University of Strathclyde

Department of Pure and Applied Chemistry

Multiplexed Nanosensing of Metal Pollutants from the Urban Environment

By

Julie Ann Docherty

A thesis submitted to the Department of Pure and Applied Chemistry, University of Strathclyde, in fulfilment of the requirements for degree of Doctor of Philosophy

2016

This thesis is the result of the author's original research. It has been composed by the author and has not been previously submitted for examination which has led to the award of a degree.

Signed: Date:

Acknowledgements

First and foremost I would like to thank my supervisors Prof. Duncan Graham, Prof. Karen Faulds, Dr. John Reglinski and Dr. Christine Davidson for providing me with the opportunity to do this PhD, and for all their help and support over the past few years. Special thanks is extended to Prof. Ewen Smith for his help and guidance throughout the project.

Next, I would like to thank the entire Bionano group, past and present, for all their support, banter and drunken antics which made the experience much more enjoyable. There are too many to individually acknowledge but most importantly, I have to thank Dr. Samuel Mabbott whose help and advice throughout my PhD has been invaluable. I also have to thank him and Dr. Steve Asiala for taking the time to correct my thesis. Thanks is also extended to Alan Hutton and Ryan Kane for helping me synthesise and NMR ligands. Next, I would like to thank Jon, Chris and Pietro for their office banter over the past 3 years or so, both the good and the bad; Rachel for making my first trip to the USA so memorable by almost getting me killed and thrown off a plane; Sian and Alex for their company in “The Ark” every Friday night and always giving me a place to crash when they made me miss my last train.

Finally, I would like to thank my family for all their support over the years.

Abstract

Surface enhanced Raman scattering (SERS) is a useful tool for the detection of metal ions due to the characteristic vibrational spectra that can be produced. Complexing different metal ions to a single ligand in solution can uniquely alter the SERS spectrum of that ligand, with the changes being specific to each individual metal ion. This approach has been used to research a nanoparticle-based sensor that can detect a number of metal ions using SERS for environmental monitoring purposes.

Research commenced by studying the small Raman reporter molecules, 4-mercaptobenzoic acid (4-MBA) and 4-mercaptopyridine (4-MPY), which were functionalised onto the surface of AgNPs. Upon addition of different metal ions, the AgNPs would aggregate resulting in an increased SERS response and characteristic frequency shifts in certain bands, which allowed discrimination of different species.

The potential of 2,2'-bipyridyl (bipy) as a chelating ligand for the SERS detection of multiple metal ions has also been investigated. It has been shown that coordination of six different metal ions to this ligand produces characteristic changes throughout the entire spectral region, and therefore the presence of a metal ion can be identified with greater confidence. Not only that, the sensitivity is also greatly improved, with both Zn(II) and Cu(II) capable of being detected below the World Health Organisation (WHO) recommended limits of 0.22 and 0.6 ppm, respectively.

Finally, the characteristic changes produced in the SERS spectrum of salen by Ni(II), Cu(II), Co(II) and Mn(II) is discussed. Although a smaller range of species can be detected compared to bipy, detection limits are significantly improved and changes produced by the different metal ions are arguably more pronounced. This approach has also been applied to real environmental freshwater samples in order to determine whether it is suitable for environmental sampling. A contaminated water sample known to contain elevated levels of Mn(II) was tested and it has been demonstrated that this method is indeed capable of detecting high levels of metal ions in natural freshwater samples.

Abbreviations

4-MBA	4-mercaptobenzoic acid
4-MPY	4-mercaptopyridine
AAS	Atomic absorption microscopy
AES	Atomic emission spectroscopy
AgNPs	Silver nanoparticles
Bipy	2,2'-bipyridyl
CE	Chemical enhancement
DLS	Dynamic light scattering
EM	Electromagnetic
EPA	Environmental Protection Agency
ETAAS	Electrothermal atomic absorption spectroscopy
f.H_2O	Freshwater
IARC	International agency for research on cancer
ICP	Inductively coupled plasmon
IR	Infrared
LOD	Limit of detection
LSPR	Localised surface plasmon resonance
MS	Mass spectrometry
NMR	Nuclear magnetic resonance
PC	Principal component
PCA	Principal component analysis
Phen	1,10'-phenanthroline
Salen	N,N'-bis(salicylidene)ethylenediamine
Salophen	N,N'-bis(salicylidene)-1,2-phenylenediamine
SALTSC	Salicylaldehye thiosemicarbazide
SEM	Scanning electron microscopy
SERS	Surface enhanced Raman scattering
SERRS	Surface enhanced resonance Raman scattering
WHO	World Health Organisation

Contents

1 Introduction 1

1.1 Background 1

1.2 Nanoparticles 1

1.3 Raman Spectroscopy 3

1.4 Surface Enhanced Raman Scattering (SERS) 6

1.4.1 The Electromagnetic Enhancement 6

1.4.2 The Chemical Enhancement (CE) 7

1.5 Surface Enhanced Resonance Raman Scattering (SERRS) 7

1.6 Heavy Metals in the Environment 9

1.7 Exposure to Heavy Metals 10

1.8 Metal Ion Detection 11

1.9 Nanoparticle-based Sensors for Metal Ion Detection 14

2 Aim 20

3 Experimental 21

3.1 Materials 21

3.2 Instrumentation 21

3.2.1 Extinction Spectroscopy 21

3.2.2 SERS 21

3.2.3 ICP-MS Analysis 22

3.2.4 DLS 22

3.2.5 SEM 22

3.2.6 NMR 22

3.3 Data Analysis 22

3.4 Nanoparticle Synthesis & Characterisation 23
3.4.1 Nanoparticle Synthesis 23
3.4.2 Extinction Spectroscopy of Colloid 23
3.4.3 DLS 25
3.4.4 SEM 25
4 MBA & MPY are not the MVPs of Metal Ion Detection 27
4.1 Experimental 27
4.1.1 Concentration Study 27
4.1.2 SERS Measurements 28
4.1.3 Extinction Spectra 28
4.2 4-MBA 28
4.2.1 Concentration Study 29
4.2.2 Addition of Metal Ions to 4-MBA-Functionalised AgNPs 31
4.2.3 PCA 35
4.3 4-MPY 39
4.3.1 Concentration Study 39
4.3.2 Addition of Metal Ions to 4-MPY- Functionalised AgNPs 41
4.3.3 PCA 44
4.3.4 Concentration Dependence Studies 46
4.4 Chapter Conclusions 48
5 The “Miracle” of Bipyridyl 50
5.1 Experimental 51
5.1.1 Solid Bipy Complexes 51
5.1.2 Concentration Study 51
5.1.3 SERS Measurements 51

5.1.4 1,10-Phenanthroline 52
5.2 Investigation of Solid Bipy Complexes 52
5.3 Concentration Study 56
5.4 SERS of Bipy-Metal Complexes 58
5.4.1 First Row Transition Metals: Fe(II) to Zn(II) 59
5.4.2 Copper 61
5.4.3 Cadmium & Chromium 62
5.5 Principal Component Analysis 63
5.6 Concentration Dependence Studies 64
5.7 1,10-Phenanthroline 67
5.8 Chapter Conclusions 68
6 It's All About That (Schiff) Base 70
6.1 Experimental 71
6.1.1 Concentration Study 71
6.1.2 SERS Measurements 72
6.1.3 Synthetic Freshwater 72
6.1.4 Real Environmental Freshwater 72
6.1.5 Seawater 73
6.1.6 Mixed Metal Ion 73
6.1.7 Salophen 74
6.1.8 SALTSC 75
6.2 Salen Concentration Study 76
6.3 The SERS of Salen Complexes 78
6.4 PCA 81
6.5 Limits of Detection (d.H_2O) 81

6.6 Synthetic Freshwater 83
6.7 Real Environmental Freshwater 84
6.8 Contaminated Freshwater 89
6.9 Seawater 91
6.10 Mixtures of Metal Ions 93
6.11 N,N'-bis(salicylaldehyde)–1,2-phenylenediamine (Salophen) 97
6.11.1 SERS of Salophen Complexes 98
6.11.2 PCA 100
6.11.3 Salophen vs. Salen 101
6.12 Salicylaldehyde Thiosemicarbazone (SALTSC) 102
6.12.1 Concentration Study 103
SERS of SALTSC-metal complexes 104
6.12.2 104
6.12.3 PCA 106
6.13 Chapter Conclusions 107
7 Conclusions 110
8 Future Work 112
9 References 114
10 Appendices 119

1 Introduction

1.1 Background

Heavy metals are a major cause of concern to the environment and human health due to their toxic, non-biodegradable and bio-accumulative properties. Although these elements are present naturally in the environment, during the past few decades widespread contamination has occurred due to anthropological activities, namely the increasing of industrialization.[1] As a result, environmental monitoring is vital to ensure that the levels present do not exceed the recommended limits set out by environmental bodies such as the World Health Organisation (WHO). Currently, the main methods used for metal ion quantitation are inductively coupled plasmon mass and atomic emission spectrometry (ICP-MS/ICP-AES) and atomic absorption spectroscopy (AAS) due to their high sensitivity and high throughput capabilities. However these techniques require the use of expensive, laboratory-based instruments that may not be available to all environmental groups, especially those in developing countries. Also, these techniques do not have the capability of providing on-site detection of metal ions. As a result, there is a need for simpler, low-cost techniques that can be used to provide the remote sensing of these species.

Nanoparticle-based sensors are becoming increasingly popular as an alternative analytical tool due to their ability to sensitively and selectively detect a wide range of analytes. Hence, this work aims to develop a portable nanosensor that is capable of detecting a number of heavy metals using surface enhanced Raman scattering (SERS). It is envisioned that this system could overcome some of the constraints of current instrumentation in use today.

1.2 Nanoparticles

Nanoparticles are a class of materials with diameters in the range of 1 to 100 nm and as a result, their properties are different to those of bulk material.[2] A historic and well-known example that demonstrates the unique properties of nanoparticles is the Lycurgus

Cup, dating back to 4th century A.D. which appears green in reflected light but ruby red in scattered light (Figure 1.1).[3] Colloidal suspensions of silver and gold nanoparticles have also been used in stained glass since the Middle Ages, where transmission through silver colloid yields yellow light, whereas transmission through gold nanoparticles produces red.[4] It was Faraday in the 1850s that first recognized that the red colour of gold colloid was due to the miniscule size of the particles.[5]

Figure 1.1: Lycurgus cup in reflected light (left) and scattered light (red)[3]

As a result, the properties of nanoparticles have been of interest for centuries and due to the ability to synthesise nanoparticles in a wide range of sizes, shapes and dielectric environments, these substrates have been used in a variety of applications.[6-9] Nanoparticles can be synthesised from a number of different metals however, gold and silver are the most commonly used substrates due to the intense plasmon resonances they possess in the visible-near infrared region of the electromagnetic spectrum. Gold nanoparticles have a strong plasmon resonance at ~520 nm and as a result, appear red in colour, whereas silver is yellow-green and has a plasmon resonance at ~400 nm.[10]

As a result, metallic nanoparticles are of great interest due to their unique physical properties. They are most commonly prepared by the chemical reduction of metal salts by reducing agents such as trisodium citrate, ethylenediaminetetraacetic acid (EDTA) or sodium borohydride. However, chemical functionalization of the nanoparticles is often required to impart selectivity and sensitivity for the specific target analytes that do not

have a sufficient affinity towards the metal surface e.g. metal ions.[10] In this case, detection is indirectly achieved by attaching reporter molecules onto the nanoparticle surface which selectively complex to the analyte. Interaction of the analyte with the reporter molecules causes aggregation of the nanoparticles, which not only changes the extinction spectrum, but also enhances the Raman scattering of the molecule.

1.3 Raman Spectroscopy

As enhanced Raman scattering can be obtained from molecules adsorbed on the surface of nanoparticles, and the vibrational modes of ligands are highly sensitive to metal ion coordination, SERS has the potential of becoming an alternative, low-cost method for detecting metal ions.[11]

Raman spectroscopy is a vibrational spectroscopic technique, which involves the inelastic scattering of photons. The theory of inelastic light scattering was first predicted by Smekal in 1923, but it was Raman who first experimentally demonstrated this phenomenon in 1928.[12, 13]

In Raman scattering, a photon interacts with a molecule and causes the electron cloud surrounding that molecule to become distorted i.e. it causes polarization. This creates an unstable "virtual state" which quickly re-radiates the photon. If the re-radiated photon has the same energy as the incident photon, it is termed Rayleigh (or elastic) scattering. However, energy can be transferred either from the incident photon to the molecule, or from the molecule to the scattered photon. In this case, a change of energy by one vibrational unit occurs and this is known as Raman (or inelastic) scattering. This is a weak process, occurring in around one in every 10^6 – 10^8 photons and therefore, Rayleigh scattering is the dominant process.[14]

There are two types of inelastic scattering that can occur depending on whether the molecule exists in the ground state or an excited state. These two processes are known as Stokes and anti-Stokes scattering respectively, and are summarised in Figure 1.2.

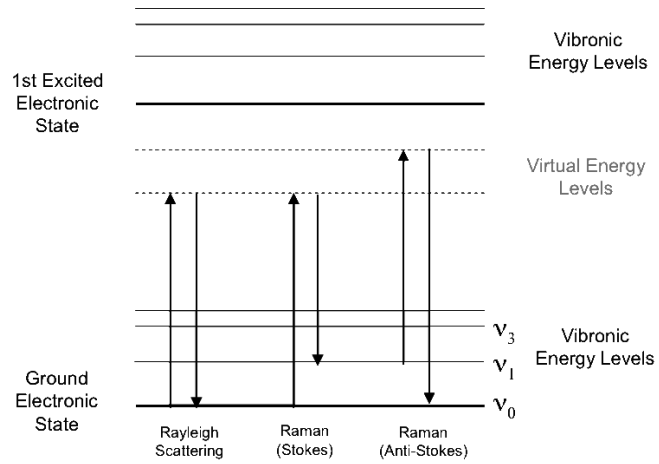

Figure 1.2: Jablonski diagram illustrating Rayleigh, Stokes and anti-Stokes scattering

In Stokes scattering, molecules are initially in the ground state and are promoted to a higher energy vibrational excited state by gaining energy from the incident photon. In anti-Stokes scattering, the molecule is initially present in an excited state and energy is transferred from the molecule to the scattered photon.[15] The intensities of Stokes and anti-Stokes scattering are dependent on the number of molecules in the ground and excited states, which can be calculated using the Boltzmann equation[14]:

$$\frac{N_1}{N_0} = \frac{g_1}{g_0} \exp\left[\frac{-\Delta E}{kT}\right] \qquad \text{(Equation 1)}$$

N_1 = the number of molecules in the lower vibrational state

N_0 = the number of molecules in the vibrational excited state

g = the degeneracy of the energy levels

ΔE = the energy difference between the two energy levels

k = Boltzmann's constant (1.3807×10^{-23} JK^{-1})

T = temperature (K)

At room temperature, the majority of molecules will be in the ground state and therefore, Stokes scattering is most commonly recorded as it will be the most intense.[14] The ratio of Stokes to anti-Stokes scattering is dependent on the temperature, and therefore increasing the temperature will result in more molecules existing in an excited state and consequently, anti-Stokes scattering can be obtained.

However, not all vibrations are Raman active. The key selection rule in Raman spectroscopy is that there must be a change in polarizability in the molecule for Raman scattering to occur. This means that symmetric vibrations give rise to the most intense scattering as they give the largest changes in polarizability.[14] This is in contrast to infrared (IR) spectroscopy where asymmetric stretches are strongest (as a change in dipole is required) and therefore, IR and Raman spectroscopy can be thought of as two complementary techniques.

The intensity of Raman scattering (I) is given by the equation:

$$I = K\, l \propto^2 \omega^4 \qquad \text{(Equation 2)}$$

Where *K* consists of constants including the speed of light, *I* is the intensity of the laser, α is the polarizability of the electrons and ω is the frequency of the incident radiation. By changing the laser power and frequency, the intensity of Raman scattering can be maximised. As the equation shows, the intensity has a 4^{th} power dependence on the excitation frequency and therefore, the lower the excitation wavelength used e.g. in the UV region, the more intense the Raman scattering. However, many compounds absorb UV radiation and this, along with the high energy of the photons in this region, means that sample degradation and burning can occur.[14]

Also, since Raman scattering is a weak effect, powerful excitation sources are required and as a result, a visible laser is usually the most common choice. However, this means that fluorescence is a major problem in Raman spectroscopy.[14] In fluorescence, light is absorbed and subsequently re-emitted at a longer wavelength after a brief interval. Since the fluorescence signals are broader and much more intense, they can therefore overwhelm weak Raman scattering, preventing detection.

Raman spectroscopy is not more widely used due to its low sensitivity, interference from fluorescence and sample degradation. However, SERS is emerging as a very powerful analytical technique that can overcome some of the problems associated with Raman spectroscopy.

1.4 Surface Enhanced Raman Scattering (SERS)

SERS is a phenomenon which greatly enhances the Raman scattering of molecules adsorbed on the surface of roughened surfaces. This effect was first discovered by Fleischmann *et al.* in 1974 when unusually high Raman signals from pyridine adsorbed on an electrochemically roughened silver electrode was observed.[16] The initial theory behind this effect was thought to be due to the increase in surface area however, Jeanmaire and Van Duyne[17] and Albrecht and Creighton[18] independently recognised in 1977 that the origin of this enhancement was due to the presence of nanostructured features.

There has been much debate surrounding the mechanism involved in SERS but it is now widely accepted that two effects contribute to this enhancement. These are the electromagnetic (EM) enhancement and the chemical enhancement (CE), which is also known as charge transfer.

1.4.1 The Electromagnetic Enhancement

When light interacts with a metallic nanoparticle, a collective oscillation of the conduction electrons occur, termed the localized surface plasmon resonance (LSPR) which is shown in Figure 1.3.[19]

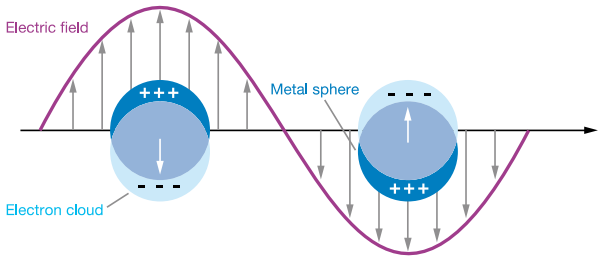

Figure 1.3: Diagram illustrating the LSPR[19]

The LSPR results in highly localized areas of EM fields, which are most intense between the interstitial sites of the metallic nanoparticles. These are called “hotspots” and any

molecules within these areas experience a much greater EM field, which therefore results in enhanced Raman scattering.[20] The EM effect is the dominant process and can provide enhancement of up to 10^{10} – 10^{11} orders of magnitude over "normal" Raman scattering.[10]

1.4.2 The Chemical Enhancement (CE)

The CE is a much weaker effect, which gives an enhancement factor of around 10 – 10^2 orders of magnitude.[20] In this process, a bond is formed between the molecule and the metal surface to give an adsorbate-metal complex. These new electronic states serve as resonant intermediates in the Raman scattering and charge can be transferred from the metal to the molecule, or vice versa.[21]

There is evidence for both the EM and CE processes however the EM effect will have a greater influence. As the CE involves an adsorbate-surface complex, this effect should only increase up to monolayer coverage.[14] The EM effect does not require direct contact between the molecule and metal however, the enhancement does drop off with distance from the surface.[20]

1.5 Surface Enhanced Resonance Raman Scattering (SERRS)

Resonance Raman scattering is a process that can provide a significant enhancement over normal Raman scattering and occurs when the energy of the excitation coincides with an electronic transition within the molecule.[22] This means that absorption or scattering can occur, however the key difference is the time scales of the two processes. Scattering is faster as it occurs before the nuclei reach equilibrium positions in the excited state. Absorption on the other hand is slower as the nuclei relax into the equilibrium geometry of the excited state.[14]

Not only can resonance Raman scattering provide an enhancement of the order 10^3 – 10^4 over normal Raman scattering, it is also selective for the part of the molecule involving the chromophore. Therefore, some bands are enhanced more than others.[14]

Figure 1.4 illustrates the process of normal (Stokes) Raman scattering, resonance Raman scattering and it also demonstrates how fluorescence has the potential to cause interference.

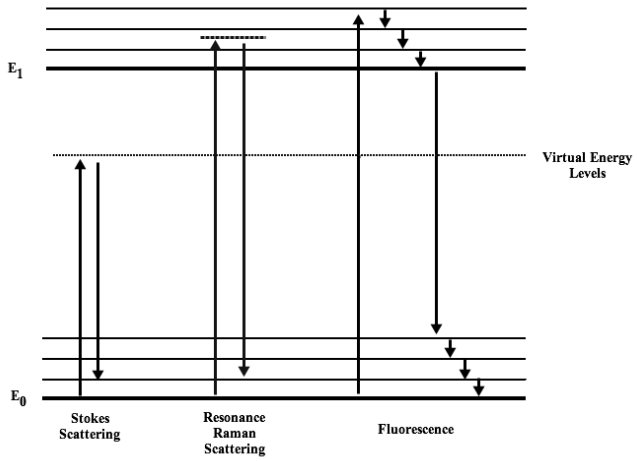

Figure 1.4: Jablonski diagram comparing Stokes scattering, resonance Raman scattering and fluorescence

However, surface enhanced resonance Raman scattering (SERRS) can help overcome the problem of fluorescence as, when a molecule with a chromophore is adsorbed onto the metal surface, fluorescence is almost completely quenched due to energy transfer to the metal.[23] Hence, SERRS can be applied to a wider range of analytes than resonance Raman scattering, as molecules considered to be fluorophores can be detected using this technique.

Furthermore, very intense scattering is obtained due to the surface plasmon resonance and also from the molecular resonance. These combined mechanisms can improve Raman scattering by up to 10^{14} orders of magnitude over "normal" Raman scattering.[14] Therefore using SERRS, it is possible to detect analytes at ultratrace levels with little or no interference from fluorescence.

1.6 Heavy Metals in the Environment

"Heavy metals" is a loosely defined term, which is generally used to indicate metals that are of environmental concern due to their toxic properties.[24] These metals and their effects on the environment and human health have been widely studied and are regularly reviewed by international bodies such as the WHO. For example, the recommended limits of heavy metals in drinking water according to the WHO are listed in Table 1.1.

Table 1.1: Recommended WHO levels of metal ions in drinking water

Heavy Metal	**WHO guideline (ppm)**
Cd	0.003
Cr	0.05
Cu	2
Pb	0.01
Mn	0.5
Ni	0.02
Zn	3

Background levels of heavy metals exist in the environment due to natural sources, such as volcanic activity and weathering of rocks.[25] However, as a result of various industrial activities, the concentration of heavy metals present in the environment may exceed the permissible limits as recommended by environmental agencies.

Heavy metals have been widely used for thousands of years and their adverse health effects have been known for some time. Despite this, their use has increased rapidly since the middle of the 19th century and it was not until the end of the 20th century that the emission of heavy metals began to fall in the developed world. In the UK for example, emissions fell by 50% between 1990 and 2000.[26] However, exposure in developing countries still remains a cause for concern.[27]

One of the most famous examples of environmental pollution is the extensive use of lead as an anti-knock agent in petrol during the 20th century. This resulted in widespread contamination throughout the environment and as a result, the use of lead in petrol began to be phased out in the 1980s, with the UK introducing a complete ban in 2000.[28, 29] Studies have shown that the prohibition of leaded petrol has resulted in a sharp decline in the average lead blood levels, as shown in Figure 1.5.[26]

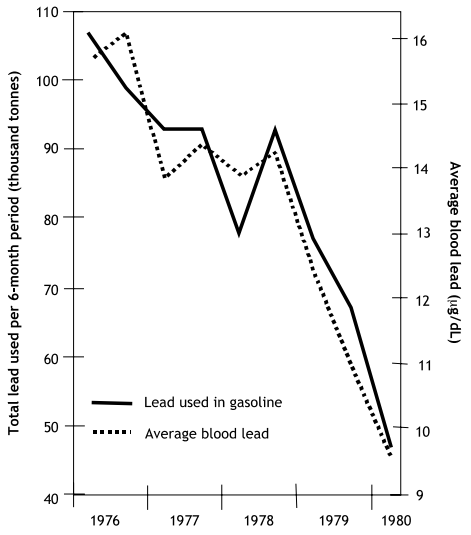

Figure 1.5: Relationship between the use of lead in petrol and average blood levels[26]

1.7 Exposure to Heavy Metals

People may be exposed to heavy metals via food, water, soil or air, although exposure can only result from direct contact between the metal and the human body, with dermal contact, inhalation and ingestion being the three main routes of exposure to humans. Figure 1.6 illustrates the relationships between environmental media, exposure media and exposure routes.[30]

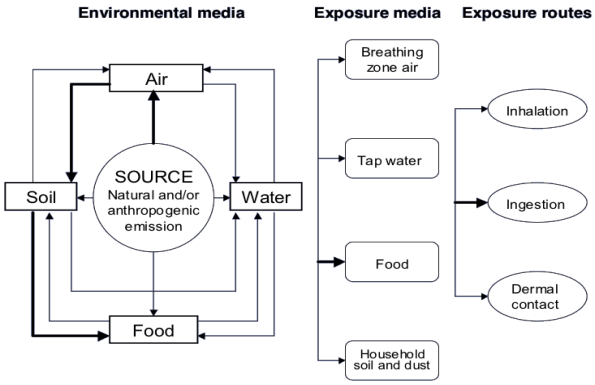

Figure 1.6: Illustration showing the relationship between environmental media and exposure media and routes[30]

The major causes of heavy metal emissions to the environment are due to anthropological activities including mining, industrial processes (foundries, smelters, oil refineries, petrochemical plants, etc.) and transportation.[31] Exposure to these elements are known to adversely affect human health, with each individual metal exhibiting specific effects.[32] A number of heavy metals and their compounds are known carcinogens, as classified by the International Agency for Research on Cancer (IARC).[33] However, over-exposure to heavy metals can also affect the central nervous system, blood composition and a number of vital organs including the lungs, liver and kidneys.[31] Due to the risks these elements pose to human health and the environment, it is vital to ensure that the levels present in the environment to do not exceed permissible limits.

1.8 Metal Ion Detection

Heavy metals are indispensable to human life as they are applied in the manufacture of a wide range of products. However, the effects of exposure to heavy metals could potentially be life threatening and therefore, regulating the levels in the environment should not be neglected. Electrothermal atomic absorption spectroscopy (ETAAS), AAS and ICP methods are most commonly used for metal ion analysis. The method of choice is usually dependent on the metal and/or concentration to be determined, along with the availability and cost of the instrumentation.[34] A summary of the main advantages and disadvantages of these techniques is given in Table 1.2, and their estimated detection limits are listed in Table 1.3.

Table 1.2: Comparison of the current methods of metal ion quantitation[34]

	Atomic Absorption Spectroscopy	**Electrothermal Atomic Absorption Spectroscopy**	**Inductively Coupled Plasmon-Atomic Emission Spectroscopy**	**Inductively Coupled Plasmon-Mass Spectrometry**
Detection limits	Very good for some elements	Excellent for some elements	Very good for most elements	Excellent for most elements
Sample throughput	10-15 s per element	3-4 min per element	1-60 elements/min	All elements in < 1 min
Interferences: **-Spectral** **-Chemical** **-Physical**	 Very few Many Some	 Very few Very many Very few	 Many Very few Very few	 Few Some Some
Sample volumes required	Large	Very small	Medium	Very small to medium
Method development	Easy	Difficult	Moderately easy	Difficult
Capital costs	Low	Medium to high	High	Very high
Running costs	Low	Medium	High	High

Table 1.3: Estimated detection limits of heavy metal ions using ETAAS, AAS and ICP methods[35]

Metal	Estimated Detection Limit		
	ETAAS (µg/L)	AAS (µg/L)	ICP (µg/L)
Cd	0.1	2	4
Cr	2	20	7
Cu	1	10	6
Mn	0.2	10	2
Ni	1	20	15
Pb	1	50	40
Zn	-	5	2

It can be seen from Table 1.2 that each technique has several advantages and disadvantages, and no one technique will suit all of the needs of a laboratory. The main drawback of these techniques is cost and availability. As a result, they may not be available to all environmental groups, nor do they allow for the remote sensing of heavy metal ions.

UV-Vis and fluorescence spectroscopy are cheaper alternatives that may be used on-site for the real-time detection of metal ions. These techniques exploit the affinity of metal ions to certain ligands and therefore complexation is required for the successful detection of these species.

UV-Vis spectroscopy is convenient as it is a simple and low-cost method, where detection is achieved by incubating metal ions with selective ligands that provide a coloured complex. The absorbance spectrum of this complex is then obtained and the Beer-Lambert law can then be applied to estimate the concentration of metal ion present. For example, dimethylglyoxime can form a coloured complex with nickel and UV-Vis spectroscopy can be used to estimate the nickel concentration down to a reported 0.1 ppm.[36] A second example of a spectroscopic reagent for UV-Vis analysis is silver diethyldithiocarbamate, which can reportedly be used to detect arsenic at 0.1 µg/mL.[37]

Fluorescence spectroscopy is also an attractive approach due to the widespread availability and high sensitivity of this technique. This has been illustrated by the development of a wide range of fluorescent sensors for the detection of metal ions.[38-44] These sensors are designed by linking a receptor molecule, which has a selective affinity for the metal ion of interest, to a fluorophore, which provides the fluorescent signal. When a target ion binds to the fluorescent probe, the compound exhibits changes in the fluorescent emission intensity, making them useful for the detection of metal ions.[45]

SERS also requires ligands to bind to the metal ions of interest and provide a vibrational profile. However, the advantage of SERS is that it provides molecularly specific data, whereas the signals for UV-Vis and fluorescence are broad and overlapping, and therefore these techniques can usually only detect one species at a time. Selective ligands which bind to a single metal ion are also required for these methods, which can be difficult as interference from other metal ions is very common. For SERS however, the sharp signals allow multiple metal ions to be detected using a single ligand, as different metal ions can produce different vibrational changes in the spectrum of the ligand. Therefore, SERS has a greater potential for multiplexed detection i.e. it has the ability to sensitively and unambiguously detect multiple species simultaneously. SERS analysis also has the potential to provide much lower detection limits than UV-Vis spectroscopy, while the sensitivity is usually comparable to that of fluorescence spectroscopy.[46] An added benefit of SERS is the availability of portable Raman spectrometers which are becoming smaller and cheaper, making this an effective detection technique for the analysis of metal ions on-site.[47]

1.9 Nanoparticle-based Sensors for Metal Ion Detection

Over the past couple of decades, nanoparticles have been investigated as potential sensors for a wide variety of analytes (chemical and biological), such as, DNA[48], explosives[49, 50], pathogens[51, 52], antigens[53], etc. These sensors allow reliable, rapid detection with minimal sample handling, and therefore demonstrate properties that are desirable for environmental screening. As a result, nanoparticle-based sensors are

expected to play an increasingly important role in the detection of environmental pollutants.

A large number of colourimetric nanoparticle-based sensors have been reported where nanoparticles are functionalised with a molecule that selectively binds to a metal ion.[54-60] As a result, aggregation occurs when the metal ion of interest is present, resulting in a visible colour change. Using extinction spectroscopy, it is then possible to record changes in the intensity and wavelength of the surface plasmon band.

For example, Xin *et al.* have developed a gold nanoparticle-based sensor for the detection of Cr^{3+} ions.[61] The gold nanoparticles (AuNPs) were functionalized with tripolyphosphate, which resulted in a colour change from red to violet in the presence of Cr^{3+}, which is shown in Figure 1.7. This system has a detection limit of 10^{-7} M by the naked eye with little interference from other metal ions, making it a simple and selective technique for the detection of Cr^{3+} ions.

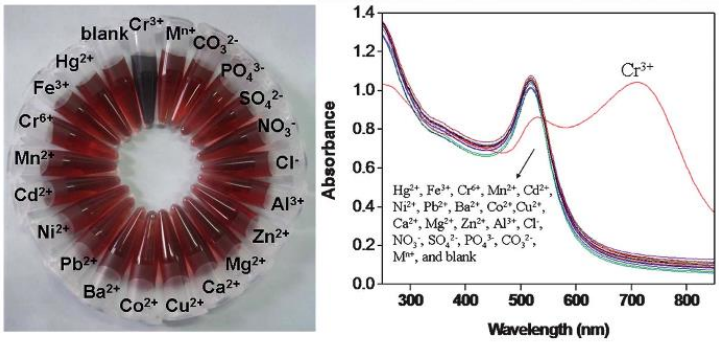

Figure 1.7: Left: tripolyphosphate functionalised AuNPs in the presence of various ions; right: extinction spectra of the AuNPs after addition of different ions (50 µM)[61]

Li and co-workers have reported the detection of Ni(II) in aqueous media using glutathione-stabilized silver nanoparticles.[62] In this system, the nanoparticle solution changes from yellow to a deep orange in the presence of Ni(II) ions, with a detection limit of 7.5×10^{-5} M. This method was shown to be highly selective as interference from a number of other metal ions was negligible; only cobalt was shown to have a moderate interference as shown in Figure 1.8.

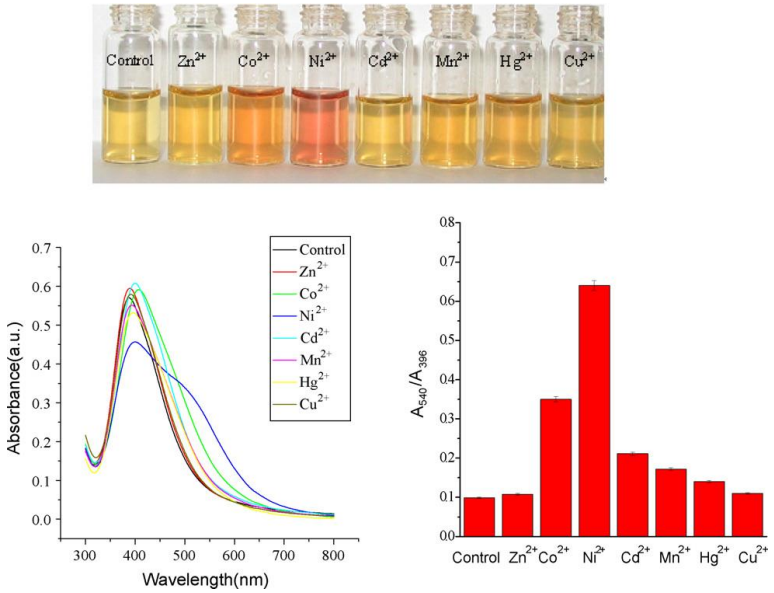

Figure 1.8: Top: glutathione-AgNPs in the presence of different metal ions. Bottom left: extinction spectra of the functionalised AgNPs in the presence of different metal ions. Bottom right: ratio of A_{540}/A_{395} for the different metal ions[62]

Although these examples demonstrate that this concept allows the rapid detection of heavy metal ions, along with simple interpretation of the results, there are major drawbacks to using these systems. Firstly, it lacks the sensitivity of conventional analytical techniques, such as AAS and ICP-MS. Secondly, the broad nature of the response means that the ability to multiplex is severely limited. One way to overcome these issues is to base the nanosensors around SERS. If the ligand used to bind to the metal ions is Raman active, SERS can be used as a sensitive detection method. Aggregation of the nanoparticles after addition of the analyte should significantly increase the SERS signal of the ligand, resulting in an off-to-on response. A large number of studies on the selective SERS detection of metal ions have previously been reported.[63-68] However, these studies can only detect one metal ion which is not ideal for environmental monitoring, as a number of heavy metals can contaminate the environment. Therefore sensors that are capable of detecting multiple metal ions would be preferential.

Recently, a number of SERS-based assays that can detect more than one heavy metal ion have emerged. This approach has been demonstrated by, Tsoutsi *et al.*, who have used terpyridine-modified silver nanoparticles to simultaneously detect Cu(II) and Co(II) ions

in the ppb range by examining the differential Raman shifts in response to these metal ions, shown in Figure 1.9.[69] The sensitivity of the nanoparticles towards these cations was similar to conventional analytical methods such as AES and AAS.

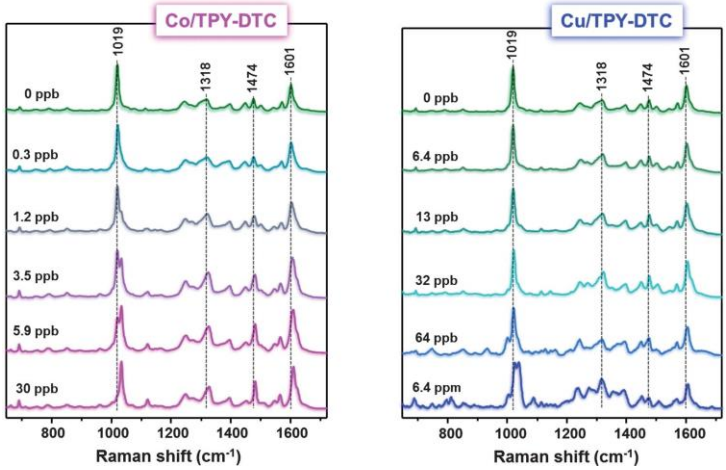

Figure 1.9: SERS spectra of the terpyridine-modified NPs with varying concentrations of Co(II) (left) and Cu(II) (right)[69]

Kim *et al.* have used cyanide for the detection of Cr(III), Fe(III), Fe(II), Ni(II) and Mn(II).[70] In this system, the metal ions interact with the cyanide via the lone pair of electrons on the nitrogen atom. The shift in the CN stretch produced by complexation of these ions is then monitored using SERS, as shown in Figure 1.10. In the presence of trivalent metal ions, this band blue-shifted by up to 64 cm^{-1}, whereas the divalent metal ions produced a blue-shift of 26 – 35 cm^{-1}. This method reported a very low detection limit of 1 fM for Co(II) which demonstrates the potential of SERS to detect metal ions at low concentrations.

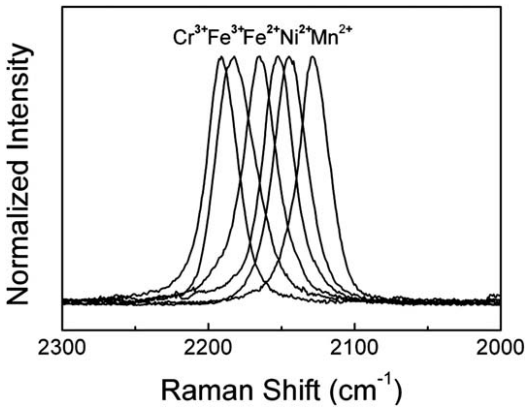

Figure 1.10: SERS spectra of CN-adsorbed Au after addition of Cr(III), Fe(III), Fe(II), Ni(II) and Mn(II)

Li *et al.* have also used dye-coded nanoparticles to detect Cu(II) and Hg(II) ions.[71] Firstly, 3,5-Dimethoxy-4-(6'-azobenzotriazolyl)phenol was attached to AgNPs to act as a SERS reporter, which was followed by the self-assembly of L-cysteine, shown in Figure 1.11. Addition of Cu(II) and Hg(II) ions resulted in the aggregation of the AgNPs, giving a good SERS response (Figure 1.12). For exclusive detection of each ion, SCN^- was added to mask Hg(II). LODs for this system were calculated to be 10 pM for Cu(II) and 1 pM for Hg(II).

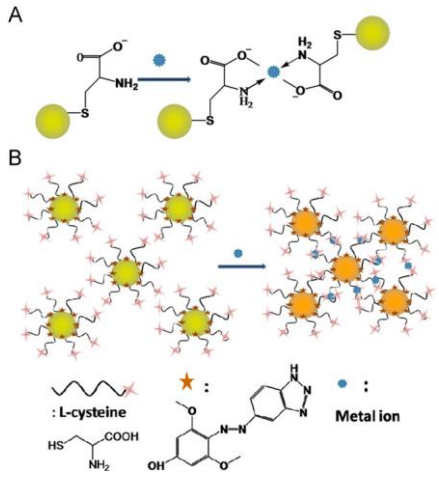

Figure 1.11: (A) Interaction of metal ions with L-cysteine functionalised nanoparticles; (B) Metal ion induced aggregation of the dye-coded nanoparticles

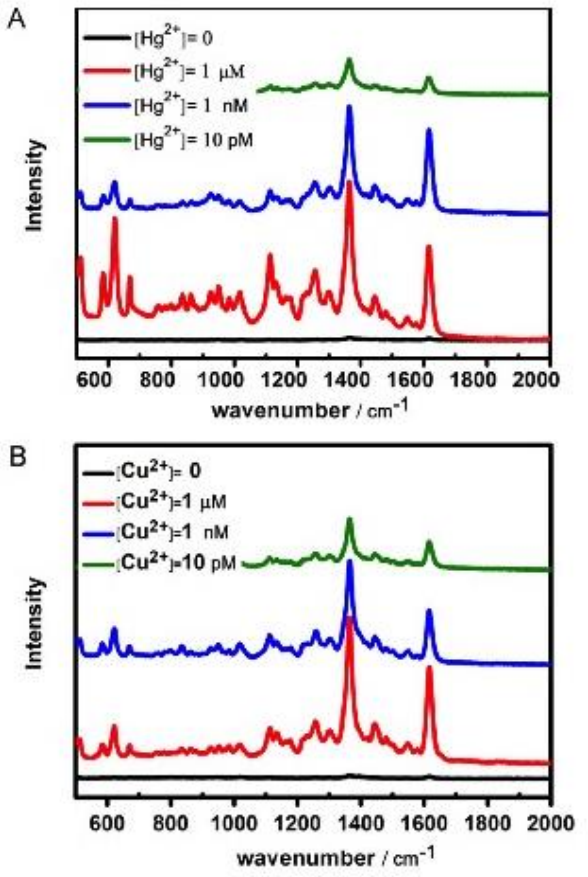

Figure 1.12: SERS spectra from Ag-L-cysteine conjugates with different concentrations of (A) Hg(II) and (B) Cu(II)

These examples therefore demonstrate the potential of SERS to detect and discriminate between more than one metal ion using a single ligand. Instead of using multiple ligands to selectively detect each metal ion of interest (which is difficult due to interference issues), it is possible to use a universal ligand to detect multiple metal ions due to the unique changes that can be produced in the SERS spectrum upon complexation.

2 Aim

The overall aim of this work is to develop a nanoparticle-based sensor that is capable of detecting multiple heavy metal ions that are hazardous to the environment. The concept behind this is based on the affinity of these ions for Raman active ligands. Binding of metal ions to these ligands can alter the SERS spectrum of the reporter molecule, with changes being specific to each metal ion. As a result, different metal ions may be discriminated based on these changes.

This work will therefore investigate the ability of certain ligands to coordinate to a range of metal ions and distinguish between these species based on the characteristic changes produced in the SERS spectrum of the ligand. Once appropriate ligands have been identified, the sensitivity will be studied in order to determine the feasibility of the system with regards to environmental screening. The WHO's recommended limits of metal ions in drinking water will be used as target LODs. Due to the complexity of real environmental samples, initial studies will be conducted by spiking distilled water (d.H_2O) with the metal ions of interest. Once an appropriate method has been optimised using d.H_2O, work will progress to using real environmental samples in order to determine if the method is feasible using more realistic samples.

3 Experimental

3.1 Materials

All chemicals and reagents were purchased from Sigma Aldrich and used as received. Metal nitrate salts were used throughout with the exception of Fe(II) where the chloride salt was used instead due to the lack of availability of the nitrate salt.

3.2 Instrumentation

3.2.1 Extinction Spectroscopy

Extinction spectra were recorded on a Varian, Cary Win-UV 300, Dual Beam Scanning UV-vis spectrometer, in the range 200 – 800 nm (Agilent, Santa Clara, CA). 1 cm path length quartz cells were used for all measurements. All extinction spectra obtained were baseline corrected using d.H_2O as a blank. Colloidal solutions were analysed using a 1 in 10 dilution with d.H_2O.

3.2.2 SERS

All SERS samples were prepared and analysed in triplicate, and an average spectrum was then obtained. SERS analysis was conducted using one of the following instruments:

An Avalon Instruments Ltd. RamanStation compact benchtop Raman spectrometer (PerkinElmer, Waltham, MA) was used to conduct rapid SERS analysis. This system uses a stabilised 532 nm external cavity diode laser (100 mW), an echelle spectrograph and an Andor Technology CCD detector. The system is fitted with a motorised x–y–z-sample stage, which accepts standard 96-well microtitre plates. The instrument's software was used to automatically drive the stage to each well in turn.

SERS measurements were also conducted using a Snowy Range Instruments Sierra Benchtop Raman Spectrometer (SnRI, Wyoming, USA). A laser wavelength of 532 nm,

laser power 50 mW, 10 s exposure time in the range of 200 – 3200 cm^{-1} was applied to all the analyses.

A WITec Alpha 300 R confocal microscope(WITec, Ulm, Germany) with a 532 nm excitation wavelength was also used for Raman measurements of solid samples.

3.2.3 ICP-MS Analysis

An Agilent 7700 instrument (Agilent Technologies, Santa Clara, USA) was used for ICP-MS analysis, which was carried out by Alexander Clunie (University of Strathclyde).

3.2.4 DLS

A Malvern Zetasizer Nano Zs system was used for dynamic light scattering (DLS) and zeta potential measurements. The measurement range for particle sizing was 0.3 nm – 10 µM, while for the zeta potential, it was 3.8 nm – 100 µM.

3.2.5 SEM

Imaging was carried out using a Hitachi S-3000N, variable pressure scanning electron microscope (SEM) with EDX 6" Tungsten electron source at an acceleration voltage of 30 kV. SEM analysis was performed by Dr. Samuel Mabbott.

3.2.6 NMR

^{1}H and ^{13}C NMR analysis was conducted using a Bruker Avance 3 (400 MHz) instrument (Billerica, Massachusetts, USA).

3.3 Data Analysis

Baseline correction of all SERS spectra collected on the Avalon Plate Reader was performed using Matlab software version 2012b (The Mathworks, Natick, MA, USA). As

SnRI Snowy Raman Instrument has a built-in baseline correction function, this was used for all spectra collected on this instrument.

PCA was also performed using Matlab software. Peak fitting was carried out using Origin9 software (OriginLab, Northampton, MA, USA).

3.4 Nanoparticle Synthesis & Characterisation

3.4.1 Nanoparticle Synthesis

Silver was chosen as the nanoparticle substrate as it provides a greater SERS enhancement over gold at 532 nm. This is due to the fact that silver has a greater scattering to absorption ratio and gold also absorbs quite strongly at around 500 nm.[72] Therefore, silver is much more effective with 532 nm excitation, which was used in this work.

Citrate reduced silver nanoparticles were prepared using a modified version of the Lee and Meisel method.[73] A 1 L 3-necked round bottom flask and glass link rod were cleaned with aqua regia ($HCl:HNO_3$ 3:1) for at least 2 hours before starting the preparation and the flask was then rinsed multiple times with $d.H_2O$. 90 mg of silver nitrate (dissolved in 10 mL $d.H_2O$) was added to 500 mL of $d.H_2O$. The solution was then heated until boiling, with vigorous stirring, and then a 1 % aqueous solution of sodium citrate was added (10 mL). The solution was left to boil for a further 20 – 30 minutes before being left to cool to room temperature.

3.4.2 Extinction Spectroscopy of Colloid

The quality of the colloid was first assessed using extinction spectroscopy. The silver citrate obtained from this method should have a λ_{max} of approximately 400 nm and a full width at half maximum (FWHM) of less than 100 nm in order to be as close to monodispersity as possible, which ensures that the colloid is of reproducible quality. As a result, all batches of colloid used throughout this research met these standards, and an

example of an extinction spectrum obtained for silver citrate nanoparticles is shown in Figure 3.1.

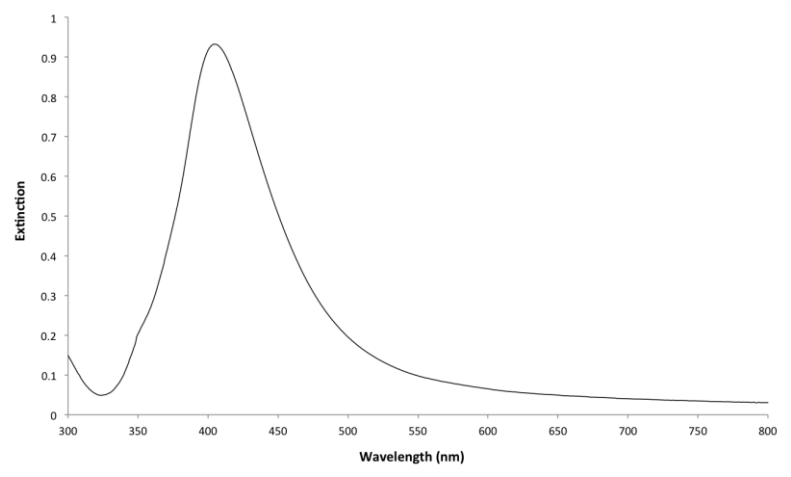

Figure 3.1: Example extinction spectrum of silver citrate colloid

The extinction spectrum can also be used to estimate the concentration of nanoparticles by applying the Beer-Lambert Law:

$$A = \varepsilon c l \qquad \text{(Equation 3)}$$

Where, A = absorbance

ε = molar absorptivity (M^{-1} cm^{-1})

c = concentration (M)

l = path length (cm)

The molar absorptivity is a measure of how strongly a chemical species absorbs light and varies with nanoparticle size. The extinction coefficient for 40 nm AgNPs is estimated to be 2.87×10^{10} M^{-1} cm^{-1}.[74] Using this value, it is therefore possible to calculate the concentration of nanoparticles, as demonstrated below:

$$c = \frac{A}{\varepsilon l}$$

$$c = \frac{0.817}{2.87 \times 10^{10} \times 1}$$

$$c = 2.85 \times 10^{-11}\ \mathrm{M}$$

However, as a 1 in 10 dilution was used to obtain the extinction spectrum, the calculated value is multiplied by 10, giving a concentration of 2.85 x 10^{-10} M, i.e. 285 pM.

3.4.3 DLS

Secondly, DLS was used to measure the size and zeta potential of the citrate-capped AgNPs. The zeta potential determines the stability of the colloid, where stable colloidal nanoparticles have been reported to have values between -30 and + 30 mV as a result of the strong electrostatic repulsion between the nanoparticles which prevent them from aggregating.[75] All batches of AgNPs used throughout this research had a size of approximately 40 nm and a zeta potential below -30 mV, which ensured the stability of the colloid.

3.4.4 SEM

Finally, SEM was the last step in assessing the quality of the synthesised colloid. A silicon wafer was washed with MeOH, dried and cleaned in an oxygen plasma chamber. The wafer was then coated with a (polydiallyldimethylammonium) chloride (PDDA) solution and left for 20 min. The solution was then removed from the wafer using a pipette before rinsing with d.H_2O and drying under a light flow of nitrogen. The wafer was then coated with 10 µL of the colloidal solution and again let for 20 min before removing the AgNPs, rinsing and drying. This step was repeated once more. Figure 3.2 gives an example of an SEM image obtained from a batch of silver citrate colloid.

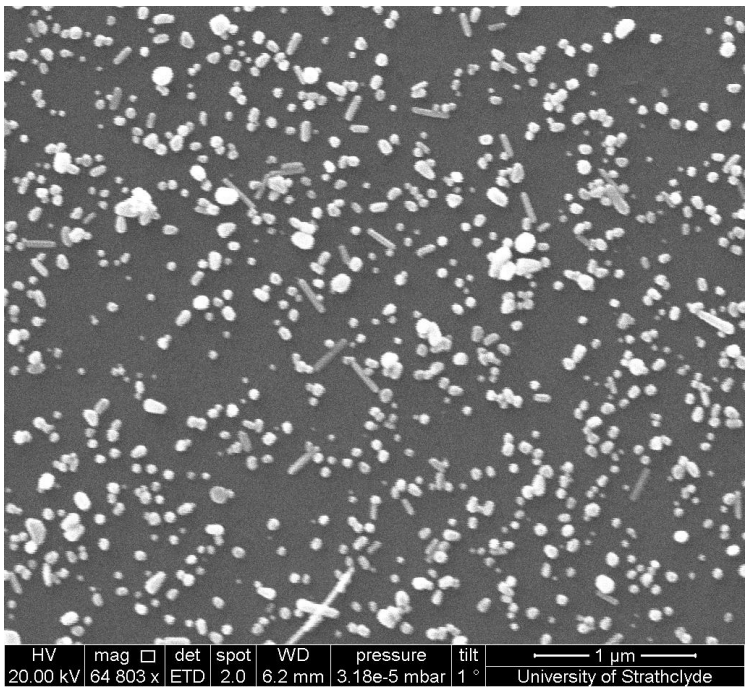

Figure 3.2: Typical SEM image for silver citrate nanoparticles

Ideally, the colloid would be monodisperse however, due to the highly reactive nature of silver ions. It is difficult to control the size and shape of citrate-reduced AgNPs and as a result, rods are also produced.

4 MBA & MPY are not the MVPs of Metal Ion Detection

4-mercaptobenzoic acid (4-MBA) is a small Raman reporter molecule that is known to provide a strong SERS signal. This was selected as a potential ligand for metal ion detection as it has previously been reported that the carboxylate stretching frequency can differ upon the coordination to different metal ions. [76] Therefore the identity of the heavy metal ions could be deduced from the changes produced in the SERS spectrum of 4-MBA. This concept was subsequently applied to a second small Raman reporter molecule, 4-mercaptopyridine (4-MPY) however for this ligand, it is presumed that the lone pair of electrons on the nitrogen atom would coordinate to the metal ions.

4.1 Experimental

4.1.1 Concentration Study

AgNPs were functionalised with varying concentrations of 4-MBA/4-MPY according to Table 4.1. 200 µL of the functionalised AgNPs were added to a 96-well microplate along with 50 µL of d.H_2O, before inducing aggregation with 10 µL of 0.1 M NaCl solution. The samples were incubated for 10 minutes to allow complete aggregation of the nanoparticles, before the SERS spectra were acquired using the Avalon plate reader (λ_{ex} = 532 nm, 10 s exposure time, 250 – 2000 cm^{-1}, 0.5 cm^{-1} resolution).

Table 4.1: Summary of the different 4-MBA/4-MPY concentrations used in the concentration study, and how the samples were prepared

Volume of AgNPs (µL)	Volume of 4-MBA/4-MPY (µL)	Concentration of 4-MBA/4-MPY added to AgNPs (µM)	Final concentration of 4-MBA/4-MPY (µM)
750	250	1000	250
750	250	100	25
750	250	10	2.5
750	250	1	0.25

4.1.2 SERS Measurements

200 µL of AgNPs functionalised with 2.5 µM 4-MBA/4-MPY were added to a 96-well plate before addition of the metal ions at the desired concentration (50 µL). The metal ions were at a high enough concentration to induce the aggregation of the AgNPs and therefore no salt was added. Again, the samples were left for 10 min to allow aggregation to occur before collecting the SERS spectra using the Avalon Plate Reader (λ_{ex} = 532 nm, 10 s exposure time, 250 – 2000 cm^{-1}, 0.5 cm^{-1} resolution).

4.1.3 Extinction Spectra

Extinction spectra were obtained by adding 75 µL of the metal ion (at 100, 350 and 500 µM) to 300 µL 4-MPY-AgNPs in a 1 cm plastic cuvette. These were allowed to aggregate before adding 2125 µL d.H_2O and acquiring the extinction spectra.

4.2 4-MBA

4-MBA is a strong Raman reporter that binds to the nanoparticle surface via the thiol group, leaving the carboxylate group free for metal ion coordination, as depicted in Figure 4.1. It was hypothesised therefore, that metal ions would influence the carboxylate stretch in the 4-MBA SERS spectrum, enabling discrimination of these species.

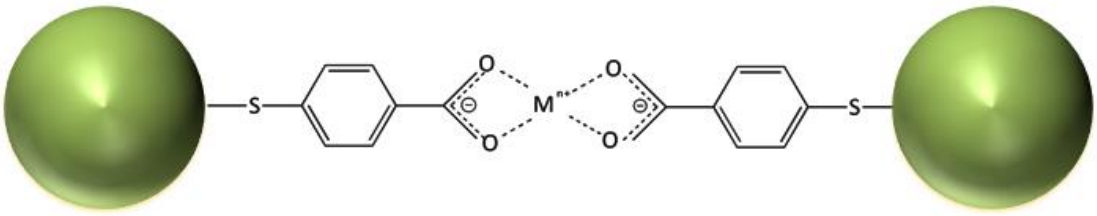

Figure 4.1: Proposed interaction of 4-MBA-functionalised AgNPs with metal ions

4.2.1 Concentration Study

Firstly, in order to determine the optimal concentration of 4-MBA required for metal ion detection, a concentration study was performed. As the majority of SERS enhancement originates from the first layer on the metal surface, it is important to ensure that there is no steric crowding or multilayer adsorption on the nanoparticle surface.[77] Therefore, in order to determine the concentration of 4-MBA required to obtain monolayer coverage, different concentrations of 4-MBA (ranging from 250 µM to 0.25 µM) was added to the nanoparticle dispersion. This was then left overnight to allow the ligands to chemisorb onto the surface of the AgNPs. The injection of 4-MBA results in the gradual displacement of citrate on the AgNP surface with the more strongly bound 4-MBA due to the formation of thiolate bonds. Sodium chloride was added to the samples in order to induce aggregation of the nanoparticles and the SERS spectra at each concentration were collected. Figure 4.2 displays the resulting spectra from this study.

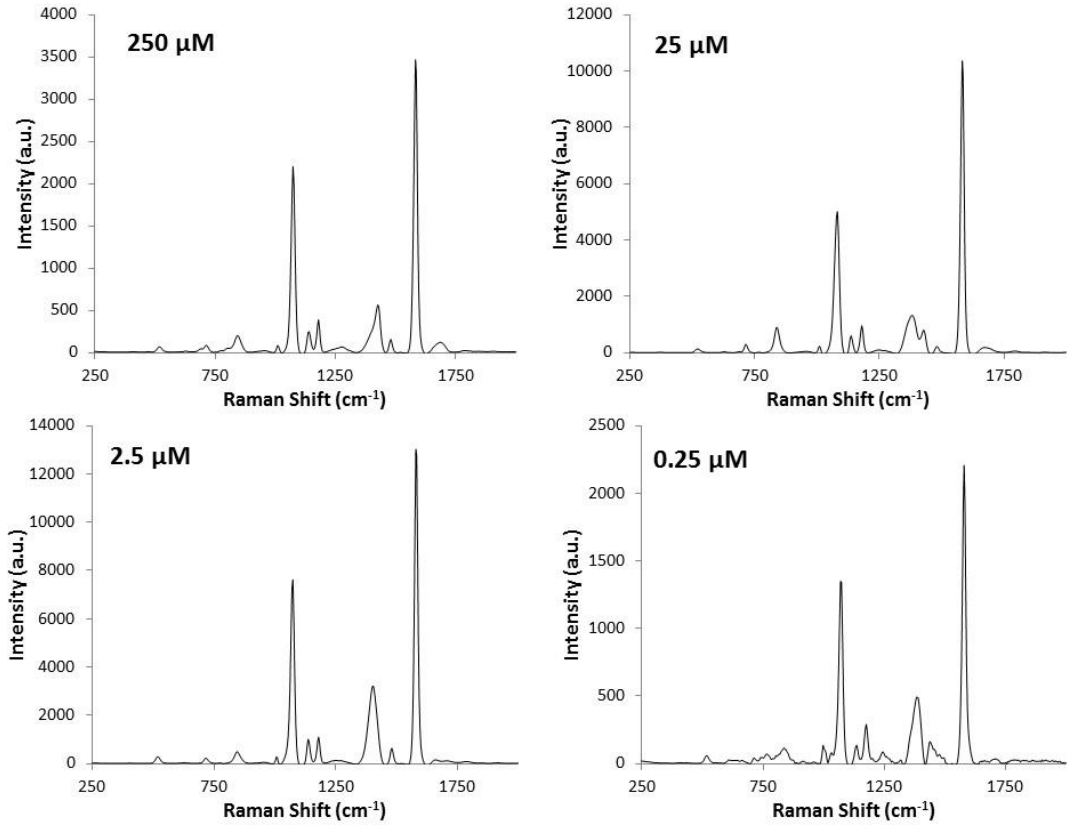

Figure 4.2: SERS spectra obtained from AgNPs functionalised with varying concentrations of 4-MBA. Top left: 250 µM; top right: 25 µM; bottom left: 2.5 µM; bottom right: 0.25 µM. (acc. time = 10s; λ_{ex} = 532 nm)

From the concentration study, it was discovered that concentrations from 250 µM to 0.25 µM gave strong SERS signals corresponding to 4-MBA. A 4-MBA concentration of 2.5 µM gave the strongest SERS response and hence this concentration was deemed to provide the monolayer coverage required. At concentrations above this, especially 250 µM, a weaker signal is obtained due to multilayer effects which will reduce the effective signal. At concentrations below this, there are too few 4-MBA molecules on the surface, hence a reduced SERS signal is observed.

It should also be noted that the carboxylate stretch (at ~1400 cm^{-1}) shifts in frequency at the different concentrations, implying that the orientation of 4-MBA on the nanoparticle surface is dependent on the concentration. At 250 µM, the COO^- stretch occurs at 1427 cm^{-1}, while at 25 µM two bands can be observed at 1427 and 1383 cm^{-1}, which is thought to be due to different orientations at the surface of the AgNPs. It is hypothesised that the lower frequency band at 1383 cm^{-1} may be due to COO^- groups interacting with the

AgNP surface while the band at 1427 cm^{-1} is due to non-bonded COO^- groups.[78] Therefore, it is presumed that at 250 µM, the majority of the 4-MBA molecules are bound to the surface via the sulfur atom hence one band at a higher frequency is present. When the concentration decreases, the ratio of surface bound to non-surface bound COO^- groups increases, and hence a second, lower frequency band appears at 25 µM which corresponds to the different orientation. At 0.25 µM, a single band at 1385 cm^{-1} is observed, along with a decreased SERS signal, implying that 4-MBA lies flat at the AgNP surface as not enough 4-MBA is present to produce monolayer coverage. As a 4-MBA concentration of 2.5 µM produces the most intense SERS spectrum, with a single COO^- peak, this concentration was deemed to be optimal. The frequency of the COO^- stretch for this concentration occurs at 1402 cm^{-1} suggesting that most of the 4-MBA molecules are orientated vertically to the surface through the sulfur atom, although some COO^- groups may still interact with the surface. The SERS assignments of 4-MBA (using the 2.5 µM spectrum) are listed in Table 4.2.

Table 4.2: SERS assignments of 4-MBA[79]

Raman Shift (cm^{-1})	**Assignment**
521 (vw)	Ring out-of-plane bending
774 (vw)	
846 (vw)	COO^- bending
953.5 (vw)	
1074 (s)	Ring breathing
1137.5 (w)	CH bending
1180 (w)	CH bending
1402.5 (m)	COO^- symmetric stretch
1481 (w)	Ring bending
1580 (vs)	Ring breathing

4.2.2 Addition of Metal Ions to 4-MBA-Functionalised AgNPs

In order to determine the feasibility of this method, seven different metal ions were added to the 4-MBA-functionalised AgNPs, which resulted in the aggregation of the

AgNPs. This can be monitored using extinction spectroscopy as shown in Figure 4.3, which compares the extinction spectra of AgNPs and 4-MBA-AgNPs before and after the addition of metal ions.

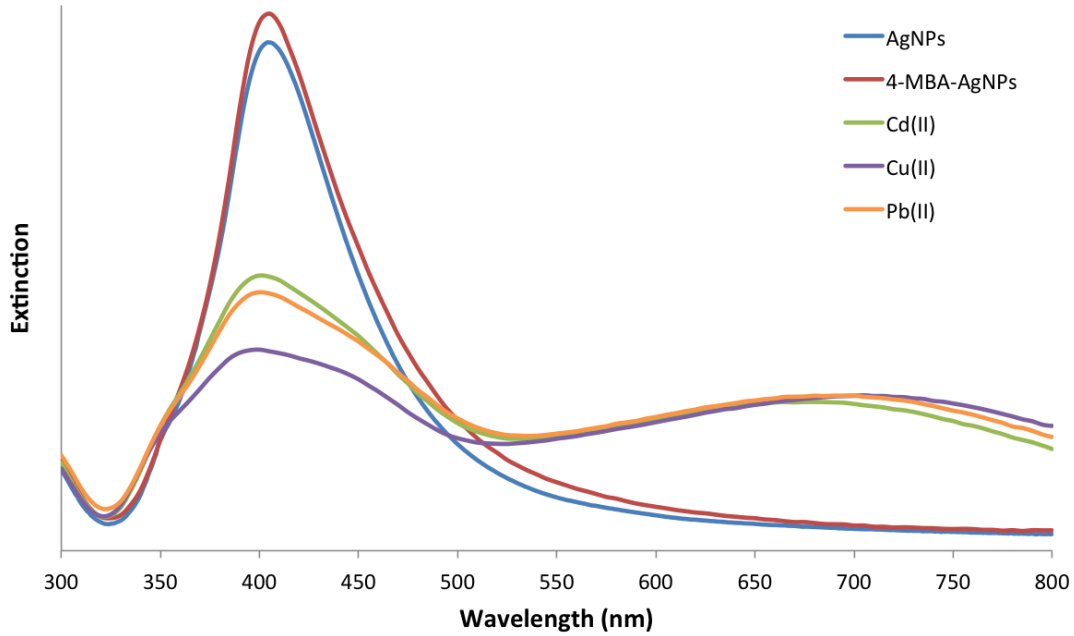

Figure 4.3: Extinction spectra of AgNPs (blue), 4-MBA-AgNPs (red) and 4-MBA-AgNPs after addition of Cd(II) (green), Cu(II) (purple) and Pb(II) (orange)

It can be seen from Figure 4.3 that there is little change in the extinction profiles of the AgNPs and 4-MBA-functionalised AgNPs, demonstrating the stability of the 4-MBA-AgNPs. After addition of metal ions to 4-MBA-AgNPs however, it is clear that aggregation occurs as the intensity of the extinction band decreases and a second band at a longer wavelength appears due to the formation of aggregates. Aggregation caused by the addition of metal ions will also result in an increased Raman signal from 4-MBA, and any unique changes produced in the SERS spectrum of this ligand, as a result of metal ion coordination, may then be detected.

The SERS spectra obtained after addition of seven different metal ions to 4-MBA-AgNPs (100 ppm) is shown in Figure 4.4.

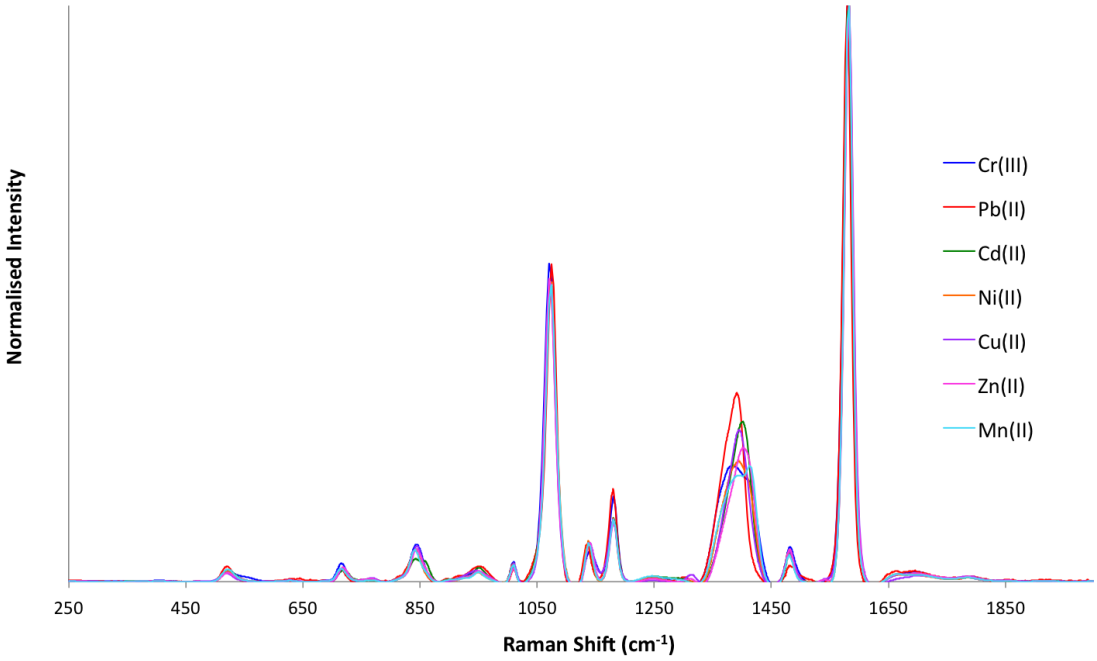

Figure 4.4: SERS spectra of 4-MBA-functionalised AgNPs after the addition of different metal ions (acc. time = 10s; λ_{ex} = 532 nm)

The spectrum of 4-MBA is dominated by two main peaks at 1074 cm^{-1} and 1580 cm^{-1}, which correspond to the aromatic ring breathing modes. However, there is little variation in these bands upon coordination of the different metal ions. The main peak of interest is the carboxylate stretching mode at ~1400 cm^{-1} since it is the carboxylate group that interacts with the metal ions. Hence, any spectroscopic changes in the spectrum due to coordination with metal ions are expected to occur in this region. It can be seen from the overlaid spectra in Figure 3.4 that coordination of the various metal ions causes this band to change in both frequency and shape. This is more apparent in Figure 4.5, where an enlargement of the carboxylate stretch is presented. The SERS shifts obtained following addition of each metal ion are also listed in Table 4.3.

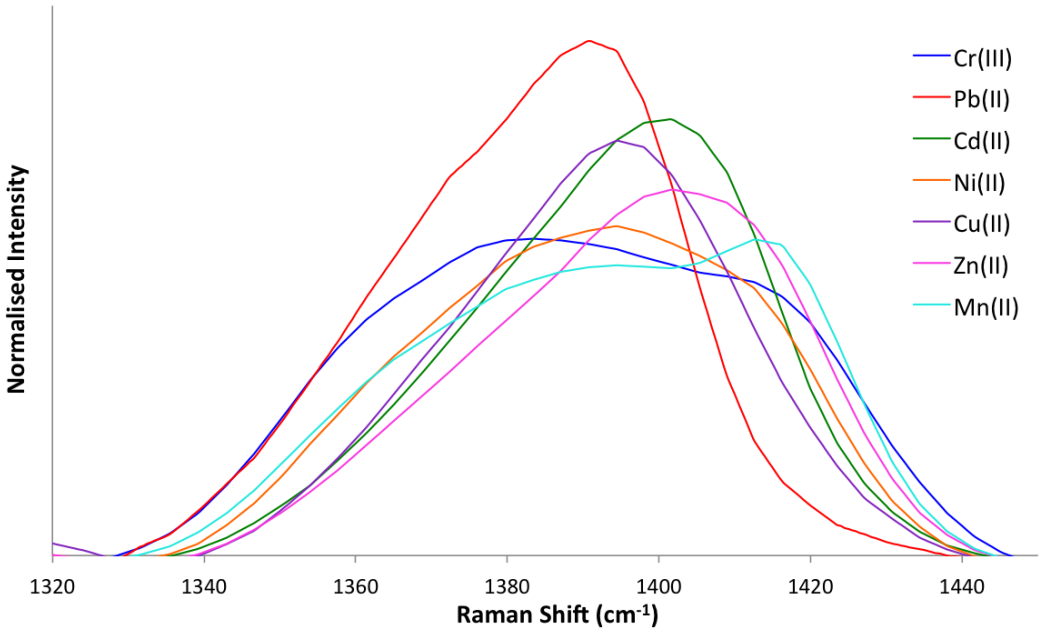

Figure 4.5: Enlargement of the carboxylate stretch showing the changes produced by the different metal ions. Cr(III), blue; Pb(II), red; Cd(II), green; Ni(II), orange; Cu(II), purple; Zn(II), pink; Mn(II), cyan (acc. time = 10s; λ_{ex} = 532 nm)

Table 4.3: Frequency of the carboxylate stretch and the ring stretches for each metal ion

Metal Ion	**Frequency of the carboxylate stretch (cm^{-1})**	**Frequency of the ring breathing stretches (cm^{-1})**	
Cr(III)	1387	1070.5	1580
Pb(II)	1391	1074.5	1579.5
Cd(II)	1401.5	1074	1583
Ni(II)	1394.5	1074	1583
Cu(II)	1394.5	1070.5	1583
Zn(II)	1402	1070.5	1583
Mn(II)	1413	1074.5	1583

It can be seen from the enlargement of the carboxylate stretch that this band shifts in frequency, and also changes shape, depending on which metal ion is present. There are a number of factors that can affect the frequency of bands in the spectra of metal

complexes, including oxidation number, coordination number, bond strength and mass of metal atom.[80] As a result, the shifts do not seem to follow any particular trend.

It can be seen from Table 4.3 that the carboxylate stretch for Zn(II) and Cd(II) occur at the same frequency for both metal ions (1402 cm^{-1}) and therefore these two species cannot be confidently distinguished. The carboxylate stretch for Ni(II) and Cu(II) also show frequency shifts of the same magnitude, occurring at 1394 cm^{-1}. However it can be seen from Figure 4.5, that the shape of the bands differ with Ni(II) showing a much broader peak than Cu(II). This could potentially be used to help discriminate between these two ions. Cr(III), Pb(II) and Mn(II) all have unique frequencies for the carboxylate stretch, occurring at 1387, 1391 and 1413 cm^{-1}, respectively. However, it should be noted that this stretch occurs at similar frequencies for certain metal ions e.g. Pb(II) and Cr(III) only differ by 4 cm^{-1}. As a result, using this single band is not enough to definitively identify each metal ion.

4.2.3 PCA

As some of the metal ions produced very similar frequencies for the carboxylate stretch, principal component analysis (PCA) was used to evaluate the possibility of differentiating the various metal ions. PCA is used to describe a dataset by reducing the dimensionality, while still retaining most of the variation within the dataset.[81] The first principal component (PC1) describes the maximum variation in the dataset and therefore contains the most information. Subsequent PCs contain less information in decreasing order and therefore, only the first few PCs are generally used to describe the variation in the dataset.[81]

Instead of using the variation of the carboxylate stretch to discriminate between the different species, PCA can be used to pick out differences throughout the entire spectral range studied. The scores plot of PC1 vs. PC2 is shown in Figure 4.6, which was obtained using the normalised spectra from all metal ions, using three replicates of three different concentrations (100, 75 and 50 ppm). The scores plot represents relationships between the different samples. Samples that group close together are said to be of similar

variability and therefore contain the same spectroscopic features, while those that are separated are said to be spectrally different to the other samples.

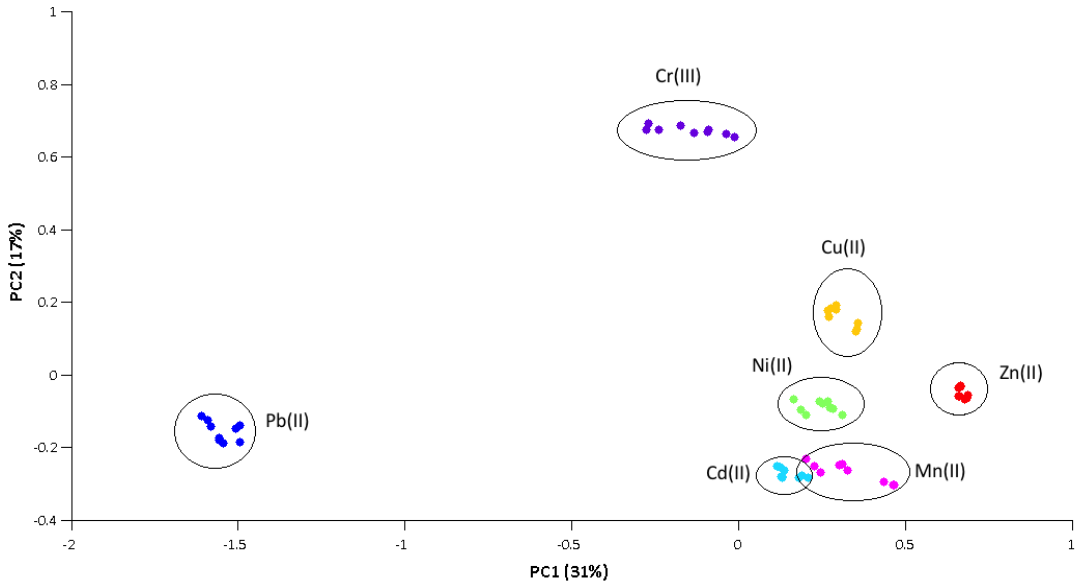

Figure 4.6: PCA scores plot of the different metal ions added to 4-MBA-functionalised AgNPs

From this plot, it can be seen that Pb(II) and Cr(III) are well-separated from the other metal ions tested, demonstrating that the SERS spectra of these ions show the most variation. Although the other metal ions are grouped relatively close together, they each form their own separate clusters, suggesting there is subtle differences between the spectra of these metal ions. However, it is evident that the groupings are very close together, potentially causing uncertainty over the identity of the metal ion present. As a result, a second scores plot was obtained by plotting PC2 vs. PC3, which is shown in Figure 4.7.

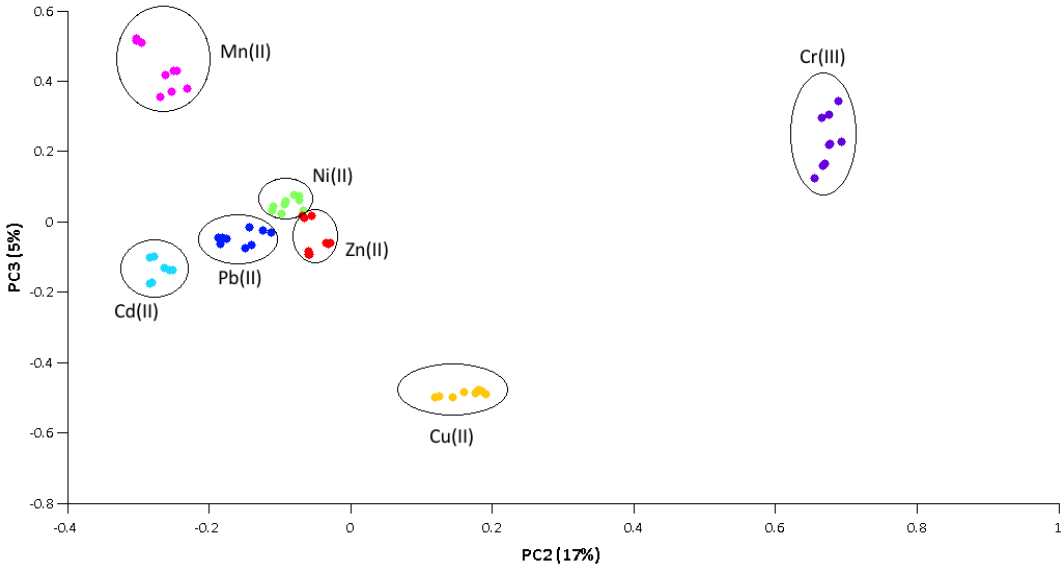

Figure 4.7: Scores plot of PC2 vs. PC3

Noticeably, Cu(II) and Mn(II) now form well-separated clusters which can be used to help distinguish these metal ions. The other species again form groupings that are close together, however, examination of both scores plots can aid the discrimination of the different metal ions.

Not only can PCA show the relationship between different samples, loadings plots can also be used to determine the source of variability between samples. The loadings plot for PC1 is shown in Figure 4.8.

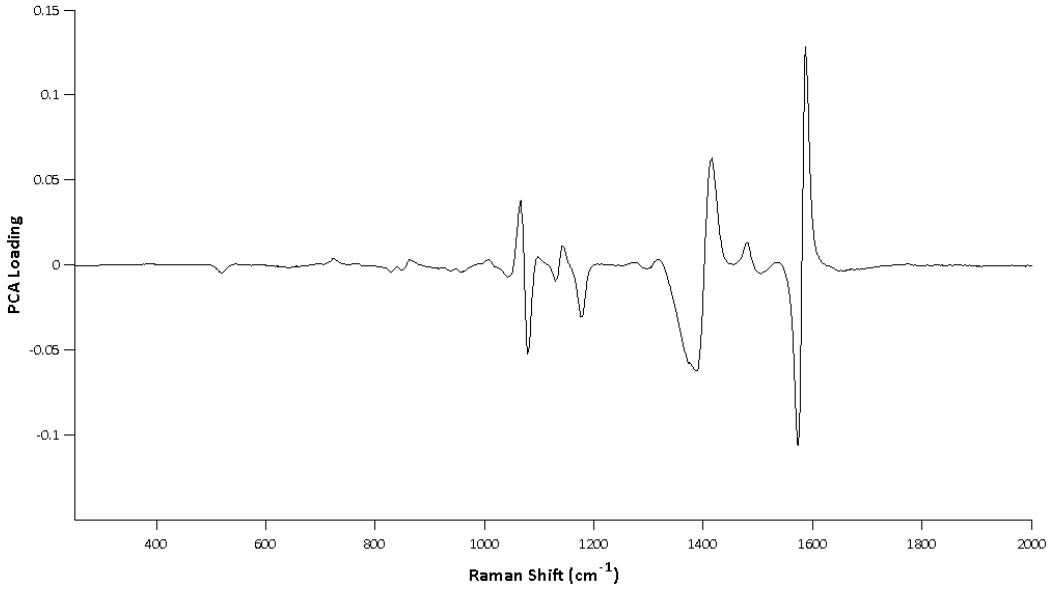

Figure 4.8: PC1 loading showing the sources of spectral variation

Three main negative peaks (at 1078, 1391 and 1574 cm^{-1}) and three main positive peaks (at 1066, 1416 and 1587 cm^{-1}) can be observed in the loadings plot. Therefore, these are the wavenumbers where the majority of variation occurs and they relate to the two ring stretches and the carboxylate stretch.

From the scores plot in Figure 4.6, it can be seen that Pb(II) has the most negative PC1 value. As a result, this ion will contain most of the features associated with the negative bands in the loadings plot. Returning to Table 4.3, it can be seen that Pb(II) does in fact contain a slightly higher frequency value for the first ring breathing stretch, and a lower frequency for the second. The COO^- stretch also occurs at 1391 cm^{-1} as the loadings plot suggests. The other metal ions have an intermediate value on the PC1 axis and therefore, does not strongly associate with either of the positive or negative loadings. The same process can be used to identify the source of variation along PC2 and PC3, and these loadings plots can be found in Appendices I and II.

As separate groupings were observed in the PCA plots, LOD studies were attempted in order to determine the sensitivity of this method. However, it was found that the frequency shifts of the carboxylate stretch were not consistent after addition of metal ions at lower concentrations. Also, due to the frequency shifts for a number of the metal

ions being quite close, uncertainty over the identity of the metal ion becomes evident, reducing the discriminatory potential of 4-MBA. Clearly this is not ideal for metal ion detection and therefore, work was discontinued with this ligand over the lack of reproducibility at lower concentrations.

4.3 4-MPY

4-MPY, like 4-MBA, is a strong Raman reporter that binds to nanoparticles via the thiol group leaving the pyridine nitrogen atoms free to bind to metal ions, as shown in Figure 4.9. Subsequently, a similar approach was used to determine the capability of 4-MPY to discriminate between different metal ions.

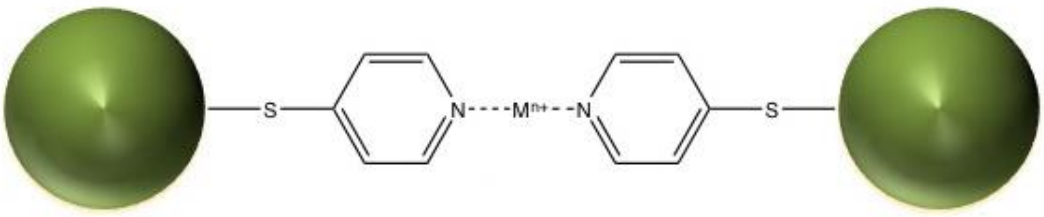

Figure 4.9: Graphical representation of 4-MPY-functionalised AgNPs and the aggregation induced by the addition of metal ions

4.3.1 Concentration Study

Firstly, a concentration study was again conducted in order to determine the concentration of 4-MPY required to produce monolayer coverage of the nanoparticles. This was achieved by adding different concentrations (250 – 0.25 µM) of 4-MPY to the nanoparticle dispersion and aggregating with salt. The results of this are displayed in Figure 4.10.

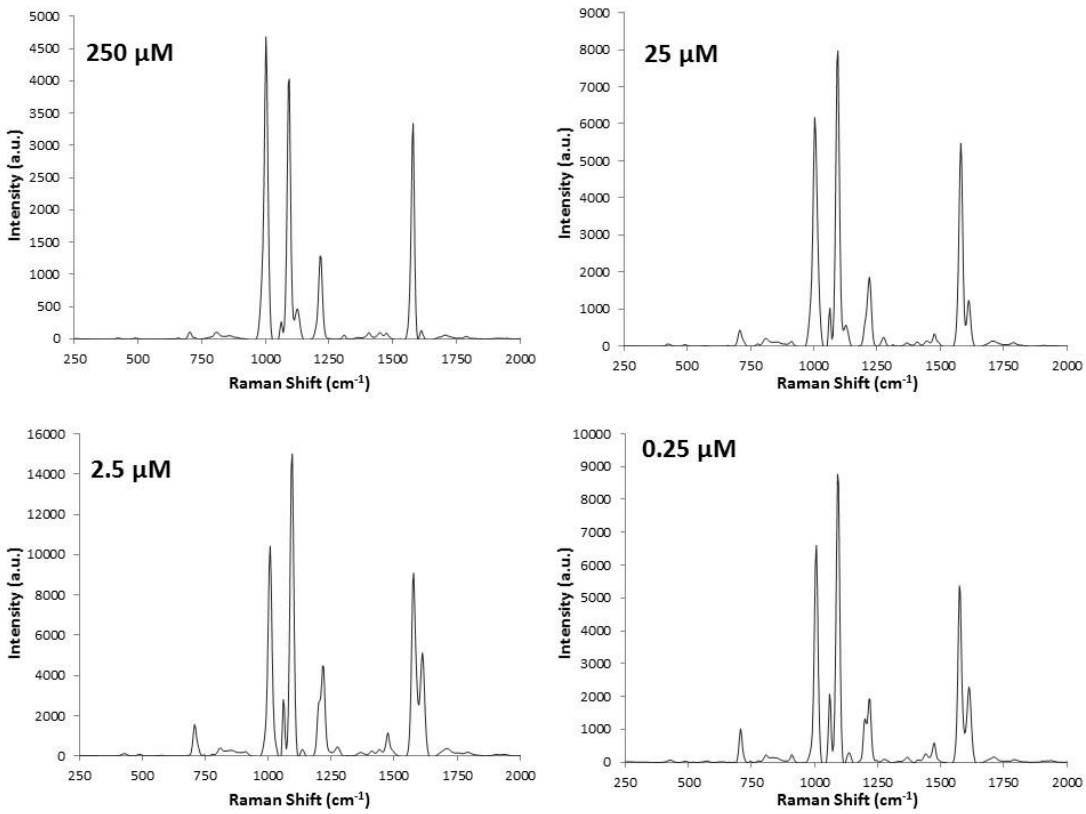

Figure 4.10: SERS spectra resulting from AgNPs functionalised with varying concentrations of 4-MPY. Top left: 250 µM; top right: 25 µM; bottom left: 2.5 µM; bottom right: 0.25 µM (λ_{ex} = 532 nm, acc. time = 10s)

At higher concentrations (250 and 25 µM) packing at the nanoparticle surface occurs which results in a decreased signal. It can be seen that a concentration of 2.5 µM was again ideal as this concentration provided the most intense SERS signal, signifying that this concentration provides monolayer coverage of the nanoparticles. The SERS intensity decreases below this concentration suggesting that not enough of the ligand is present to fully cover the surface of the nanoparticles. As a result, a 4-MPY concentration of 2.5 µM was used throughout this work and the SERS assignments of 4-MPY are listed in Table 4.4.

Table 4.4: Frequencies and assignments of the bands produced in the SERS spectrum of 4-MPY[82, 83]

Raman Shift (cm^{-1})	Assignment
706 (w)	Out-of-plane C-H deformation
1006.5 (s)	Ring breathing
1058.5 (m)	In-plane C-H deformation
1094 (vs)	Ring breathing/C-S stretch
1133.5 (w)	C-H deformation
1215 (m)	In-plane C-H deformation
1275.5 (w)	In-plane C-H deformation
1365 (vw)	C-C stretch
1409 (vw)	Ring stretch
1441.5 (vw)	Ring Stretch
1474 (w)	Ring stretch
1576 (s)	Ring stretch with N
1611 (m)	Ring stretch with N

4.3.2 Addition of Metal Ions to 4-MPY- Functionalised AgNPs

To evaluate the interaction of the surface-bound 4-MPY with different metal ions, the Ag-MPY conjugates were mixed with different metal ion solutions and the SERS spectra obtained. The resulting spectra from each of the metal ions are compared in Figure 4.11. The spectral range is reduced in order to emphasise the frequency shifts however, the full range spectra can be found in Appendix III.

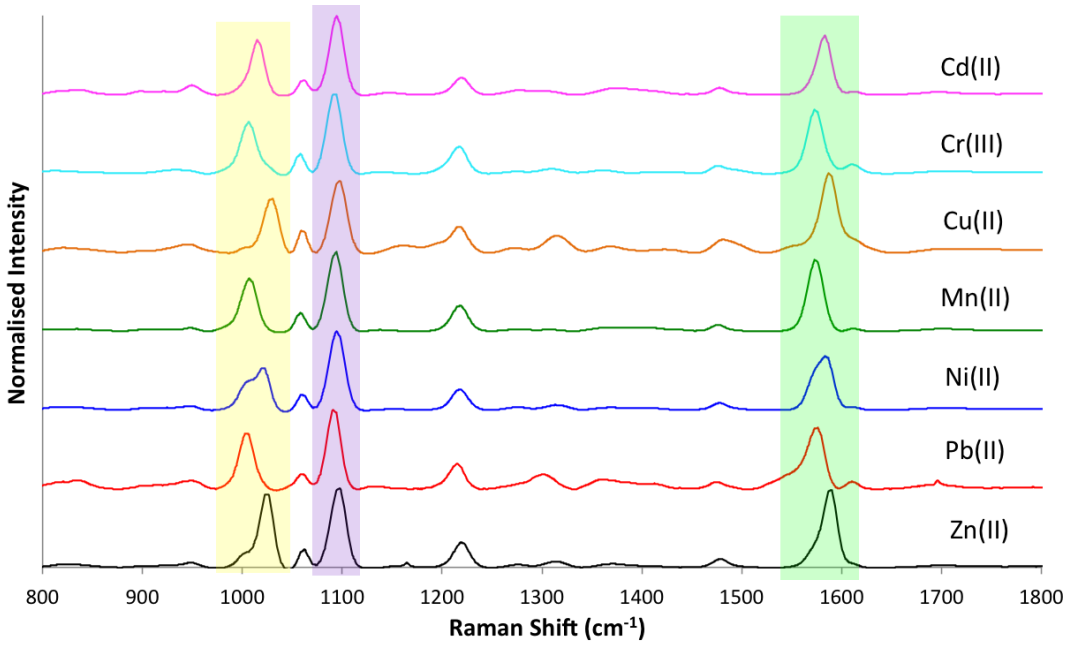

Figure 4.11: Comparison of the SERS spectra obtained from 4-MPY-functionalised AgNPs after the addition of different metal ions. Zn(II), black; Pb(II), red; Ni(II), blue; Mn(II), green; Cu(II), orange; Cr(III), cyan; Cd(II), pink (λ_{ex} = 532 nm, acc. time = 10s)

For 4-MPY, three strong bands can be observed at approximately 1007, 1094 and 1576 cm^{-1}, with the former two stretches relating to ring breathing modes and the latter a ring stretch. These are the bands that shift upon coordination of metal ions. As the ring breathing mode (highlighted in the purple box) demonstrated larger and more unique shifts for each metal ion, this was the main marker band used for the identification of metal ions. The other two bands also demonstrated frequency shifts, although these were less characteristic of each metal ion. Nevertheless, they could still be used to support the identity of the coordinating metal ion. The frequency shifts of these three peaks for all metal ions are listed in Table 4.5.

Table 4.5: Frequencies of the ring vibrations observed for each metal ion

Metal Ion	Frequency of Ring Breathing Stretches (cm^{-1})		Frequency of Ring Stretch with N (cm^{-1})
Cd(II)	1014.5	1094	1583
Cu(II)	1030.5	1097.5	1587
Cr(III)	1006.5	1090.5	1573
Mn(II)	1006.5	1094	1573
Ni(II)	1022	1094.5	1583.5
Pb(II)	1002.5	1090.5	1576
Zn(II)	1026	1098	1590

These frequency shifts arise from the different metal ions binding to the lone pair of electrons on the nitrogen atom of the pyridine ring. This will therefore change the electron density in the ring and hence the polarizability of the aromatic group, which results in changes to the frequency of these bands. Again, no trend could be deciphered from the frequency shifts, suggesting that a number of factors influence these shifts. The shifts also do not seem to be related to those observed for 4-MBA, likely due to pyridine being a softer Lewis base than carboxylate and consequently, the metal ions will have different affinities for the different ligands.

From Table 4.5, it can be seen that Cr(III) and Mn(II) have the same frequency for the first ring breathing stretch, highlighted in the yellow box (1006.5 cm^{-1}), which could possibly be due to both metal ions being hard Lewis acids.[84] This peak also occurs at the same frequency as seen in the concentration study, where the 4-MPY functionalised AgNPs were aggregated with NaCl. This suggests that these metal ions do not strongly coordinate to 4-MPY and therefore do not have a large effect on the polarizability of the aromatic ring. For the other metal ions, the frequency of the ring stretch shifts by different values allowing them to be discriminated from one another.

The second ring breathing stretch (purple box) and the ring stretch with nitrogen (blue box) also show variations depending on which metal ion is coordinated. However, as can be observed in Table 4.5, a number of metal ions have the same frequency, or very similar

frequencies. As a result, these bands alone cannot be used to distinguish between the metal ions; instead they were used to support the identification of the different species.

4.3.3 PCA

As changes could be observed between the SERS spectra of the different metal ions, PCA was once again used to reduce the dimensionality and highlight the relationships between the samples. This was achieved using the normalised SERS spectra of all metal ions. Three replicates of five different concentrations (150 – 70 ppm) are represented in the PCA scores plot shown in Figure 4.12.

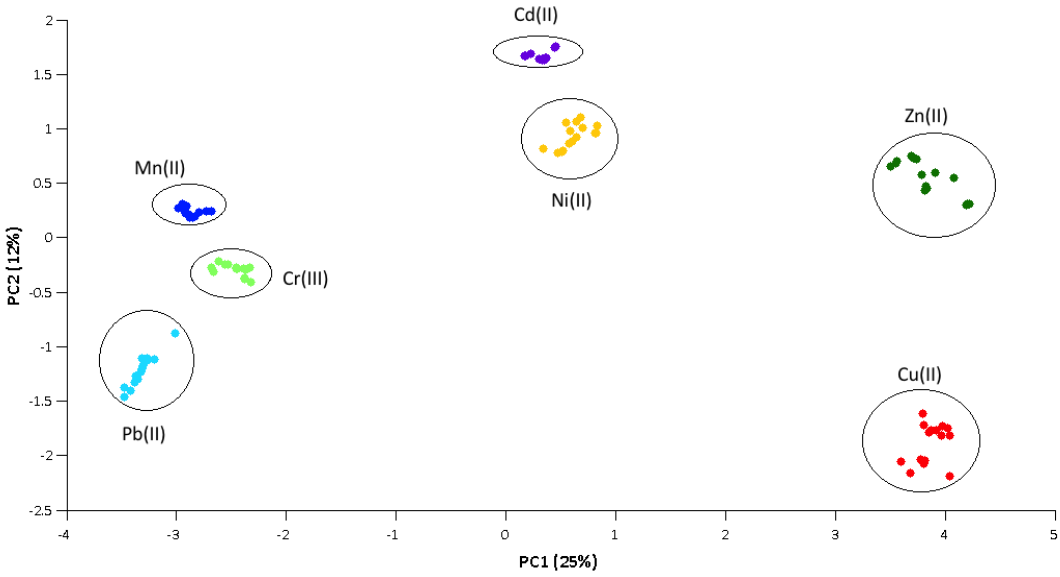

Figure 4.12: PCA scores plot of the seven metal ions analysed. Cd(II), purple; Ni(II), yellow; Zn(II), dark green; Cu(II), red; Mn(II), dark blue; Cr(III), light green; Pb(II), light blue

It can be seen from the scores plot that the metal ions are well-separated, demonstrating that the PCs clearly represent the variance between the different samples. Again, loadings can be used to provide a further insight into the source of spectral variability. The loadings plot for PC1 is shown in Figure 4.13.

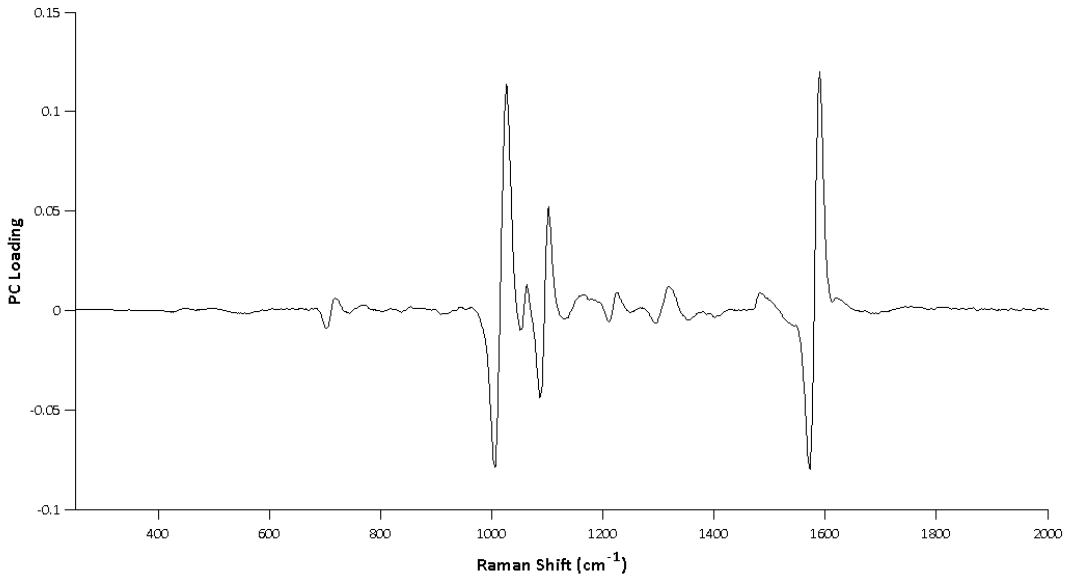

Figure 4.13: Loadings plot associated with PC1

The loadings plot shows a strong positive band at 1026 cm^{-1} and a second strong negative band at 1006 cm^{-1}, which relates to the ring breathing vibration. As a result, metal ions that induce a frequency shift to higher values are expected to have a positive value for PC1, while those metal ions that have a low frequency for this vibration should have a negative value. Returning to Table 4.5 and the scores plot, it can be seen that this is true. Cu(II) and Zn(II) have the highest shifts at 1030 and 1026 cm^{-1}, respectively and lie at the most positive values on PC1. Pb(II), Cr(III) and Mn(II) all have the lowest frequencies and therefore appear at negative values on PC1. Cd(II) and Ni(II) have intermediary shifts of 1014 and 1022 cm^{-1}, respectively and therefore lie between these groupings.

Two other strong bands related to the ring stretch with nitrogen can also be observed in the loadings plot at 1576 cm^{-1} (negative) and 1590 cm^{-1} (positive). Again, it can be seen from Table 4.5 that Cu(II) and Zn(II) also show the largest frequency values for this stretch, occurring at 1587 and 1590 cm^{-1}, respectively. Pb(II), Cr(III) and Mn(II) again have the smallest frequency values (between 1573 and 1576 cm^{-1}). PCA has therefore confirmed that the ring stretches show the most variation in the SERS spectrum of 4-MPY and can be used to discriminate between the different metal ions. The loadings plot for PC2 can be found in Appendix IV.

4.3.4 Concentration Dependence Studies

The concentrations used for the initial study were very high compared to the levels of heavy metals usually found in the environment. As a result, detection limit studies were conducted for each metal ion in order to determine the sensitivity of this approach, and whether it would be practicable for environmental monitoring. The concentration relationships obtained for each metal ion are shown in Figure 4.14, and these were obtained by plotting the intensity of the ring breathing stretch against concentration. The calculated detection limits are listed in Table 4.6 and compared to the recommended WHO guidelines for drinking water.

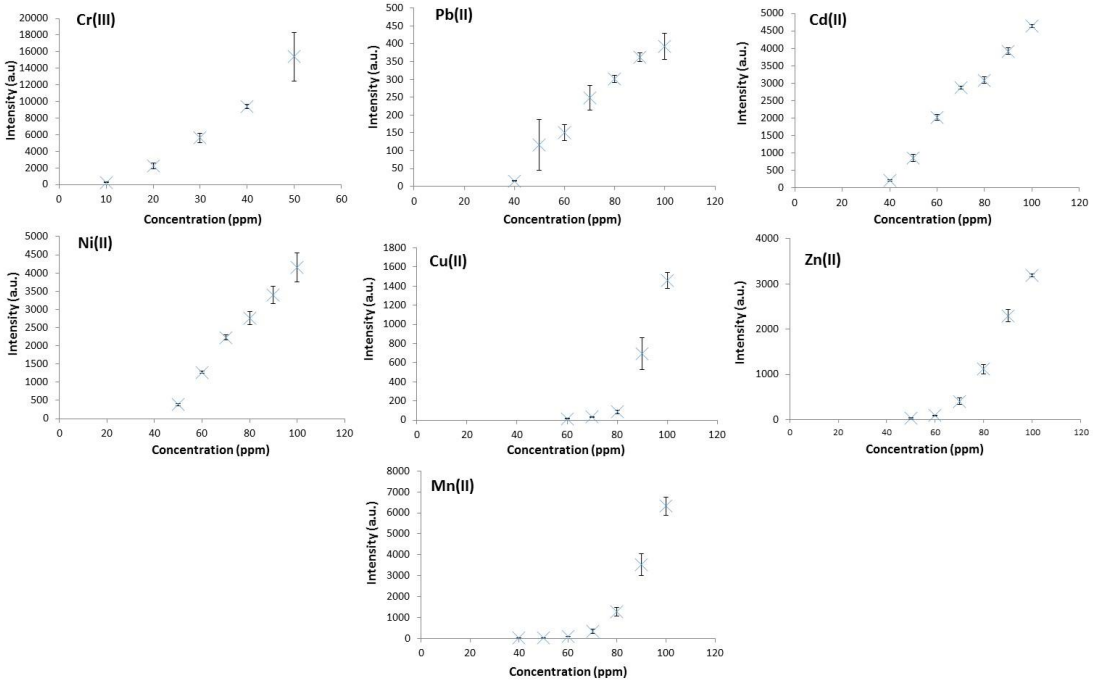

Figure 4.14: Concentration relationships obtained for each metal ion. Top row from left to right: Cd(II) ($I_{1014.5}$ vs. conc.); Cu(II) ($I_{1030.5}$ vs. conc.); Cr(III) ($I_{1006.5}$ vs. conc.). Middle row from left to right: Mn(II) ($I_{1006.5}$ vs. conc.); Ni(II) (I_{1022} vs. conc.); Pb(II) ($I_{1002.5}$ vs. conc.). Bottom row: Zn(II) (I_{1026} vs. conc.). Error bars represent the standard deviation between three replicates (λ_{ex} = 532 nm, acc. time = 10s)

Table 4.6: Detection limits calculated for the seven metal ions tested and compared to the recommended WHO limits in drinking water. Errors associated with the detection limits were obtained by multiplying the %RSD by the detection limit

Metal Ion	Detection Limit (ppm)	WHO Recommended Limit in Drinking Water (ppm)
Cd(II)	40 ± 1.1	0.003
Cu(II)	60 ± 7.2	2
Cr(III)	10 ± 1.3	0.05
Mn(II)	40 ± 4.4	0.5
Ni(II)	50 ± 3.4	0.02
Pb(II)	40 ± 4.7	0.01
Zn(II)	50 ± 2.6	3

From Table 4.6, it is clear that 4-MPY does not provide the sensitivity required for environmental monitoring, as the detection limits are much greater than the recommended WHO limits. Concentrations below the detection limit did not provide a SERS signal characteristic of 4-MPY as the concentrations were too low to induce the aggregation of the AgNPs. This was corroborated by the extinction spectra obtained for two of the metal ions of interest (Cd(II) and Mn(II)), at three different concentrations; 90, 70 and 20 ppm. These extinction spectra are shown in Figure 4.15.

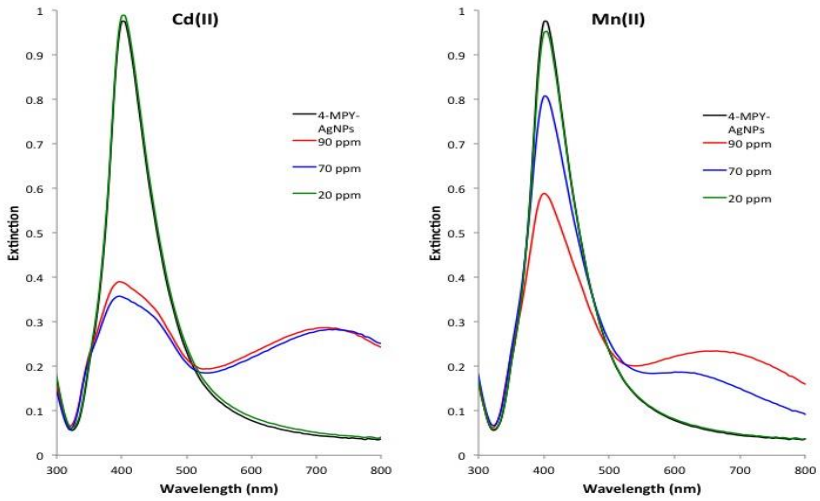

Figure 4.15: Extinction spectra for 4-MPY-AgNPs after addition of three different concentrations of Cd(II) (left) and Mn(II) (right)

It can be seen that, at higher concentrations, aggregation occurs as evidenced by the decrease in intensity of the surface plasmon band, and the emergence of a second band at a longer wavelength. At the lowest concentration however, no change is observed in the extinction profile compared to that of the control (4-MPY functionalised AgNPs only). This therefore demonstrates that the extent of aggregation affects the SERS response obtained and as low concentrations do not induce aggregation, detection of the metal ions cannot be achieved. An attempt was made to overcome this issue by adding a salt solution in order to induce aggregation however, the unique shifts produced by the different metal ions was lost. Due to the lack of sensitivity, this ligand was deemed inadequate for the requirements of environmental monitoring and work was therefore discontinued.

4.4 Chapter Conclusions

In this chapter, AgNPs have been functionalised with the small Raman reporter molecules, 4-MBA and 4-MPY, which were subsequently aggregated by the addition of various metal ions. The SERS spectra obtained showed differences between the different metal ions, and therefore each metal ion could be discriminated based on these unique variations.

The carboxylate stretch was the primary source of variation between the metal ions in the 4-MBA SERS spectrum, however, this stretch was not found to be reproducible at lower concentrations and as a result, this ligand was not considered to be reliable for the discrimination of metal ions.

4-MPY was then tested as a possible ligand for metal ion identification; this time the ring vibrations showed the most variation. The frequency shifts induced by the different metal ions were found to be more pronounced and reproducible than for 4-MBA. Detection limits for each metal ion were subsequently estimated however, these were much greater than the recommended WHO limits in drinking water and as a result, this approach would not be suitable for the environmental monitoring of metal ions.

Although the sensitivity associated with these small reporter molecules were insufficient for environmental monitoring, they did demonstrate that metal ions can uniquely alter the SERS spectra of the ligands, resulting in the discrimination between different metal ions. It was concluded therefore that, although these ligands were unsuitable, SERS has the potential to provide a new route for metal ion detection. It can be concluded from this work that the ligand design is vital for the aims of this project. Therefore, in order to develop a method capable of detecting the analytes of interest at the levels necessary, different ligands would have to be investigated.

5 The “Miracle” of Bipyridyl

As discussed in the previous chapter, ligand selection is crucial for the SERS detection of metal ions. It has been shown that attaching a ligand to the nanoparticle surface and aggregating with metal ions is a possible method of detecting metal ions using SERS. However, this restricts the number of ligands that can be used as Raman reporter molecules as two functional groups are necessary; one to bind to the nanoparticle surface and one to coordinate to the metal ions. As a result, a slightly different approach has been used in this chapter where the metal ions are coordinated to the ligand before adding this complex to the nanoparticle solution.

2,2-bipyridyl (bipy) is a bidentate chelating ligand which forms complexes with various heavy metal ions. In fact, bipy can be used as a colourimetric reagent for the detection of Fe(II) ions as it forms an intense red-coloured complex.[85] It was therefore thought that this could be a useful ligand, as it is capable of complexing to a number of metal ions of interest whilst providing a strong SERS response. It was hypothesised therefore that the coordination of different metal ions would alter the bipy spectrum in a characteristic manner, resulting in the detection of these species. A representation of bipy-metal ion complexes (in the tris form) is shown in Figure 5.1. As there is no functional group for the ligand to bind to the nanoparticle surface, physisorption of the bipy-metal ion complex should occur.

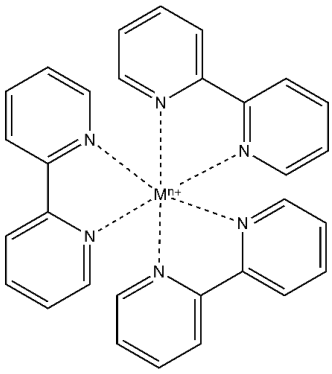

Figure 5.1: Diagram representing the coordination of bipy to metal ions (in the tris form)

5.1 Experimental

5.1.1 Solid Bipy Complexes

Tris(N,N'-bipyridyl)zinc nitrate, Bis(N,N'-bipyridyl) O,O'-nitrato-zinc nitrate and (N,N'-bipyridyl)zinc bromide were prepared by Dr. John Reglinski using reported methods.[86] Raman spectra of these solid complexes were obtained using the WITec Raman instrument (λ_{ex} = 532 nm, 10 s exposure time, 250 – 3000 cm^{-1}).

5.1.2 Concentration Study

25 µL of different bipy concentrations were added to both d.H_2O and a 10 µM Zn(II) solution (25 µL). These were left overnight before adding to 200 µL of AgNPs, aggregating with 10 µL 0.1 M NaCl and acquiring the SERS spectra on the Avalon plate reader (λ_{ex} = 532 nm, 10 s exposure time, 250 – 2000 cm^{-1}, 0.5 cm^{-1} resolution). See Table 5.1 for a summary of the sample preparation procedure.

Table 5.1: Summary of the concentrations used throughout the bipy concentration study

Volume of AgNPs (µL)	Volume of d.H_2O/Zn(II) (µL)	Volume of bipy (µL)	Starting concentration of bipy (µM)	Final concentration of bipy (µM)
200	25	25	500	50
200	25	25	400	40
200	25	25	300	30
200	25	25	200	20

5.1.3 SERS Measurements

A 5 mM stock solution of bipy was prepared by dissolving 3.9 mg in 5 mL methanol. This was then subsequently diluted with water to give a 400 µM solution of bipy. 25 µL of this stock solution was added to 25 µL of different metal ions at the desired concentration

and left overnight to allow complete coordination. They were added to a 96-well plate along with 200 µL AgNPs, which were then aggregated with NaCl and analysed using the Avalon Plate Reader (λ_{ex} = 532 nm, 10 s exposure time, 250 – 2000 cm^{-1}, 0.5 cm^{-1} resolution). The sample preparation procedure is summarised in Table 5.2 using three example concentrations.

Table 5.2: Summary of sample preparation for bipy-metal complexes

Volume of AgNPs (µL)	Volume of bipy (µL)	Volume of metal ion (µL)	Starting concentration of metal ion (µM)	Final concentration of metal ion (µM)
200	25	25	50	5
200	25	25	25	2.5
200	25	25	10	1

5.1.4 1,10-Phenanthroline

A 5 mM stock solution of 1,10-phenanthroline was prepared by dissolving 4.5 mg in 5 mL MeOH, which was subsequently diluted down to 400 µM. 25 µL of this was added to 25 µL of metal ions (50 µM) before leaving overnight to allow complete coordination. The phen complexes were then added to 200 µL of AgNPs in a 96-well plate and aggregated with 10 µL 0.1 M NaCl. SERS spectra were then collected using the Avalon Plate Reader (λ_{ex} = 532 nm, 10 s exposure time, 250 – 2000 cm^{-1}, 0.5 cm^{-1} resolution).

5.2 Investigation of Solid Bipy Complexes

An important consideration when developing methods for metal ion detection using SERS is the different geometries complexes may produce. Bipy for example can form either mono, bis or tris complexes depending on the metal ion and ligand concentration. As SERS is sensitive to geometrical changes, this can affect the spectra produced. Consequently, this could potentially complicate the identification, as only perturbations associated with the different metal ions, and not geometry, are desired in the vibrational

spectrum of the bipy ligand. This has been exhibited using the solid bipy complexes of Zn(II). Each of the Zn(II)-bipy complexes in their mono, bis and tris forms were synthesised and their Raman spectra acquired. These are shown in Figure 5.2, along with the Raman spectrum of solid bipy i.e. the free ligand.

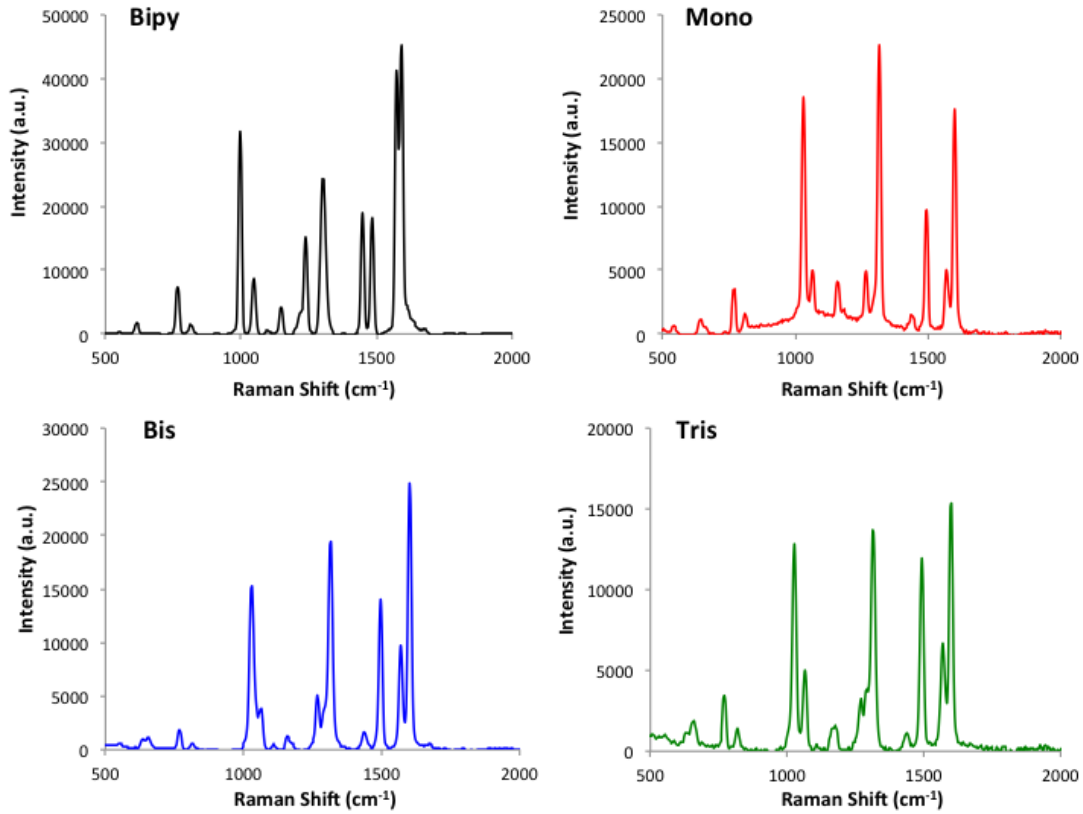

Figure 5.2: Raman spectra of the solid Zn(II)-bipy complexes. Top left, uncomplexed bipy (black); top right, mono (red); bottom left, bis (blue); bottom right, tris (green). (λ_{ex} = 532 nm, acc. time = 10s)

Initial inspection of the spectra indicated slight differences between the three forms, such as changes to the intensity ratios and slight frequency shifts of certain bands. Therefore PCA was used to shed further light on the spectral differences as shown in the scores plot in Figure 5.3.

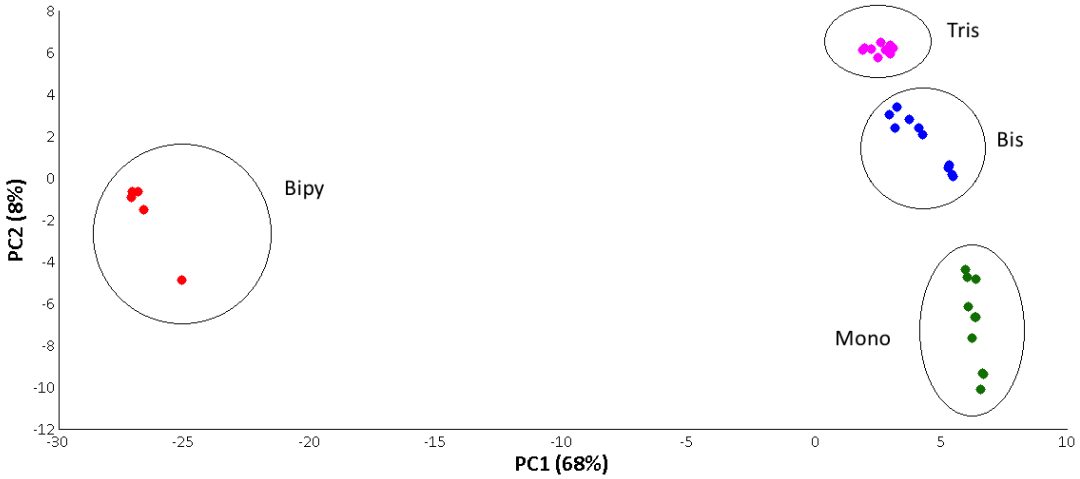

Figure 5.3: PCA scores plot of the solid Zn(II)-bipy complexes. Uncomplexed bipy, red; mono, green; bis, blue; tris, pink.

It should be noted that the Raman spectrum of the solid uncomplexed bipy was also obtained, which is significantly different from the bipy-Zn(II) complexes, illustrating the effect that complexation of metal ions have on the vibrational spectra of certain ligands. The uncomplexed bipy is clearly separated from the metal-bipy complexes along PC1. However, the main point of interest is that each of the three forms are separated along PC2, highlighting the variability between the mono, bis and tris complexes. As a result, the loadings plot for PC2 was subsequently used to establish the origin of spectral variations that give rise to the groupings, and this is shown in Figure 5.4 (the loadings plot for PC1 can be found in Appendix V).

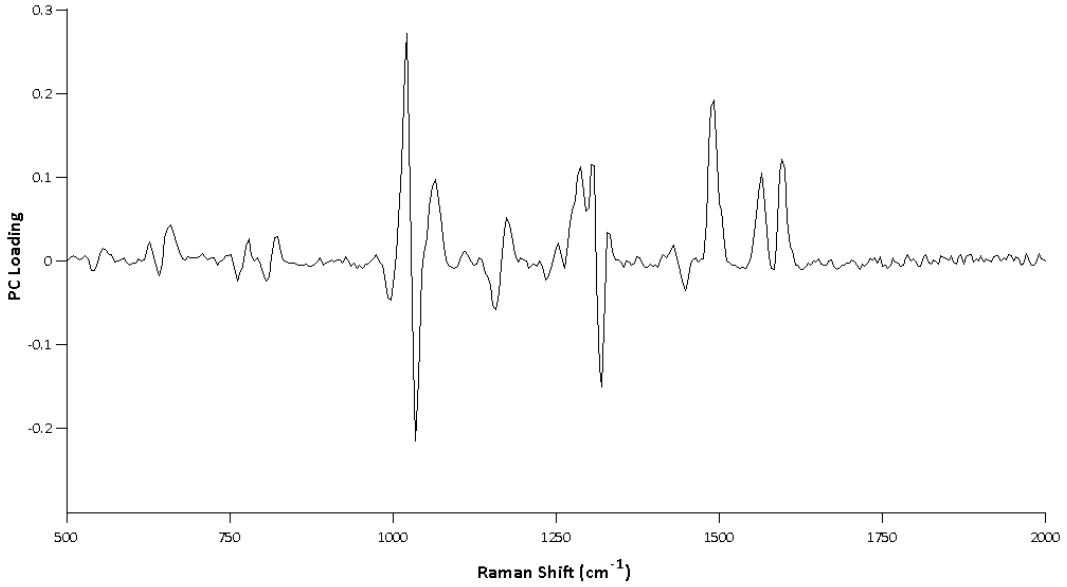

Figure 5.4: PC2 loadings plot illustrating which peaks show the most variation between the different bipy geometries

From the scores plot in Figure 5.3, it can be seen that the tris form has a positive value for PC2, which means that the positive bands in the loadings plot for PC2 are more prominent in the Raman spectrum of the tris complex. As the mono form has a negative value for PC2, negative bands in the loadings plot are therefore more prominent for the mono complex.

From the loadings plot it can be seen that the two strongest bands occur at 1023 cm^{-1} (positive) and 1035 cm^{-1} (negative). From this evidence, it can be expected that the tris complex will have a slightly lower frequency for this band compared to the other complexes. Returning to the Raman spectra, it can be seen that this is accurate, as the band for the tris form occurs at 1027 cm^{-1} compared to the mono and bis forms, where this stretch occurs at 1031 cm^{-1}. Further differences can be observed at the stretch around 1300 cm^{-1}, where the mono and bis forms have identical frequencies with a stretch at 1317 cm^{-1}. However, the tris form shifts slightly in frequency to 1313 cm^{-1}. It is evident that the tris form can be clearly discriminated from the other two geometries whereas the mono and bis forms share very similar features. However these can also be distinguished using the band around 1500 cm^{-1}. For the mono form, this band occurs at 1493 cm^{-1} and for the bis form, 1497 cm^{-1}. This demonstrates the usefulness of the

loadings plot for identifying subtle variations from the spectra of different samples. From the Raman spectra in Figure 5.2, it can also be seen that intensity changes occur in certain bands depending on which form the metal complexes adopt. These changes in frequency and intensity due to the different geometries are not desirable as the aim of this work is to detect metal ions based on the unique changes these species produce in the bipy spectrum. The differences resulting from the three different complex forms could potentially interfere with the identification of the metal ions.

It was therefore hypothesised that one way to overcome this issue would be to use an excess of the bipy ligand, as it has been suggested that the metal complexes would be more likely to exist in the tris state if an excess is present.[87, 88] Consequently, only features from the tris complex would observed in the SERS spectrum of the bipy ligand, which would encourage reproducibility and reliability in the identification of the metal ions.

5.3 Concentration Study

A concentration study was initially conducted in order to determine the excess bipy required to produce the tris complexes. This was achieved by adding increasing concentrations of bipy (20 – 50 μM) to a 10 μM solution of Zn(II) before addition to AgNPs, aggregating with NaCl and acquiring the SERS spectra. Strong SERS signals were obtained for all concentrations studied and therefore, the effect Zn(II) has on the bipy spectrum was used to determine a suitable bipy concentration which produces exclusively the tris forms. It was discovered that the spectra obtained from the higher bipy concentrations are noticeably different to those obtained using lower bipy concentrations. This is shown in Figure 5.5, where the spectra obtained from 50, 40, 30 and 20 μM bipy are compared, along with the spectrum from 40 μM uncomplexed bipy i.e. no Zn(II) solution was added.

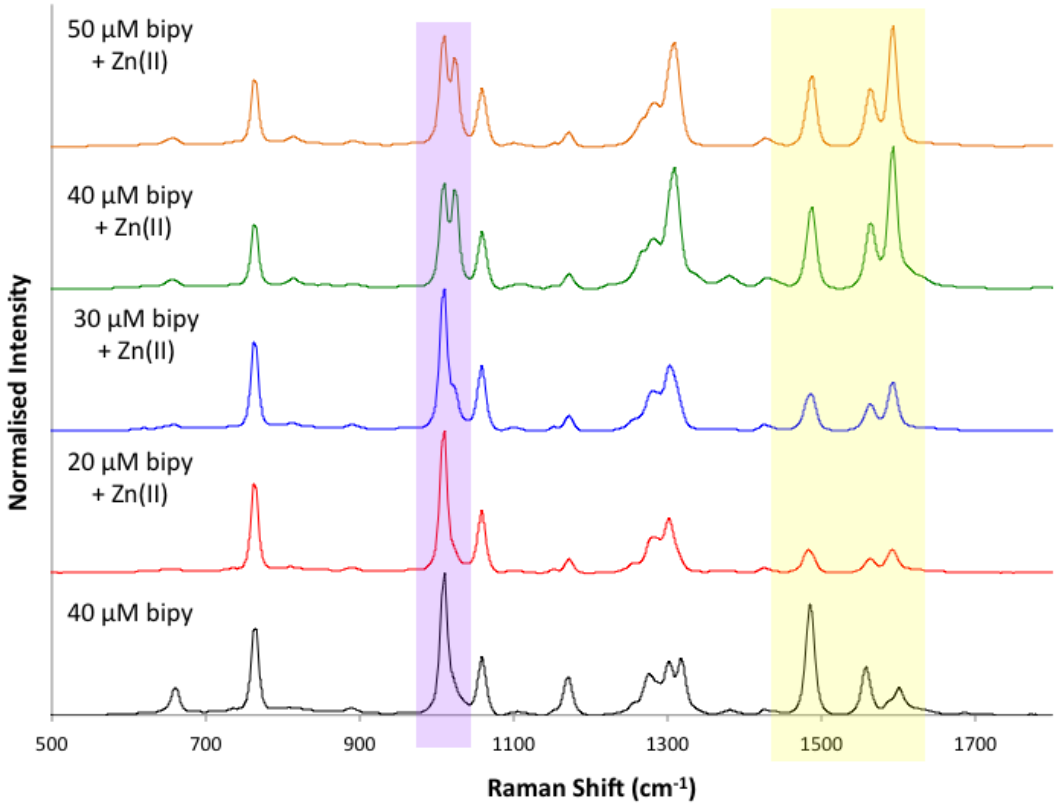

Figure 5.5: Comparison of the SERS spectra of 10 µM Zn(II) added to different concentrations of bipy: 20 µM, red; 30 µM, blue; 40 µM, green; 50 µM, orange. The spectrum of 40 µM uncomplexed bipy is also shown, black. (λ_{ex} = 532 nm, acc. time = 10s)

The two obvious differences are outlined in the purple and yellow boxes. Firstly, at the higher concentrations, it is clear that a second band is present next to the ring breathing mode (highlighted by the purple box). Secondly, there is a large increase in intensity of the aromatic stretches at concentrations above 30 µM (yellow box). At concentrations below 40 µM, the intensity of these bands are greatly diminished, and it is the ring breathing mode at 1010 cm^{-1} which is the most intense band in the spectrum. These differences are likely due to the complexes forming the tris state in excess bipy, as previously postulated, while at decreased concentrations, the mono or bis forms of Zn(II)-bipy are likely produced and hence different spectra are obtained. As the spectra are consistent above 40 µM, it can be established that this is a sufficient concentration to produce the tris forms of the metal-bipy complexes. As a result, a bipy concentration of 40 µM was used throughout this work.

5.4 SERS of Bipy-Metal Complexes

As the free ligand gives strong SERS signals, in order to discriminate between the different metal ions of interest, they must induce changes in the bipy spectrum that are unique to each individual ion. In order to assess this approach, aqueous solutions of six different metal ions, Fe(II), Ni(II), Zn(II), Cu(II), Cd(II) and Cr(III), were combined with the bipy ligand before adding to AgNPs. The AgNPs were aggregated with NaCl and the SERS spectra obtained. A comparison of these SERS spectra is shown in Figure 5.6, and the frequencies of the main bands for all metal ions are listed in Table 5.3, along with their assignments.

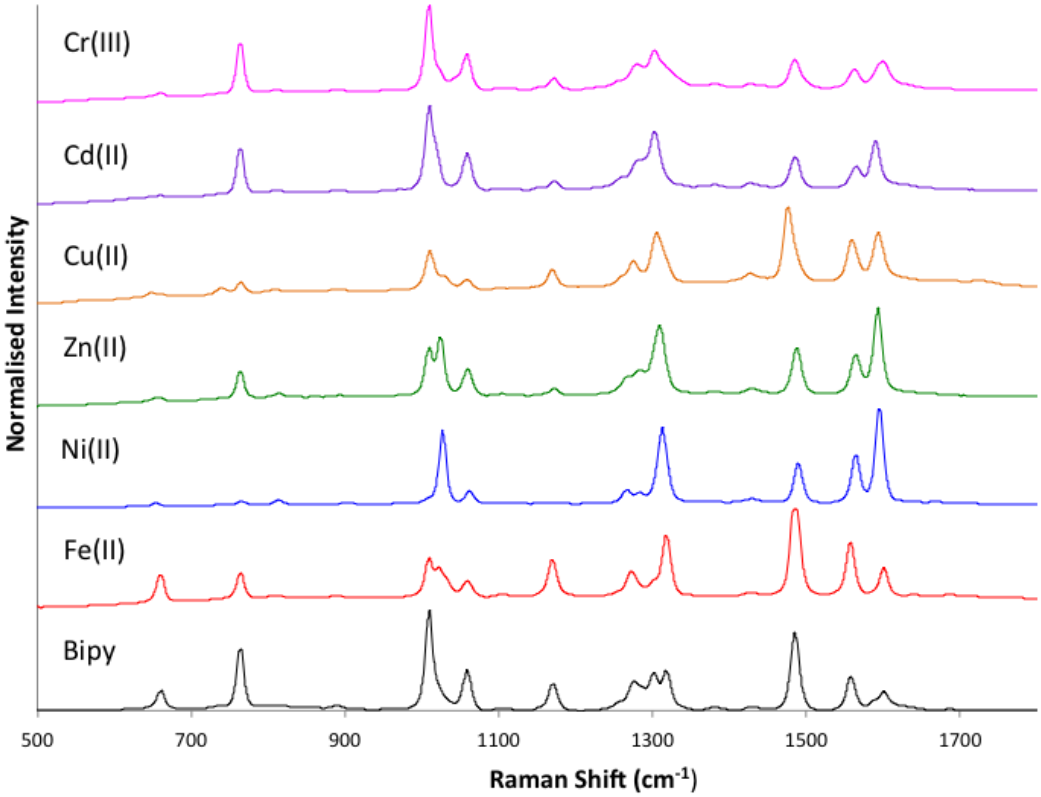

Figure 5.6: Comparison of the SERS spectra of each metal-bipy complex studied. Uncomplexed bipy, black; Fe(II), red; Ni(II), blue; Zn(II), green; Cu(II), orange; Cd(II), purple; Cr(III), pink (λ_{ex} = 532 nm, acc. time = 10s)

Table 5.3: Comparison of the frequencies of the main bands in SERS spectra of each metal-bipy complex, along with their assignments[89, 90]

Frequency (cm^{-1})							Assignment
Free bipy	**Fe(II)**	**Ni(II)**	**Zn(II)**	**Cu(II)**	**Cd(II)**	**Cr(III)**	
1010	1010 (sh. 1022)	1026	1010 1022	1010 (sh. 1030)	1010	1006	Ring breathing
1275	1279	1267	1268	1275		1279 (sh. 1258)	Ring str. C-C, C-N + C-C inter-ring str. + C-H i.p. def.
1302		1283	1283		1302 (sh: 1280, 1262)	1302	C-C inter-ring str. (trans)
1317	1309	1309	1309	1312			C-C inter-ring str. (cis)
1485, 1558, 1600	1488, 1562, 1593	1488, 1565, 1594	1488, 1565, 1593	1474, 1559, 1590	1485, 1565, 1590	1484, 1562, 1600	Aromatic stretches

It can be seen from the comparison of the spectra that each metal ion produces characteristic changes in the bipy spectrum that is unique to each ion. The following sections discuss the frequency shifts and intensity changes observed for each metal-bipy complex.

5.4.1 First Row Transition Metals: Fe(II) to Zn(II)

Fe(II) is known to form a red-coloured complex with bipy and this has an absorption maximum at 522 nm, which is close to the exciting wavelength of 532 nm.[91] Therefore, the excitation frequency is close to that of an electronic transition in this complex and as

a result, resonance Raman scattering is obtained which produces an enhanced SERS spectrum for Fe(II). Although a 4:1 bipy to metal ion ratio was deemed optimal, signal saturation occurred when 10 μM Fe(II) was used and so, a 1 μM Fe(II) concentration had to be used to allow clear comparison with the other metal ions.

From the spectra, it can be seen that the main difference between Fe(II) and Ni(II)/Zn(II) is the ratio of the aromatic stretches (1400 – 1600 cm^{-1}). Binding of metal ions to the bipy nitrogen atoms is expected to profoundly alter the electronic distribution within the heterocycles and thus, these vibrations are strongly perturbed. For Fe(II), the stretch occurring at 1484 cm^{-1} is the most intense band in the spectrum, whereas for Ni(II) and Zn(II), the ring stretch at 1590 cm^{-1} is the strongest band. Therefore, these stretches can be used to immediately discriminate Fe(II) from these two metal ions.

Although the ratio of these aromatic bands are the same for both the uncomplexed bipy and the Fe(II)-bipy complex, the intensity of the aromatic stretches are greatly increased when Fe(II) is present due to the resonance effect and thus, this can be used to help differentiate Fe(II) from the free ligand. It is also evident that the 1484 cm^{-1} stretch is the most intense in the Fe(II)-bipy spectrum, whereas for the uncomplexed ligand, it is the ring breathing mode at 1010 cm^{-1} which is the strongest. These features can therefore be used to aid the identification of Fe(II).

Changes in the bands around 1300 cm^{-1} also occur upon the complexation of metal ions. From the bipy spectrum, two inter-ring stretches can be observed, one thought to be due to the cis conformation of bipy, and the other due to the trans conformation.[90] Upon complexation, it can be seen that the peak corresponding to the cis conformation is greatly enhanced, while the intensity of the trans inter-ring stretch is decreased. As the inter-ring stretches due to the cis and trans conformations are of similar intensity in the spectrum of the free bipy, it is hypothesised that both conformations are present when bipy is uncomplexed however, only the cis conformation will complex to metal ions. This explains why the inter-ring stretch attributed to the cis form is greatly enhanced upon complexation with metal ions, while the band due to the trans form diminishes. However, due to a slight excess of bipy used, some of the ligand molecules will remain

uncomplexed and therefore, a weak trans stretch can still be observed. For Fe(II), this trans band is not apparent in the spectrum, likely due to the resonance effect which greatly increases the intensity of the SERS signal of the Fe(II) complexes. As a result, this region of the spectrum can also be used to support the discrimination of metal ions.

Finally, the ring breathing mode changes dramatically according to which metal ion is present. For Fe(II) and Zn(II), two bands are visible at 1010 and 1022 cm^{-1}, whereas for Ni(II) only one is visible at 1026 cm^{-1}. From Table 5.3, it can be seen that only the Ni(II) ion produces a single band at a higher frequency. However, it has previously been reported that bipy can also adopt a cisoid formation, as well as the cis and trans orientations, which can produce an upwards shift of the ring breathing mode.[89, 90] It is hypothesised therefore, that Ni(II)-bipy complexes predominantly adopt the cisoid orientation, resulting in one band at a higher frequency. The Fe(II) and Zn(II) complexes presumably take up this formation also, but to a lesser extent and hence, bands associated with both the cis and cisoid orientations are present.

5.4.2 Copper

It is a well-known fact that copper complexes are subject to the Jahn-Teller effect, which distorts the geometry of Cu(II) complexes. Consequently, the Cu(II)-bipy complex produced a vastly different spectrum to all other metal ions investigated, as can be seen in the comparison of the SERS spectra in Figure 5.6.

Amongst the most informative of these changes is the aromatic stretch that occurs at 1474 cm^{-1} for the Cu(II)-bipy complex. This band can be used as an immediate indicator for Cu(II) coordination as this band occurs between 1484 and 1488 cm^{-1} for all other metal ions. This relatively large shift of ~10 cm^{-1} is unique to Cu(II) and is likely due to the distortion in geometry as a result of the Jahn-Teller effect. It can also be seen that the ratio of the three aromatic stretches are different in comparison to the other metal ions and therefore, this can also be used to support the identification of Cu(II). Once again, only one ring stretch occurs for this complex at 1312 cm^{-1}, which is likely due to the majority of the bipy ligand existing in the cis conformation after coordination with Cu(II).

Although the ring breathing mode occurs at the same frequency as for the free ligand (1010 cm^{-1}), a slight shoulder is visible at 1026 cm^{-1}, which suggests that, while the majority of the Cu(II)-bipy complexes adopt the cis formation, some are present in the cisoid formation. Evidently, Cu(II) induces strong characteristic changes in the SERS spectrum of the ligand that allows for immediate identification of this metal ion.

5.4.3 Cadmium & Chromium

It has been illustrated that certain first row transition metal ions produce specific changes in the SERS spectrum of bipy upon complexation which can be used to easily differentiate each metal ion. However, it was also discovered that Cr(III), a trivalent ion, and Cd(II), a second row transition metal, also generate unique SERS spectra, again pictured in Figure 5.6.

These two ions do not change the spectrum of bipy as profoundly as the other metal ions previously discussed. For example, it is obvious that the intensity of the aromatic stretches do not increase as drastically as for the first row transition metal ions. This therefore suggests that these metal ions do not interact as strongly with bipy as the spectrum is less perturbed. The SERS spectra of these ions also show similarities to the SERS spectrum of Zn(II) in the presence of lower bipy concentrations, such as the much weaker aromatic stretches (Figure 5.6). Therefore, these ions may not form the tris complex, even in excess bipy; the mono or bis complex could possibly form, which could explain why the spectra of these ions do not change quite as drastically as the other metal ions discussed. However, close inspection of the SERS spectra of the Cd(II)-bipy and Cr(III)-bipy complexes reveals that there are slight variations which can be used to aid the identification of these species.

Firstly, it can be seen from Table 5.3, that Cr(III) induces a slight downwards shift of the ring breathing mode (from 1010 to 1006 cm^{-1}) which can be used to tentatively identify the presence of Cr(III). The region around 1300 cm^{-1} also differs slightly between these species, as it can be seen that Cr(III) has two main bands, one with a slight shoulder, whereas Cd(II) only has one band with two shoulders. This region is also somewhat

altered compared to the uncomplexed bipy spectrum, illustrating that this region can be used to help distinguish these ions from one other, and also from the free ligand. However, the main marker band that can be used to differentiate Cd(II) and Cr(III) is the aromatic stretch which occurs at 1590 cm^{-1} and 1600 cm^{-1}, respectively. This difference of 10 cm^{-1} allows clear differentiation between these two metal ions. It should also be noted that the intensity ratio of these bands vary slightly and so this can also be used to support the discrimination of these species.

5.5 Principal Component Analysis

It has been demonstrated that, by complexing bipy to different metal ions, these ions may be discriminated based on the characteristic changes they produce in the SERS spectrum of the ligand. These differences can be clearly seen by examination of the spectra however, as Cr(III) and Cd(II) do not alter the bipy spectrum to the same extent as the other metal ions, PCA was applied to the dataset in order to provide a clear representation of the variability between the different metal-bipy complexes. The scores plot from this is shown in Figure 5.7, which was obtained using three replicates of each metal ion at a concentration of 10 μM (1 μM was used for Fe(II) due to the stronger SERS signal).

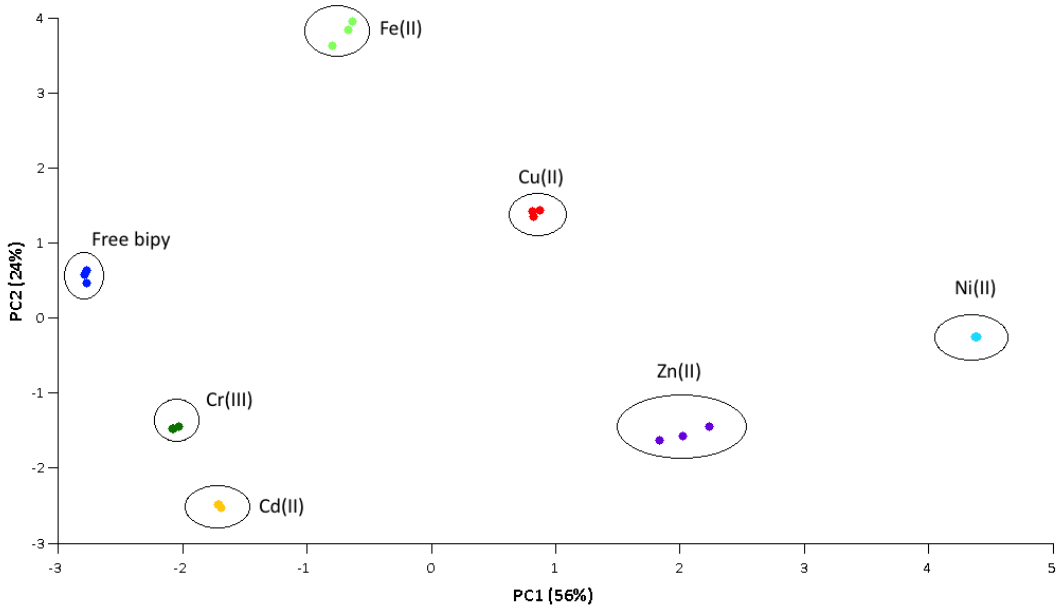

Figure 5.7: PCA scores plot of the different metal-bipy complexes studied. Free bipy, dark blue; Fe(II), light green; Ni(II), light blue; Zn(II), purple; Cu(II), red; Cd(II), yellow; Cr(III), dark green

It can be seen from the scores plot that the different metal ions form well-separated clusters demonstrating that each metal-bipy complex has distinct spectroscopic features that allow them to be unambiguously identified. Cd(II) and Cr(III), which altered the SERS spectrum of bipy less profoundly than the other species, also form separate clusters demonstrating they can also be confidently discriminated. The loadings plots for PC1 and PC2 are shown in Appendices VI and VII, where they demonstrate that the main sources of variation lie in the bands previously discussed.

5.6 Concentration Dependence Studies

As the aim of this research is to develop a system for the detection of heavy metals ions in environmental samples, it was necessary to determine if this ligand provided the sensitivity required for environmental monitoring. To get an idea of whether this ligand is suitable, detection limit studies were conducted for all metal ions. The bipy concentration was kept constant (40 µM) while the metal ion concentration was decreased. The concentration relationships obtained for each metal ion are shown in Figure 5.8 and the detection limits are listed in Table 5.4.

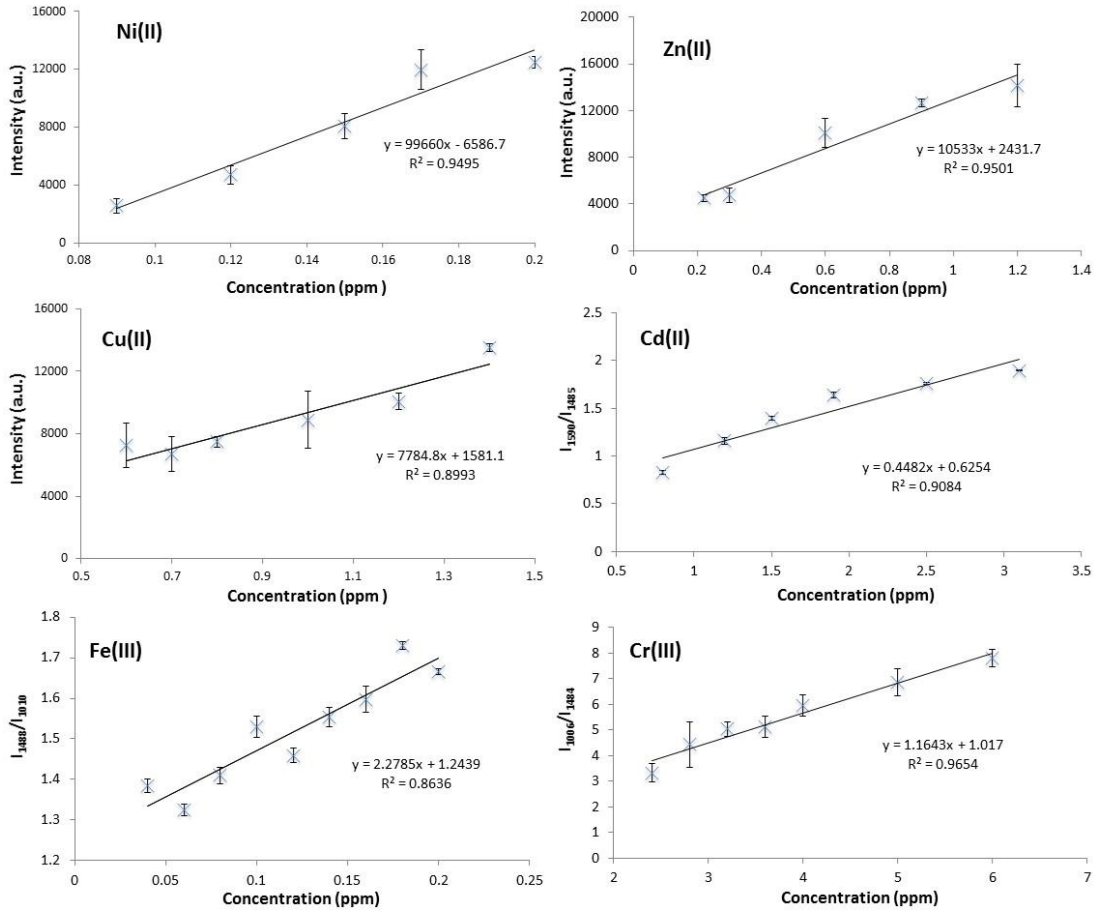

Figure 5.8: Concentration relationships for all metal ions. Ni(II) (I_{1026} vs. conc.), top left; Zn(II) (I_{1022} vs. conc.), top right; Cu(II) (I_{1474} vs. conc.), middle left; Cd(II) (I_{1590}/I_{1485} vs. conc.), middle right; Fe(II) (I_{1488}/I_{1010} vs. conc.), bottom left; Cr(III) (I_{1006}/I_{1484} vs. conc.), bottom left. Error bars represent the standard deviation between three replicates (λ_{ex} = 532 nm, acc. time = 10s)

Table 5.4: Observable detection limits for all metal ions, along with the associated uncertainty. These limits are compared to the WHO's recommended limits in drinking water.

Metal Ion	Observable Detection Limit (ppm)	WHO guideline (ppm)
Ni(II)	0.09 ± 0.009	0.02
Zn(II)	0.22 ± 0.02	3
Cu(II)	0.6 ± 0.06	2
Fe(II)	0.04 ± 0.0005	-
Cd(II)	0.8 ± 0.01	0.003
Cr(III)	2.4 ± 0.2	0.005

The graphs for Ni(II), Zn(II) and Cu(II) were obtained using a band that was discernible by eye and specific to each of these ions (1026, 1022 and 1474 cm^{-1}, respectively). The intensities of these bands were plotted against concentration in ppm, as environmental limits are usually defined using these units. However, as the free bipy ligand also produces a strong SERS signal, observable detection limits were estimated, which was the lowest metal ion concentration that clearly altered the spectrum of bipy in the unique manner that is expected. Below this concentration, the SERS profile of the free ligand dominates and therefore, positive identification of the metal ions was not possible.

Table 5.4 compares the observable detection limits to the WHO's recommended guidelines in drinking water. Errors associated with each detection limit were also calculated by multiplying the %RSD by the observable detection limit. It can be seen from the table that the observable limits for Zn(II) and Cu(II) fall below WHO's guideline at concentrations of 0.22 and 0.6 ppm, respectively, suggesting that this system could be capable of detecting hazardous levels of these metal ions in drinking water. Clearly however, the detection limit for Ni(II) would have to be improved in order to detect this species at the levels necessary, as the concentration this system can detect is more than four times higher than the WHO's recommendation.

For Fe(II), Cd(II) and Cr(III), a slightly different approach was used to determine the lowest observable detection limits. As intensity changes were the most defining feature in the SERS spectra for these ions, the intensity ratio of two peaks were plotted against concentration. The observable detection limits are also displayed in Table 5.4, however, Fe(II) does not have a limit set out by the WHO as Fe(II) salts in drinking water are insoluble and therefore precipitate out as Fe(III) hydroxide.[92] However, it is clear that the limits for Cd(II) and Cr(III) would also have to be vastly improved in order to meet the WHO's guidelines, as currently they are much higher than the recommended levels.

As only two of the metal ions provided detection limits below the target levels, it is evident that further work would have to be undertaken in order to lower these values, such as a pre-concentration step. It was therefore decided that work should be discontinued with bipy in order to concentrate on other ligands that have the potential

to provide more sensitive analysis, without resorting to more complex sample preparation procedures.

5.7 1,10-Phenanthroline

As bipy was capable of discriminating between a number of metal ions, it was decided that 1,10-phenanthroline (phen) should also be studied for comparison, as this compound has a similar structure to bipy, shown in Figure 5.9.

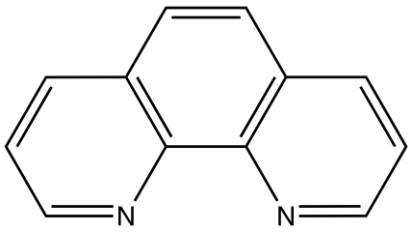

Figure 5.9: Structure of 1,10-phenanthroline (phen)

Phen was studied in the same manner as described for bipy. The SERS spectra of phen complexes, with the same six metal ions studied using bipy, is shown in Figure 5.10 (using 40 µM phen and a 10 µM metal ion solution).

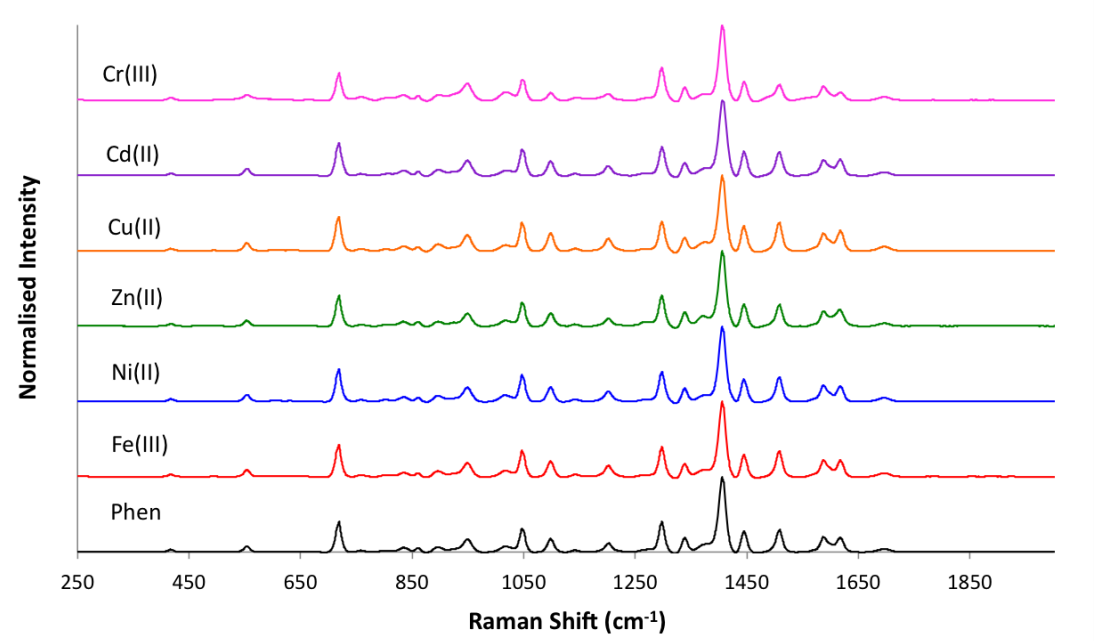

Figure 5.10: SERS response of phen compared to different metal-phen complexes. Phen, black; Fe(III), red; Ni(II), blue; Zn(II), green; Cu(II), orange; Cd(II), purple; Cr(III), pink (λ_{ex} = 532 nm, acc. time = 10s)

It can be seen from the SERS spectra that coordination of metal ions to phen did not appear to alter the SERS spectrum of this ligand. It is hypothesised that this is due to the more rigid structure of phen, as all the aromatic rings are fused together and therefore they are much more constrained. From the comparison of the bipy and phen ligands, it was therefore hypothesised that, for metal ions to inflict changes in the SERS spectra of ligands, flexibility of the ligand structure is required.

5.8 Chapter Conclusions

To conclude this chapter, it has been demonstrated that bipy can potentially be used as a universal ligand to detect a number of heavy metal ions. By complexing the ligand to the metal ions, before adding to AgNPs and acquiring the SERS spectra, it has been shown that a number of metal ions (Fe(II), Ni(II), Zn(II), Cu(II), Cd(II) and Cr(III)) give a unique SERS spectrum. The characteristic changes that are specific to each metal ion may then be used to discriminate between these species. PCA was used to group the results according to the variation in their spectra, and each complex formed distinct clusters demonstrating that they are different from one another. Finally, concentration

dependence studies of all metal ions were conducted to give an idea of the sensitivity of this system. An estimated detection limit of 0.22 ppm was calculated for Zn(II), and 0.6 ppm for Cu(II), both of which are below WHO's recommended levels in drinking water. This suggests that this system may be sensitive enough for the environmental sensing of these ions. However, the detection limits for the other species exceed the recommended levels and therefore, this system cannot be used directly for the reliable detection of these metal ions. For comparison purposes, phen was also studied however, unlike bipy, no unique changes in the SERS spectrum of this ligand was produced by the coordination of different metal ions. It is hypothesised therefore, that in order to impose changes in the spectra of ligands, flexibility of the chelating ligand is required.

Although this system is not as sensitive as other reported methods in the literature, a wide range of metal ions could be discriminated using a single, simple ligand. Variations in a number of bands were observed in the spectra of different metal-bipy complexes, as opposed to subtle shifts in a couple of bands as seen for 4-MBA and 4-MPY in Chapter 4. As a result, bipy appeared to support the hypothesis that chelating ligands produce more pronounced changes in the SERS spectra as opposed to the small Raman reporter molecules.

6 It's All About That (Schiff) Base

It was demonstrated in Chapter 4 that small Raman reporter molecules lacked the sensitivity required; however, in Chapter 5, different bipy-metal complexes were shown to produce a number of changes throughout the SERS spectrum of the ligand. The sensitivity was also vastly improved using bipy and consequently, research continued with the focus on chelating ligands. As Schiff bases are common ligands in coordination chemistry, N,N'-bis(salicylidene)ethylenediamine (salen) was selected as it was thought that the SERS spectrum of this ligand would also be sensitive to metal ion chelation.[93, 94]

Schiff bases were first discovered in 1864 by Hugo Schiff and are derived from the condensation between a carbonyl compound and a primary amine.[95] Schiff bases are essential in the field of coordination chemistry, where they are able to coordinate to most metal ions via the imine nitrogen and another functional group, usually linked to the carbonyl compound.[96] These ligands are therefore very versatile and are used in a wide variety of applications. For example, Schiff base complexes have been used extensively in catalysis due to their high catalytic activity in a number of reactions at high temperature (>100°C), and in the presence of moisture.[97, 98] Their pharmacological properties have also been widely studied, including antiviral, antibacterial and antifungal activity.[99-103] Other applications include uses in the food industry, dye industry and analytical chemistry.[93] Schiff bases have also been used for the quantitative determination of heavy metals as they are excellent chelating agents and so have been exploited for this purpose using both colourimetric and fluorometric methods.[104-108] Recently however, these two techniques have been combined to provide a single sensor for the detection of more than one metal ion.[109, 110] Although UV-Vis and fluorescence are useful techniques, the drawbacks include a lack of sensitivity/selectivity and are liable to interference from other metal ions. The main drawback is the inability to multiplex due to the broad, overlapping signals obtained using these methods.

In this chapter, salen has been used as the ligand of choice and its structure is shown in Figure 6.1. Salen-type ligands are a particular class of Schiff base and are commonly used to describe the [O,N,N,O] tetradentate bis-Schiff base ligands. These are synthesised by

reacting salicylaldehyde (or its derivatives) with 1,2-diamines. This produces a chelating Schiff base with four coordinating sites and two axial sites free to ancillary ligands. As a result, these ligands are similar to porphyrins, however they are much more easily prepared.[96]

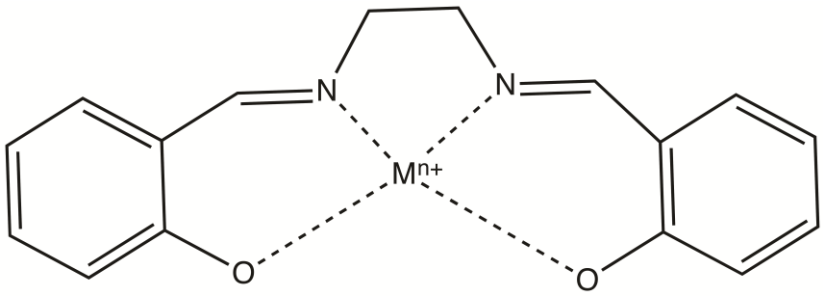

Figure 6.1: Illustration of metal-salen complexes

6.1 Experimental

6.1.1 Concentration Study

25 µL of different salen concentrations (50, 25, 10, 5 µM) were added to both 25 µL of d.H_2O, and a 1 µM Ni(II) solution. These were left overnight before adding to 200 µL AgNPs and aggregating with 10 µL 0.1 M MgBr. Three replicates of each sample were obtained using the Avalon plate reader (λ_{ex} = 532 nm, 10 s exposure time, 250 – 2000 cm^{-1}, 0.5 cm^{-1} resolution). The sample preparation procedure is summarised in Table 6.1.

Table 6.1: Summary of the samples used in the salen concentration study

Volume of AgNPs (µL)	**Volume of d.H_2O/Ni(II) (µL)**	**Volume of salen (µL)**	**Starting concentration of salen (µM)**	**Final concentration of salen (µM)**
200	25	25	500	50
200	25	25	250	25
200	25	25	100	10
200	25	25	50	5

6.1.2 SERS Measurements

A 5 mM stock solution of salen was prepared by dissolving 6.7 mg in 5 mL acetone, which was subsequently diluted to 100 µM. 25 µL of this was added to 25 µL of the metal ion (in d.H_2O), before addition of 200 µL AgNPs and aggregation with 0.1 M MgBr. SERS measurements were obtained using the Avalon Plate Reader reader (λ_{ex} = 532 nm, 10 s exposure time, 250 – 2000 cm^{-1}, 0.5 cm^{-1} resolution).

6.1.3 Synthetic Freshwater

1 L of soft synthetic f.H_2O was prepared according to a EPA recipe, as shown in Table 6.2.[111]

Table 6.2: Preparation of the synthetic f.H_2O according to the EPA

Reagent Added (mg/L)			
$NaHCO_3$	$CaSO_4.2H_2O$	$MgSO_4$	KCl
48	30	30	2

The metal ion stock solutions were then made up, and diluted, using this synthetic f.H_2O. SERS measurements were conducted in the same manner as previously discussed except this time, they were conducted using the portable Snowy Raman spectrometer (λ_{ex} = 532 nm, 10 s exposure time, 250 – 3200 cm^{-1}).

6.1.4 Real Environmental Freshwater

f.H_2O was collected from Loch Thom, Greenock, Scotland. Usually, environmental samples are preserved with a 2% nitric acid solution in order to stabilise the metal ions in solution. However, as nitric acid induces aggregation when added to AgNPs, preservation with nitric acid could not be conducted. As a result, the f.H_2O samples were analysed as soon as possible after collection. It should be noted that an aliquot of the f.H_2O was taken for ICP-MS analysis, and this was preserved in 2% nitric acid.

The detection limit studies were conducted by spiking the f.H_2O with each of the metal ions (Ni(II), Cu(II), Co(II) and Mn(II)) at different concentrations. The SERS spectrum of the unspiked f.H_2O sample was also obtained. These measurements were conducted using the portable Snowy Raman Instrument (λ_{ex} = 532 nm, 10 s exposure time, 250 – 3200 cm^{-1}).

Contaminated water was collected from Gourock burn, Gourock, Scotland which is known to have leachate issues from a nearby landfill site. Again, an aliquot was preserved in 2% nitric acid for ICP-MS analysis, and the SERS analysis was conducted the day after collection on the portable Snowy Raman spectrometer (λ_{ex} = 532 nm, 10 s exposure time, 250 – 3200 cm^{-1}).

6.1.5 Seawater

Natural seawater was bought from Sigma Aldrich and this was spiked with each of the metal ions interest. Again, the metal ion solutions in the seawater were added to salen, before adding to AgNPs. However, no salt was required as aggregation occurred immediately after addition to the AgNPs due to the high salinity of the seawater. SERS analysis was conducted using the Avalon Plate Reader (λ_{ex} = 532 nm, 10 s exposure time, 250 – 2000 cm^{-1}, 0.5 cm^{-1} resolution).

6.1.6 Mixed Metal Ion

12.5 µL of each of the two metal ions (25 µM in d.H_2O) were combined before adding this mixture to 25 µL 100 µM salen. This was left overnight before adding to 200 µL AgNPs and aggregating with 10 µL 0.1M MgBr. The SERS spectra of each salen-mixture were acquired using the Avalon Plate reader (λ_{ex} = 532 nm, 10 s exposure time, 250 – 2000 cm^{-1}). Table 6.3 summarises this sample preparation procedure.

Table 6.3: Summary of the preparation method used for the mixed metal ion SERS analysis

Volume of each metal ion (µL)	Volume of salen (µL)	Starting concentration of each metal ion (µM)	Final concentration of each metal ion (µM)
12.5	25	25	1.25

6.1.7 Salophen

Salophen was synthesised according to the reaction scheme in Figure 6.2.

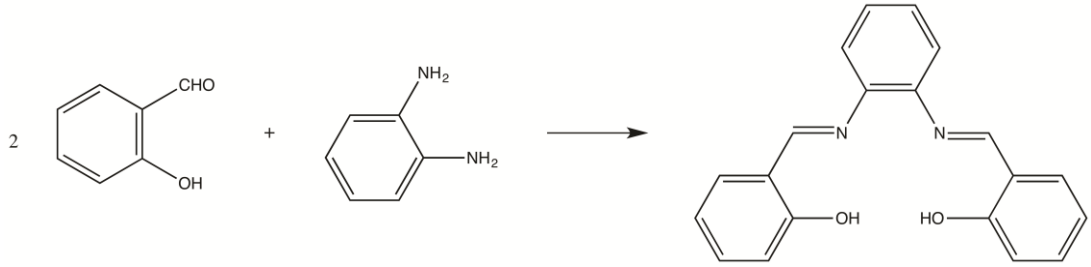

Figure 6.2: Reaction scheme of the salophen synthesis

5 mmol of salicylaldehyde was added to 2.5 mmol of 1,2-phenylenediamine (in 20 mL EtOH). This was then refluxed for 3 – 4 hours to ensure the completion of the reaction. The reaction mixture was then left to cool to room temperature before filtering the precipitate and recrystallizing with EtOH. ^{1}H and ^{13}C NMR was used to characterise the ligand and these are shown in Appendices XX and XXI.

^{1}H NMR (400 MHz, $CDCl_3$): δ11.04 (s, OH), 9.28 (s, HC=N), 7.6 – 6.9 (m, aromatic)

^{13}C NMR (101 MHz, $CDCl_3$): δ163.25, 160.87, 141.97, 136.5, 133.1, 132.18, 127.24, 119.31, 118.60, 116.85

A 5mM stock solution of salophen was prepared by dissolving 7.9 mg in 5 mL acetone, before dilution to 5 µM. 25 µL of this was then added to 25 µL 5 µM of the metal ions. These complexes were left overnight before adding to 200 µL AgNPs in a 96-well plate

with 10 µL 0.1 M MgBr. SERS spectra were obtained using the Avalon Plate Reader (10 s exposure time, 250 – 3000 cm^{-1}, 0.5 cm^{-1} resolution).

6.1.8 SALTSC

A SERS concentration study of SALTSC was conducted by adding varying concentrations of SALTSC to both d.H_2O and a solution of 10 µM Ni(II). The SERS spectra of these samples were collected using the Avalon Plate Reader (10 s exposure time, 250 – 3000 cm^{-1}, 0.5 cm^{-1} resolution) and Table 6.4 summarises the sample preparation.

Table 6.4: Preparation of samples used for the SALTSC concentration study

Volume of AgNPs (µL)	**Volume of d.H_2O/Ni(II) solution (µL)**	**Volume of SALTSC (µL)**	**Starting concentration of SALTSC (µM)**	**Final concentration of SALTSC (µM)**
200	25	25	100	10
200	25	25	75	7.5
200	25	25	50	5
200	25	25	25	2.5
200	25	25	10	1

A 5mM stock solution of SALTSC was prepared by dissolving 4.9 mg in 5 mL acetone. This was diluted to 50 µM before adding 25 µL of this, to 25 µL of the metal ion solutions (25 µM). After leaving overnight, the SALTSC-metal complexes were added to a 96-well plate along with 200 µL of AgNPs, which were subsequently aggregated with 10 µL 0.1 M MgBr. SERS spectra were collected on the Avalon Plate Reader (10 s exposure time, 250 – 3000 cm^{-1}, 0.5 cm^{-1} resolution).

6.2 Salen Concentration Study

In order to determine a suitable concentration of salen required to give the optimal SERS response, a concentration study was conducted. This was achieved by adding 1 µM Ni(II) to varying concentrations of salen. The salen-metal complexes were then added to AgNPs and aggregated with MgBr before collecting the SERS spectra. The SERS spectra of the different salen concentrations with no metal ions added were also obtained for comparison. When no metal ions are present, a weak SERS response is obtained. However, upon the addition of a 1 µM Ni(II) solution, strong SERS signals were observed. This can be seen in Figure 6.3, where the SERS spectrum of salen without background correction is compared to that of the Ni(II)-salen complex.

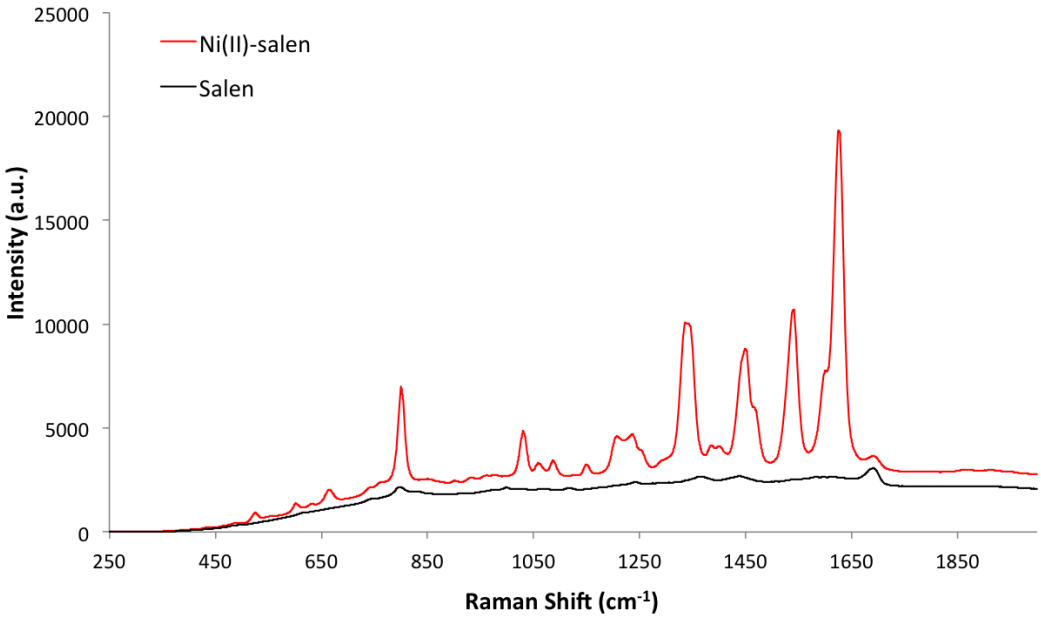

Figure 6.3: Comparison of the SERS spectrum of salen (black) to the spectrum of the Ni(II)-salen complex (red) (λ_{ex} = 532 nm, acc. time = 10s)

A tentative explanation for this substantial increase in the SERS response is thought to be due to "cross-resonance" where π-electrons of the salen and d-electrons of the metal are delocalised in the chelate ring. As a result of this delocalisation, the polarizability of

the metal complex is greater than the ligand itself, resulting in an increase in the SERS response.[112-114]

All concentrations of the uncomplexed salen resulted in the same weak SERS response as observed in Figure 6.3, and therefore, the intensity increase upon coordination of Ni(II) was used to determine the optimal salen concentration. Figure 6.4 shows the background-corrected SERS spectra obtained from adding 1 µM Ni(II) to varying concentrations of salen (50 – 5 µM).

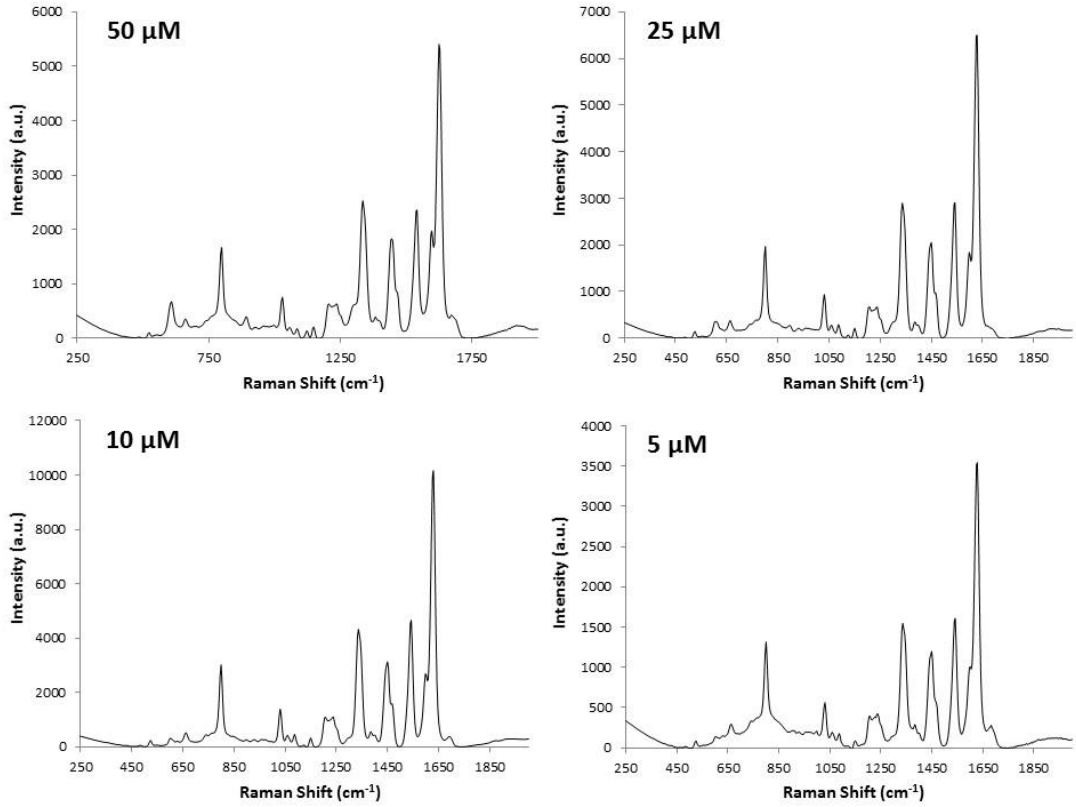

Figure 6.4: SERS spectra from the salen concentration study after addition of 1 µM Ni(II). Top left, 50 µM; top right, 25 µM; bottom left, 10 µM; bottom right, 5 µM (λ_{ex} = 532 nm, acc. time = 10s)

From the spectra, it can be seen that a salen concentration of 10 µM provides the highest SERS intensity compared to the other concentrations. This implies that at higher concentrations of salen (50 and 25 µM), there are too many ligand molecules at the surface of the nanoparticles to produce monolayer coverage, and instead multilayers are

formed, resulting in a decreased SERS response. Below 10 µM, there are too few ligand molecules to provide the monolayer coverage required to give the optimum SERS response, again resulting in a loss in signal. As a result, a salen concentration of 10 µM was deemed optimal and this concentration is used throughout this work.

6.3 The SERS of Salen Complexes

In order to test the SERS response of different salen-metal complexes, a solution of salen (10 µM) was added to different metal ion solutions, which were then left overnight to ensure that complete coordination occurred. A range of metal ions were tested with salen – Co(II), Cu(II), Cr(II), Fe(III), Mn(II), Ni(II), Pb(II) and Zn(II) – however only Co(II), Cu(II), Mn(II) and Ni(II) gave a strong SERS profile (see Appendix VIII for the SERS response of the other ions). Figure 6.5 shows a comparison of the SERS spectrum of the uncomplexed salen ligand to the spectra of salen complexed to 5 µM Ni(II), Co(II), Cu(II) and Mn(II). The frequency and assignments of all bands are listed in Table 6.5.

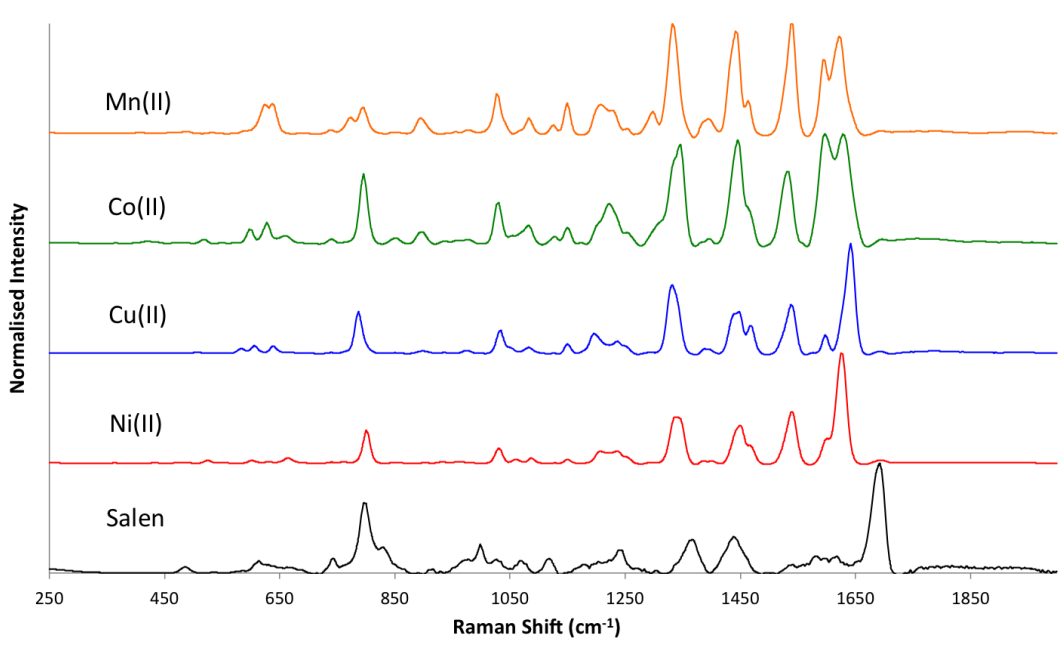

Figure 6.5: Comparison of the SERS spectra obtained from the different salen-metal complexes and the free ligand. Salen, black; Ni(II), red; Cu(II), blue; Co(II), green; Mn(II), orange (λ_{ex} = 532 nm, acc. time = 10s)

Table 6.5: Frequencies and tentative assignments of the bands observed in the spectra of the salen-metal ion complexes[80, 115]

	Ni(II)	Co(II)	Cu(II)	Mn(II)	Assignment
Frequency (cm^{-1})	1627.5 (s)	1628 (s)	1641.5 (s)	1621.5 (s)	RCH=N-R_2 (Schiff bases) + ν(C=C)
	1600.5 (sh)	1597 (s)	1597 (w)	1597 (s)	
	1541 (m)	1531 (m)	1538 (m)	1538 (s)	Aromatic ring stretches
			1467 (m)	1463.5 (m)	
	1449 (m)	1445.5 (s)	1448.5 (m)	1441.5 (s)	
			1387.5 (w)	1394.5 (w)	
	1335.5 (m)	1346.5 (s)	1331.5 (m)	1332 (s)	
				1298 (w)	
	1237.5 (w)	1222.5 (m)	1237.5 (w)	1226.5 (m)	ν(C-C)
	1207.5 (w)		1195.5 (w)	1207 (m)	-$(CH_2)_2$-
	1149 (w)	1149 (w)	1149 (w)	1149 (m)	ν(C-H)
		1129.5 (w)		1125.5 (w)	ν(C-N)/ ν(C-O)/ ν(C-C)
	1086.5 (w)	1082.5 (w)	1082.5 (w)	1082.5 (w)	
	1058.5 (w)				
	1030.5 (w)	1030.5 (m)	1034.5 (m)	1026.5 (m)	Ring breathing
				978 (w)	ν(C-H)
		896 (w)		896 (w)	
		850.5 (w)			
	800 (m)	795.5 (m)	787.5 (m)	795.5 (m)	
				774.5 (w)	
		740.5 (w)		740.5 (w)	
	663 (w)	662 (w)			Metal-ligand vibrations
	632 (w)	627.5 (w)	640.5 (w)	636.5 (m)	
	601 (w)	597 (w)	605.5 (w)		
			583.5 (w)		

From Figure 6.5, it can be seen that each metal ion uniquely alters the spectrum of salen, and these differences can be used to easily distinguish between the different metal ions. The most noticeable change in the spectra occurs at the bands around 1600 cm^{-1}, which are mainly attributed to the C=N stretches of Schiff bases, however the aromatic vibrations will also have an influence on this band. For Ni(II), a strong peak is observed at 1627 cm^{-1} with a shoulder at 1600 cm^{-1}. However, when Cu(II) is complexed to salen, this band shifts to 1641 cm^{-1} with a weak band at 1597 cm^{-1}. For Co(II) and Mn(II), these bands also vary significantly with two strong peaks at 1628 cm^{-1} and 1597 cm^{-1}, and 1621 cm^{-1} and 1597 cm^{-1}, respectively. These differences are due to the metal ions binding to the imine nitrogen atoms of the salen ligand, changing the vibrational properties of these bonds, resulting in frequency shifts of the C=N stretches. These distinct changes can therefore be used to confidently identify which metal ion is coordinated to salen.

Not only are the C=N stretches changed upon coordination, the aromatic bands also differ depending on which metal ion is present. From Table 6.5, it can be seen that an aromatic stretch occurs at 1531 cm^{-1} for Co(II), however for all other ions, this stretch appears between 1538 and 1541 cm^{-1}. This relatively large shift of ~7 cm^{-1} allows this band to be an indicator for the presence of Co(II). The second aromatic stretch occurs at different frequencies for all metal ions: 1449, 1467, 1445 and 1463 cm^{-1} for Ni(II), Cu(II), Co(II) and Mn(II), respectively. The changes in the frequency of the aromatic stretches are due to the coordination of the metal ions to the groups attached to the aromatic rings (the oxygen and nitrogen atoms). Coordination of metal ions causes a change in the electron density and polarizability of the ring groups, and this results in a change to the frequency of these bands. As a result, the aromatic stretches can also be used to confirm the identity of the metal ion coordinated to salen.

It should also be noted that, below 700 cm^{-1}, a number of weak bands are present which arise from metal-ligand vibrations. These are regarded as arising from vibrations of the chelate rings that involve the metal ions.

6.4 PCA

Although the changes produced by the different metal ions are clearly observable from the SERS spectra, PCA was used to highlight the differences, as shown in Figure 6.6. PCA was conducted using 18 samples of each metal ion; three replicates of six different concentrations (2.5, 2, 1.5, 0.75, 0.5 and 0.25 μM). It can be seen from the scores plot that each metal ion forms well-separated clusters, which emphasises the fact that the metal-salen complexes have different spectroscopic features allowing them to be unambiguously identified. Little variation between the different concentrations is also observed, which demonstrates the reproducibility of this technique. The corresponding loadings plots can be found in Appendices IX and X.

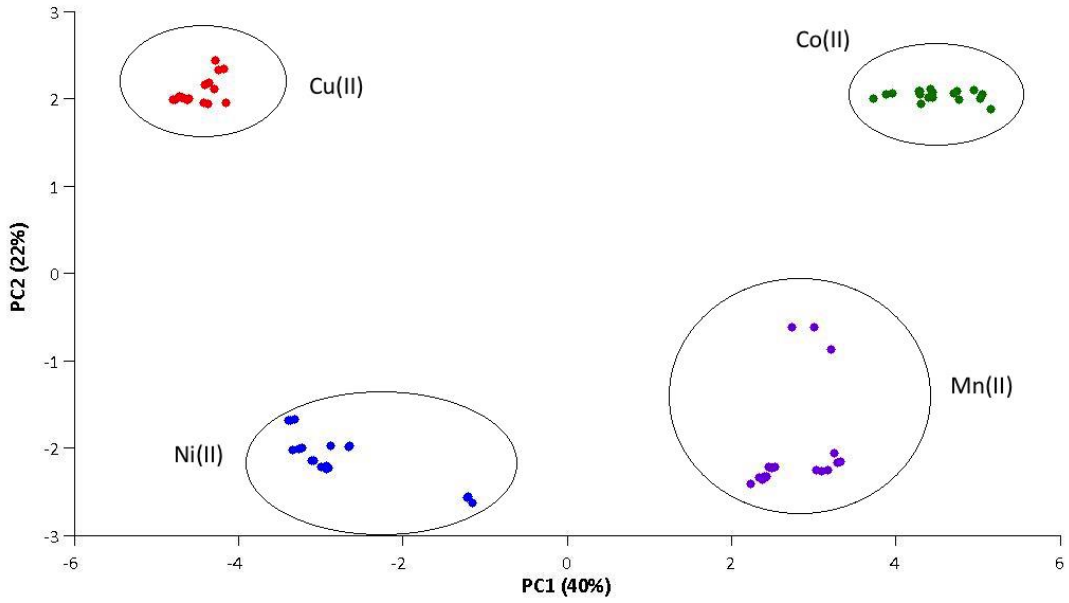

Figure 6.6: PCA scores plot of the four metal ions of interest using three replicates of six different concentrations. Ni(II), blue; Cu(II), red; Co(II), green; Mn(II), purple

6.5 Limits of Detection (d.H_2O)

In order to determine the sensitivity of this method, LOD graphs were obtained for each metal ion, as shown in Figure 6.7. These were obtained by taking the most intense and unique peak for each metal ion, and plotting its intensity against the concentration. The LODs were then calculated by dividing 3x standard deviation of the blank sample (i.e. the

uncomplexed salen) by the gradient of the straight line. Errors associated with each LOD were also calculated by multiplying the %RSD of each sample by the calculated LOD.

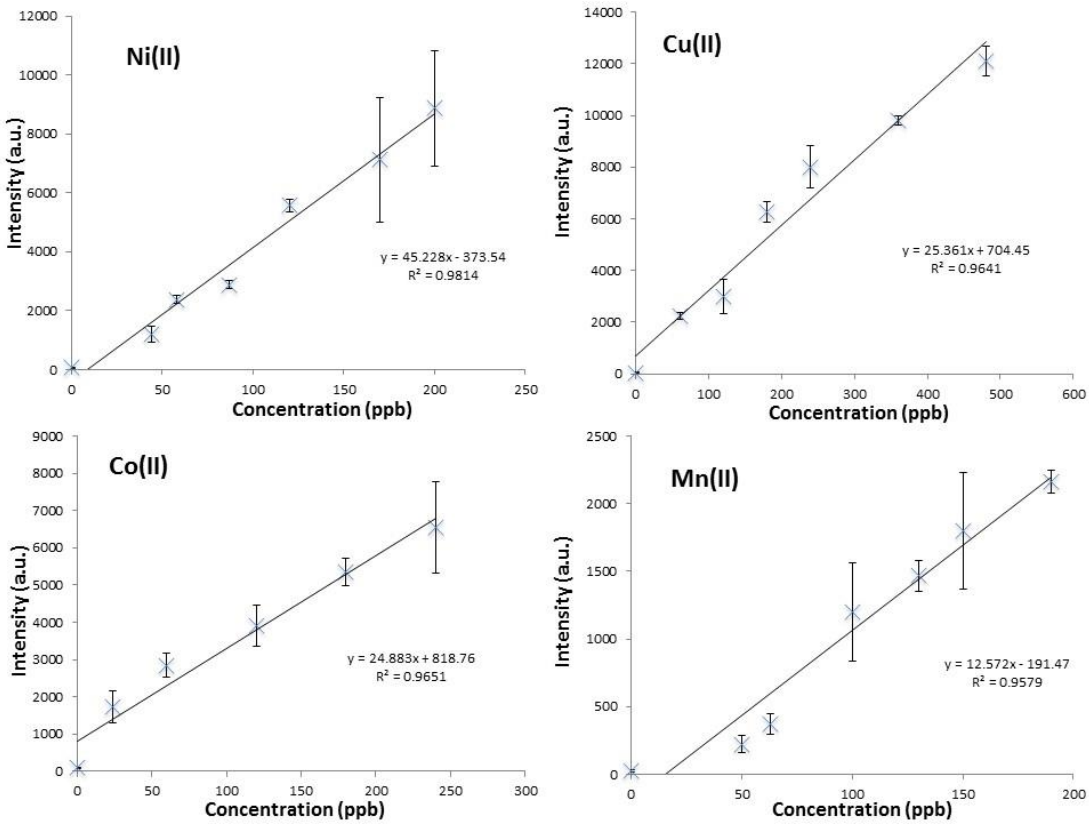

Figure 6.7: LOD graphs obtained for each salen-metal ion complex. Top left, Ni(II) (I_{1627} vs. conc.); top right, Cu(II) (I_{1641} vs. conc.); bottom left, Co(II) (I_{1597} vs. conc.); bottom right, Mn(II) (I_{1332} vs. conc.). Error bars represent the standard deviation of three replicates (λ_{ex} = 532 nm, acc. time = 10s)

The LODs obtained for each metal ion are listed in Table 6.6, where they are also compared to the recommended WHO guidelines for drinking water. It can be seen from this table that Ni(II), Cu(II) and Mn(II) can all be detected below their recommended limits, demonstrating the potential of this method to detect these metal ions at levels deemed harmful by the WHO. The WHO has not assigned a guideline for Co(II) as it is very rarely found in drinking water at high levels, with concentrations usually ranging from 0.1 – 5 ppb. However, Co(II) still poses a threat to the environment through other media such as soil.[116]

Table 6.6: Comparison of the detection limits calculated using d.H_2O, synthetic f.H_2O and f.H_2O obtained from Loch Thom. The recommended WHO guidelines for drinking water are also listed.

Metal Ion	**d.H_2O (ppm)**	**Synthetic f.H_2O (ppm)**	**f.H_2O from Loch Thom (ppm)**	**WHO drinking water limit (ppm)**
Cu(II)	0.002 ± 0.0001	0.001 ± 0.00009	0.48 ± 0.02	2
Ni(II)	0.001 ± 0.0002	0.004 ± 0.0005	0.73 ± 0.03	0.02
Mn(II)	0.002 ± 0.0002	0 ± 0	0.63 ± 0.02	0.5
Co(II)	0.0006 ± 0.00009	0.007 ± 0.0004	0.12 ± 0.005	-

6.6 Synthetic Freshwater

Due to the complexity of real environmental samples, it was decided to gradually increase the complexity of the sample matrices by initially moving from to d.H_2O to synthetic freshwater (f.H_2O). This was prepared according to a recipe reported by the EPA,[111] which was subsequently spiked with each of the metal ions of interest.

SERS spectra obtained using the synthetic f.H_2O were found to be almost identical to those from the d.H_2O, demonstrating that the contents of the synthetic f.H_2O did not interfere with the analysis (see Appendix XI for the comparison). LODs using the synthetic f.H_2O were therefore acquired using a portable Raman instrument, and the graphs obtained are shown in Figure 6.8. The LODs calculated from these graphs are also listed in Table 6.6, where it can be seen that the LODs are reasonably similar to those obtained using d.H_2O (i.e. within an order of magnitude), showing that the synthetic f.H_2O does not drastically affect the SERS analysis of the metal ions.

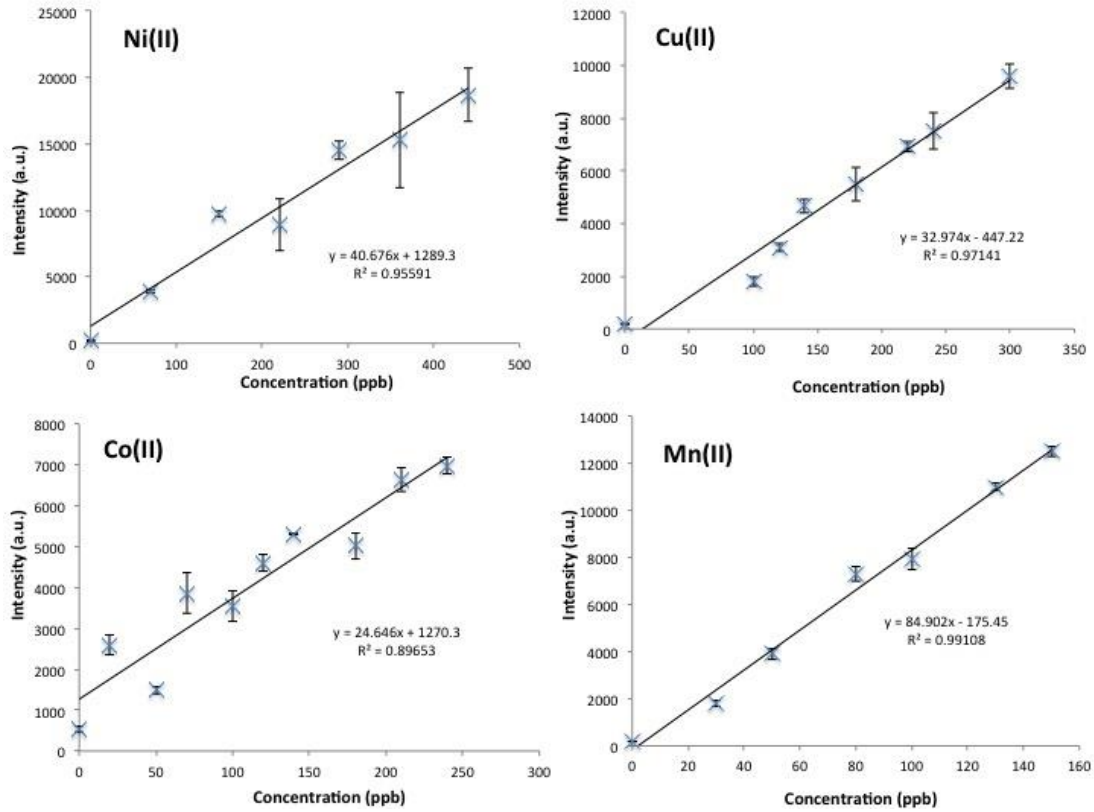

Figure 6.8: LOD graphs for each metal ion using synthetic freshwater. Top left, Ni(II) (I_{1627} vs. conc.); top right, Cu(II) (I_{1641} vs. conc.); bottom left, Co(II) (I_{1597} vs. conc.); bottom right, Mn(II) (I_{1332} vs. conc.). Error bars represent the standard deviation of three replicates (λ_{ex} = 532 nm, acc. time = 10s)

6.7 Real Environmental Freshwater

As no interference was observed from the contents of the synthetic f.H_2O, real f.H_2O was collected from Loch Thom, Greenock, Scotland in order to test the capability of this system with a true environmental sample.

The f.H_2O collected was analysed using ICP-MS in order to determine the composition of the sample. The results of the semi-quantitative analysis are listed in Appendix XII. Quantitative analysis of the metal ions of interest was also conducted in order to provide an accurate concentration of these ions. The concentration of Ni(II), Cu(II), Co(II) and Mn(II) were found to be 0.9 ± 0.001, 3.7 ± 1.6 , 0.1 ± 0.01 and 17.3 ± 0.08 ppb, respectively (n=3).

Firstly, the SERS spectrum of the f.H_2O, as it was collected, was obtained (i.e. it was not spiked with metal ions). However, a strong response from the f.H_2O was observed, as shown in Figure 6.9.

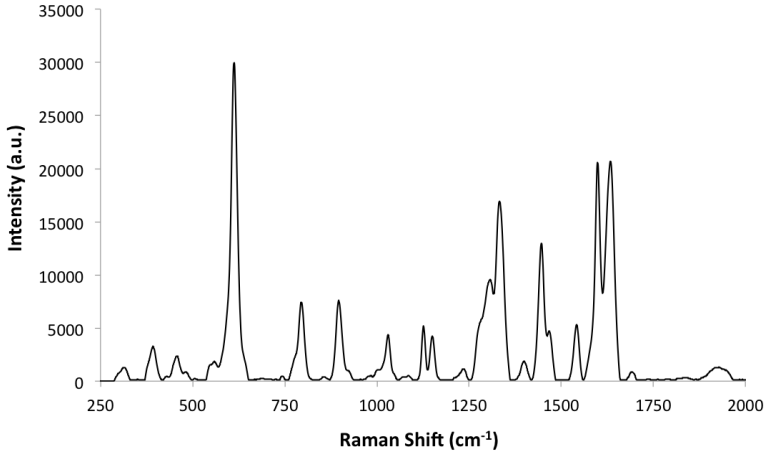

Figure 6.9: SERS spectrum obtained from the unspiked f.H_2O sample collected from Loch Thom. (λ_{ex} = 532 nm, acc. time = 10s)

This response from the f.H_2O did not match the profile expected from Ni(II), Cu(II), Co(II) or Mn(II) and therefore, it was postulated that this signal was due to another metal ion present in the f.H_2O sample. From the ICP-MS semi-quantitative analysis, the metal ions present at the highest concentrations were Ca (1 ppm), Na (600 ppb), K (500 ppb), Mg (200 ppb) and Fe (100 ppb). As a result, each of these ions was tested with salen in the same manner as before. d.H_2O was spiked with 10 µM of each species however only Fe gave an increased SERS response, which is compared to the f.H_2O SERS spectrum in Figure 6.10. The results from the other ions are shown in Appendix XIII.

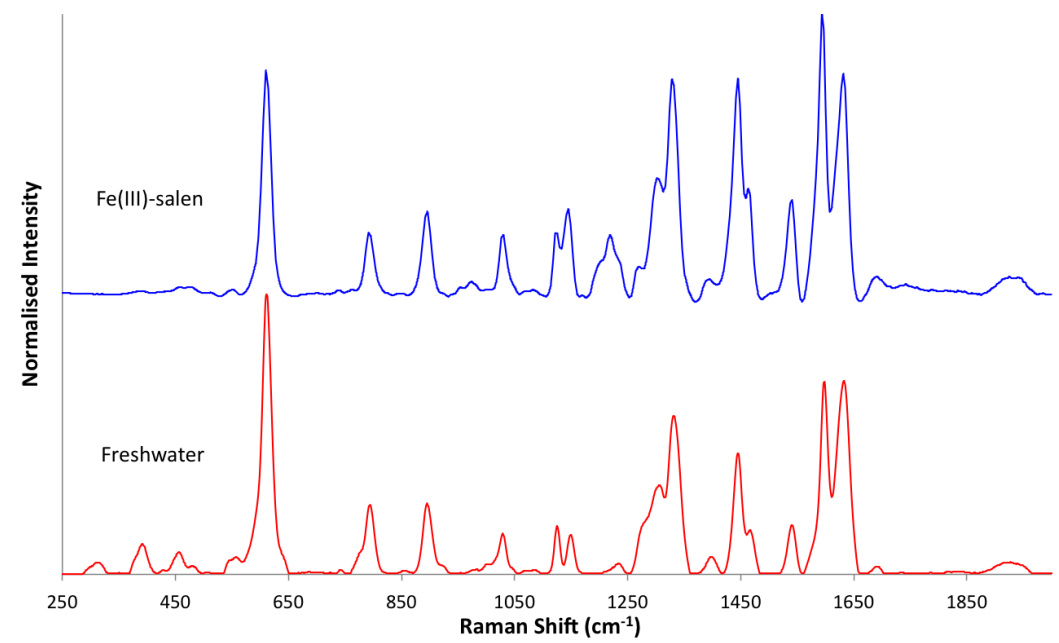

Figure 6.10: Comparison of the SERS spectrum obtained from the f.H_2O (red) to the Fe(III)-salen complex in d.H_2O water (blue) (λ_{ex} = 532 nm, acc. time = 10s)

It can be seen from the comparison that the Fe(III)-salen complex shares very similar SERS features to that of the f.H_2O sample. However, there are differences between the two spectra which could be due to the different sample matrices. Despite the similarity, it was found that the SERS response of the Fe(III)-SERS complex was much weaker than that of the f.H_2O (around 1500 counts for Fe(III)-salen vs. 30000 counts for f.H_2O) and therefore, Fe could not be confidently identified as the interfering source. It is postulated therefore, that the more complex sample matrix of the f.H_2O may somehow enhance the signal from Fe however, another possibility is that the signal is a result of organic material present in the f.H_2O. It is not likely that the interferent is due to other metal ions in the sample as they are all present at very low concentrations. Nevertheless, little could be done about the interferent and therefore, the f.H_2O was spiked with the four metal ions of interest (at a concentration of 0.5 µM) as they were not present in the sample at high enough levels for detection. The SERS spectra were then obtained in order to determine if Ni(II), Cu(II), Co(II) and Mn(II) could still be detected in the presence of the interferent. Figure 6.11 compares the spectra obtained using the f.H_2O to those from d.H_2O.

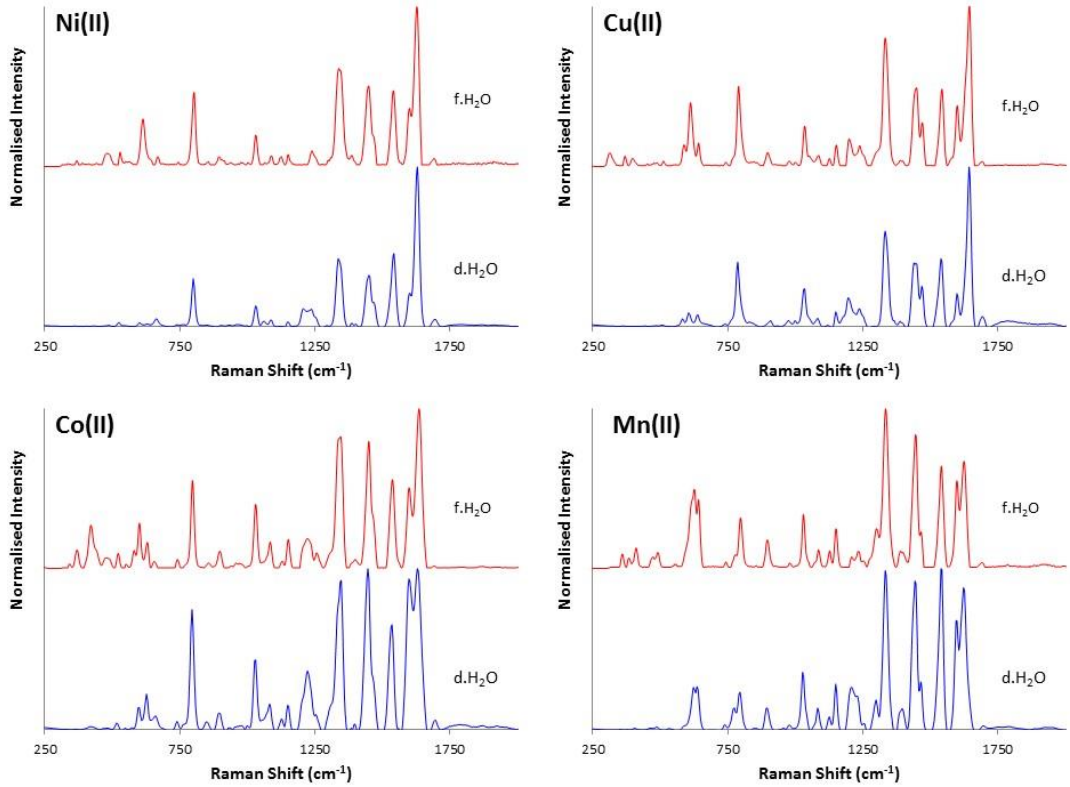

Figure 6.11: SERS spectra obtained from d.H_2O water (blue) vs. spectra obtained from the spiked f.H_2O obtained from Loch Thom (red). Top left: Ni(II); top right: Cu(II); bottom left: Co(II); bottom right: Mn(II) (λ_{ex} = 532 nm, acc. time = 10s)

It can be seen from Figure 6.11 that the spectra are very similar, with only minor differences detected. These minor differences are likely due to the fact that the natural f.H_2O has a more complex composition, including the interferent. However, the spectra closely resemble each other enough that the positive identification of each metal ion can still be achieved.

As Ni(II), Cu(II), Co(II) and Mn(II) could be detected in the natural f.H_2O sample after spiking, detection limit studies were conducted in order to determine if the detection limits were affected by the different sample matrix of the f.H_2O. However, it was difficult to calculate the accurate and precise LODs due to the interferent. It was found that, at lower concentrations of the spiked metal ions, the SERS spectrum from the interferent would dominate, masking the features that are specific to the metal ions of interest. The blank sample would also produce a very strong SERS profile (see Figure 6.9), and as a result, concentration relationships were plotted, as shown in Figure 6.12.

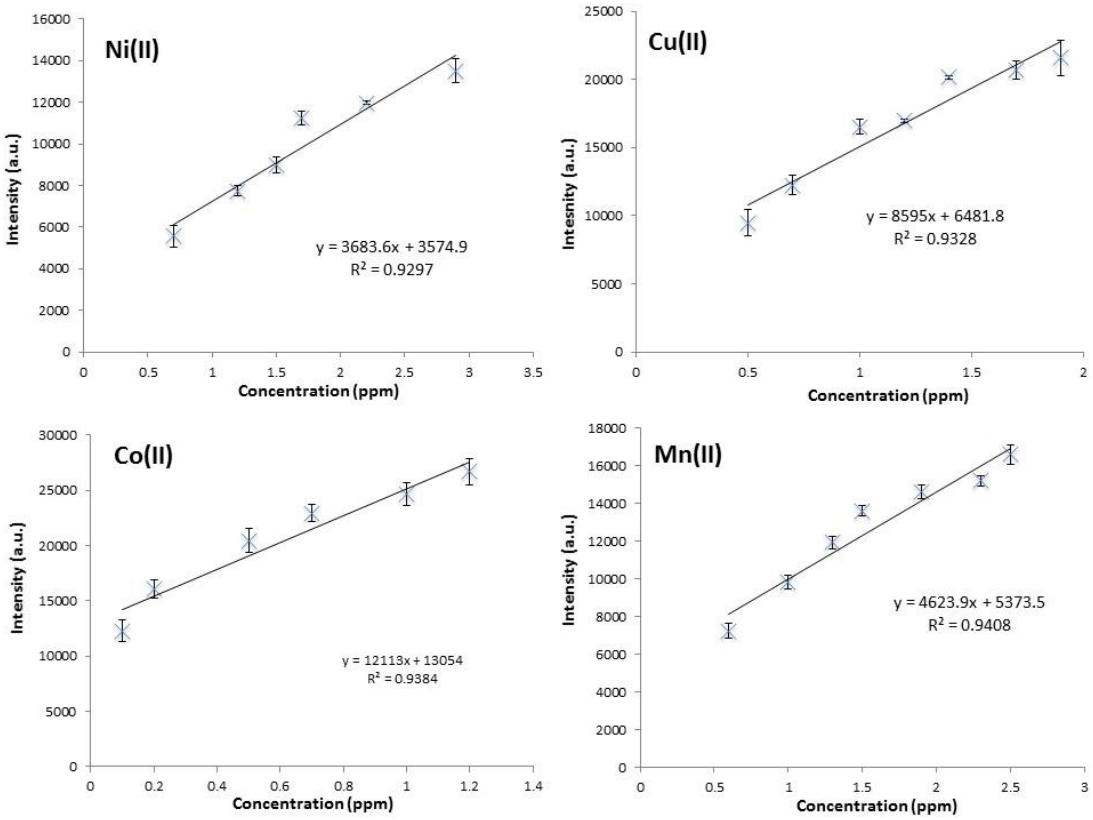

Figure 6.12: Concentration relationships of each metal-salen complex in f.H_2O. Top left, Ni(II) (I_{1627} vs. conc.); top right, Cu(II) (I_{1641} vs. conc.); bottom left, Co(II) (I_{1597} vs. conc.); bottom right, Mn(II) (I_{1332} vs. conc.). Error bars represent the standard deviation of three replicates (λ_{ex} = 532 nm, acc. time = 10s)

The concentration relationships were used to calculate observable detection limits, which were obtained using the lowest metal ion concentration that provided the unique SERS spectrum associated with each metal ion. Below this concentration the SERS profile of the interferent dominated, and therefore the presence of the metal ions could not be confidently detected. These lowest observable concentrations are compared to the LODs obtained using d.H_2O water and synthetic f.H_2O in Table 6.6. It can be seen that the lowest observable concentrations for the metal-salen complexes in natural f.H_2O are significantly higher due to the interferent and as a result, only Cu(II) can be detected below the recommended WHO guidelines. Mn(II) is close to the recommended limit, only being 0.13 ppm out, however the detection limit for Ni(II) would have to be greatly improved for this system to be used in the environmental monitoring of Ni(II).

Although the detection limits are much greater for the real f.H_2O samples, the levels of metal ions found naturally in this water sample do not pose an environmental threat, as this system proved by not producing a SERS response specific to each of the species of interest.

6.8 Contaminated Freshwater

As this system was tested with a natural f.H_2O sample that did not contain high levels of the metal ions of interest, work progressed to applying the method to a contaminated f.H_2O sample obtained from Gourock burn, Gourock, Scotland which is known to have leachate issues from a nearby landfill site. The SERS spectrum of the contaminated f.H_2O was obtained using the same method as previously described. It was found that the SERS spectrum from the contaminated water was almost identical to that of the Mn(II)-salen complex. This is shown in Figure 6.13, and Table 6.7 compares the frequencies of the bands that occur in both spectra.

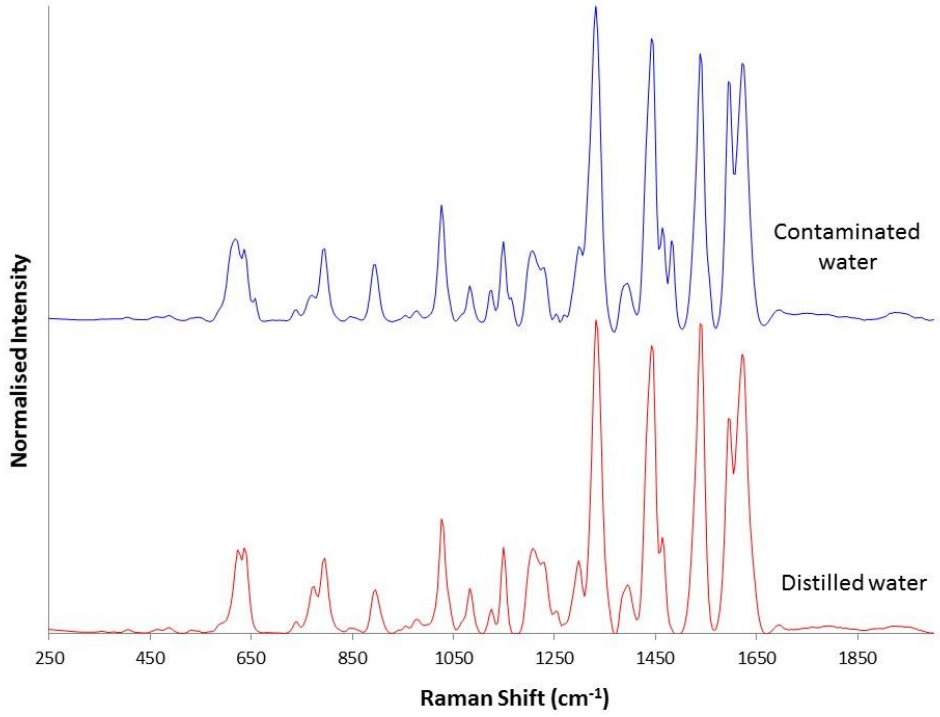

Figure 6.13: SERS spectrum obtained from contaminated water sample (top, blue) versus the SERS spectrum from d.H_2O water spiked with Mn(II) (bottom, red). (λ_{ex} = 532 nm, acc. time = 10s)

Table 6.7: Comparison of the bands observed in the SERS spectrum of Mn(II)-salen in d.H_2O and those in f.H_2O

Frequency of Mn(II)-salen bands using d.H_2O (cm^{-1})	**Frequency of Mn(II)-salen bands using f.H_2O (cm^{-1})**
1621.5 (s)	1621.5
1597 (s)	1594
1538 (s)	1538
	1481.5
1463.5 (m)	1463.5
1441.5 (s)	1442
1394.5 (w)	1394
1332 (s)	1331.5
1298 (w)	1298.5
1226.5 (m)	1229.5
1207 (m)	1207
1149 (m)	1149
1125.5 (w)	1125.5
1082.5 (w)	1082.5
1026.5 (m)	1026.5
978 (w)	978
896 (w)	895.5
795.5 (m)	795.5
774.5 (w)	770
740.5 (w)	740
636.5 (m)	636.5
	614.5

There are minor differences between the two spectra (around 1450 cm^{-1} and 1275 cm^{-1}, for example), however these are attributed to the different sample matrices, as more analytes are present in the contaminated water sample. The spectra closely resemble each other enough to positively identify the presence of Mn(II) in the contaminated

water sample, and this was confirmed using ICP-MS analysis which showed a Mn(II) concentration of 833 ± 37 ppb was present (n=3). The concentrations of Ni(II), Cu(II) and Co(II) present in the sample were 1.7 ± 0.04, 1.9 ± 0.07 and 0.6 ± 0.02 ppb, respectively. An indication of the Mn(II) concentration from the SERS analysis was obtained using the concentration relationships shown in Figure 6.12, which was then compared to the ICP-MS results. The band at 1332 cm^{-1} (i.e. that used to plot the concentration relationship for Mn(II)) was found to have an intensity of approximately 7000 counts (see Appendix XIV). From the concentration relationship in Figure 6.12, this implies that Mn(II) was present in the contaminated f.H_2O sample at ~700 ppb, which is reasonably similar to the ICP-MS value. Therefore, not only can this approach detect high levels of metal ions in f.H_2O samples, it can also provide a reasonable estimate of the concentration present.

6.9 Seawater

After using the system with f.H_2O to detect the metal ions of interest, it was decided to test it with seawater, which has a higher salinity than f.H_2O. The same procedure was used as before, where the seawater was spiked with Ni(II), Cu(II), Co(II) and Mn(II), before complexation with salen and addition to AgNPs. This time however, the high salinity of the seawater caused immediate aggregation of the AgNPs and as a result, no salt was required to induce aggregation. The SERS spectra of each metal-salen complex was again acquired and compared to previous results. Figure 6.14 compares the SERS spectra obtained for each metal ion (at a concentration of 0.5 µM) in seawater to those in d.H_2O water.

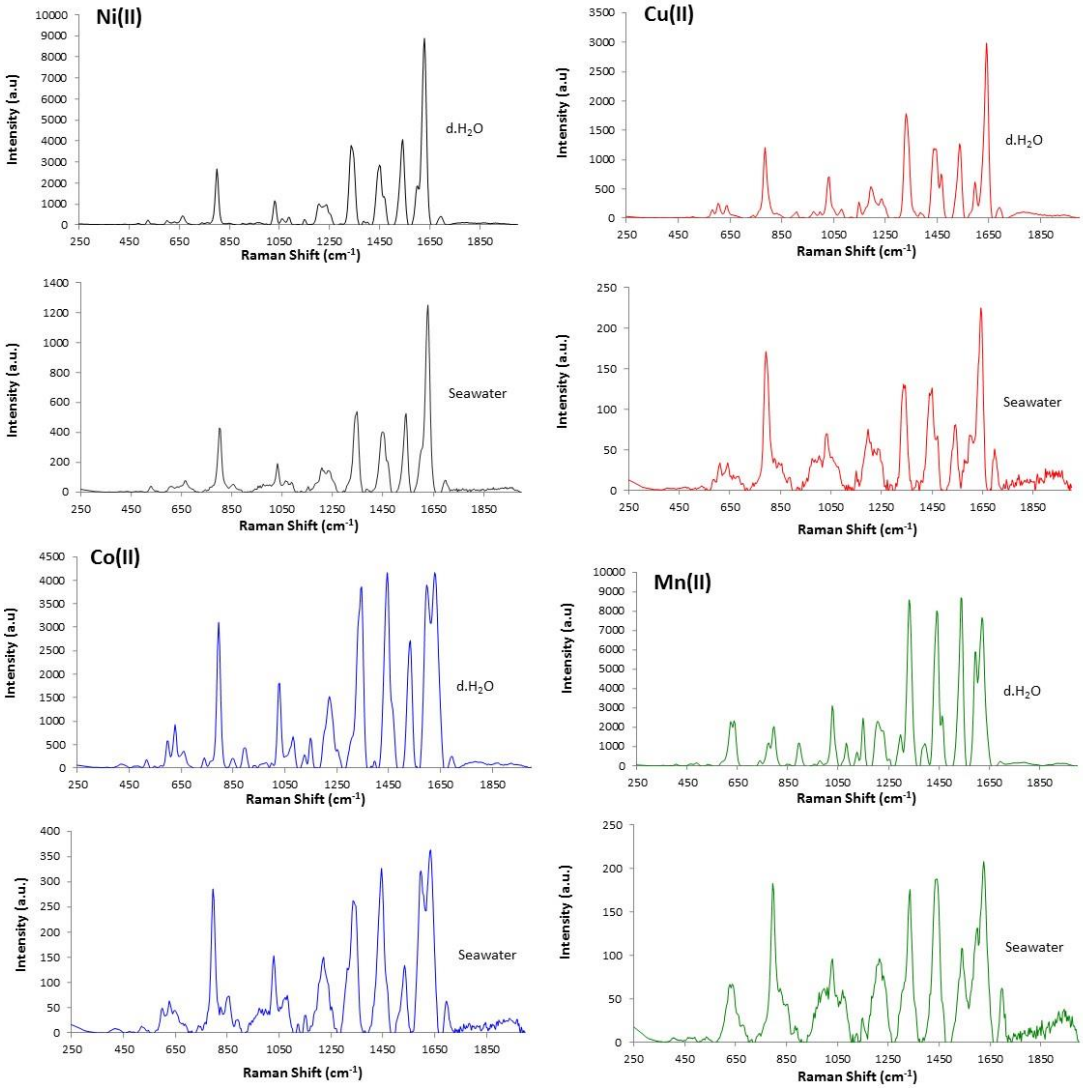

Figure 6.14: SERS spectra obtained from metal ions (0.5 µM) in d.H_2O water vs. those in seawater. Top left, Ni(II), black; top right, Cu(II), red; bottom left, Co(II), blue; bottom right, Mn(II), green (λ_{ex} = 532 nm, acc. time = 10s)

It can be seen from Figure 6.14, that the intensity of the SERS response is greatly decreased in seawater. This is likely due to the high chloride content in the seawater causing the AgNPs to over-aggregate and precipitate from the solution, decreasing the SERS signal. An attempt to overcome this issue was made by adding $AgNO_3$ to the salen-metal complexes in seawater. This would precipitate the chloride out of the solution as AgCl, therefore reducing the chloride content and preventing the suspected over-aggregation. This was conducted by adding 100 µL of 5 M $AgNO_3$ to 900 µL of the Ni(II) in seawater. After the AgCl precipitate had formed, a 25 µL aliquot was added to 25 µL of salen which was left overnight. This was then added to AgNPs but again, the AgNPs

aggregated immediately. The SERS spectrum of this sample was collected and compared to the initial Ni(II)-salen spectrum in seawater however, little change in the intensity was observed (see Appendix XVI). This suggests that either a high concentration of chloride still exists or other salts present in the seawater are still causing over-aggregation of the AgNPs, resulting in a greatly reduced SERS signal. Attempts to decrease the salt concentration was discontinued as the idea of this system is to provide a low-cost and simple method for metal ion detection that can be used for field-deployment. As much more complex sample preparation would be required for this system to work in seawater, this went counter to the aims of this project.

6.10 Mixtures of Metal Ions

Obviously environmental samples may contain more than one of the metal ions of interest and as a result, research was conducted in order to determine if this system is capable of detecting multiple metal ions in a single sample. This was achieved by adding two metal ions to the salen solution (at identical concentrations), before adding to AgNPs and acquiring the SERS spectra. This was done for all possible metal ion combinations. Figure 6.15 compares the resulting SERS spectrum from a mixture of Cu(II) and Mn(II) to those of the single spectra.

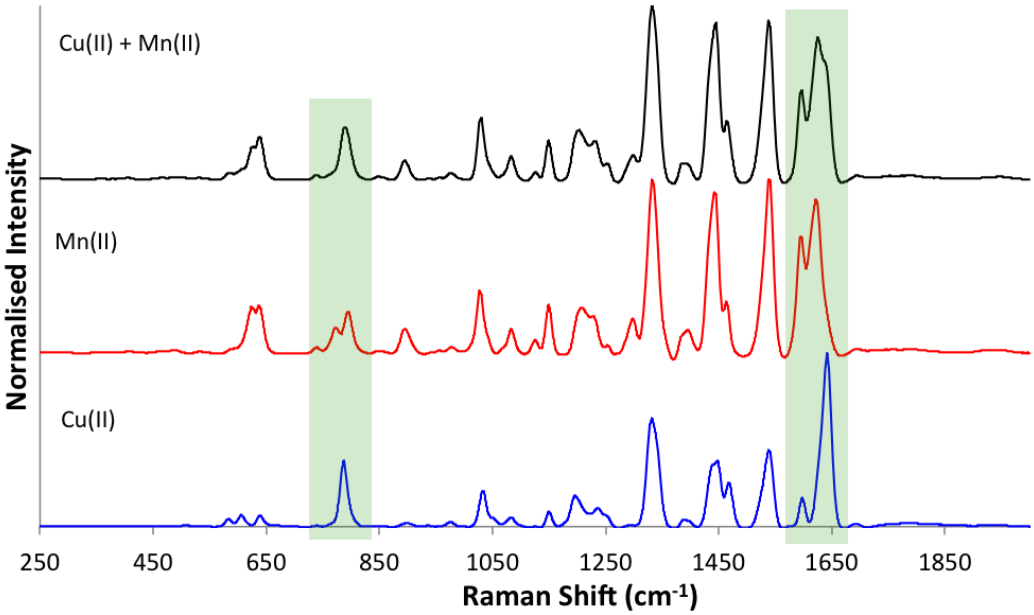

Figure 6.15: Comparison of the SERS spectrum obtained from a mixture of Cu(II) and Mn(II) (top, black) to the spectra of the single metal ions Mn(II) (middle, red) and Cu(II) (bottom, blue) (λ_{ex} = 532 nm, acc. time = 10s)

The SERS spectrum from the mixture of Cu(II) and Mn(II) is dominated by features that are specific to Mn(II)-salen complexes. However, there are subtle differences that suggest that Cu(II) does have a slight effect on the mixed metal spectrum, which are highlighted in the green boxes in Figure 6.15. Firstly, the C=N stretches around 1600 cm^{-1} have the same frequencies as for Mn(II) however, the band at 1624 cm^{-1} changed shape suggesting there was an overlap of peaks. As a result, curve fitting was applied to this band to allow separation of the components and this is shown in Figure 6.16.

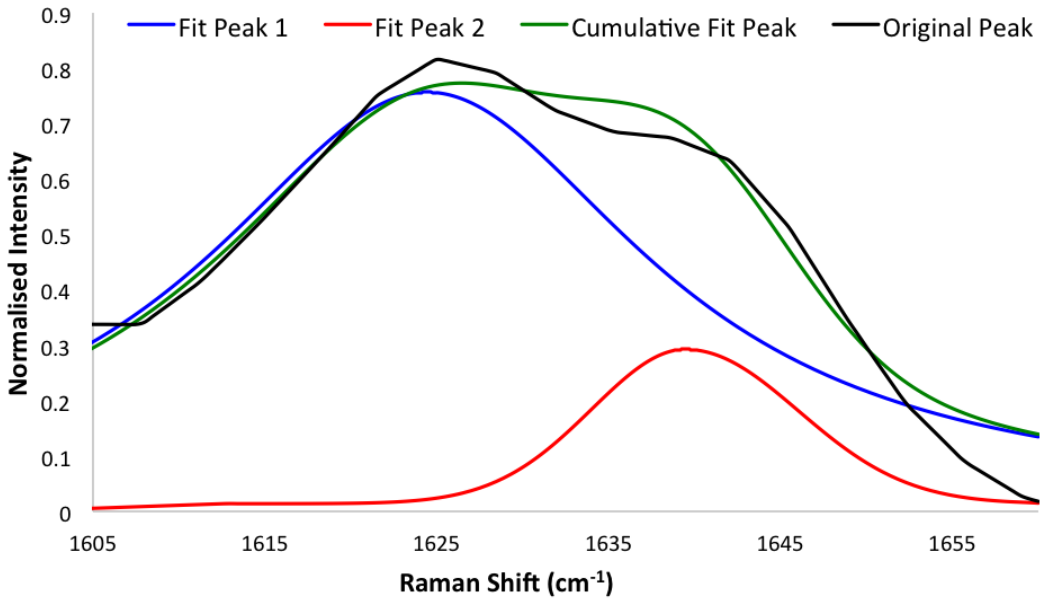

Figure 6.16: C=N stretching band from the mixed sample (black) with the corresponding curve bands fitted at 1624 cm^{-1} (blue) and 1639 cm^{-1} (red). The cumulative fit peak is also shown (green)

The curve-fitting model separated the two peaks at frequencies of 1624 and 1639 cm^{-1}, which matches the frequencies of this band for Mn(II) and Cu(II), respectively. This therefore helped to verify the overlap of these two bands, and hence provide a small indicator for the presence of Cu(II). A single band at 787 cm^{-1} in the mixed-metal spectrum is also a feature found in the Cu(II)-salen spectrum, but not for Mn(II) where two bands are observed. Consequently, this subtle difference can also be used to indicate the presence of a competing species. As the spectrum closely resembles Mn(II)-salen complexes with only minor differences produced by Cu(II), it would be very easy to miss the presence of the second species. If this were to be used for environmental samples, the minor differences could easily be attributable to the more complex sample matrix.

A second example is shown in Figure 6.17 using a mixture of Co(II) and Mn(II), with Table 6.8 comparing the frequencies of the main bands of interest.

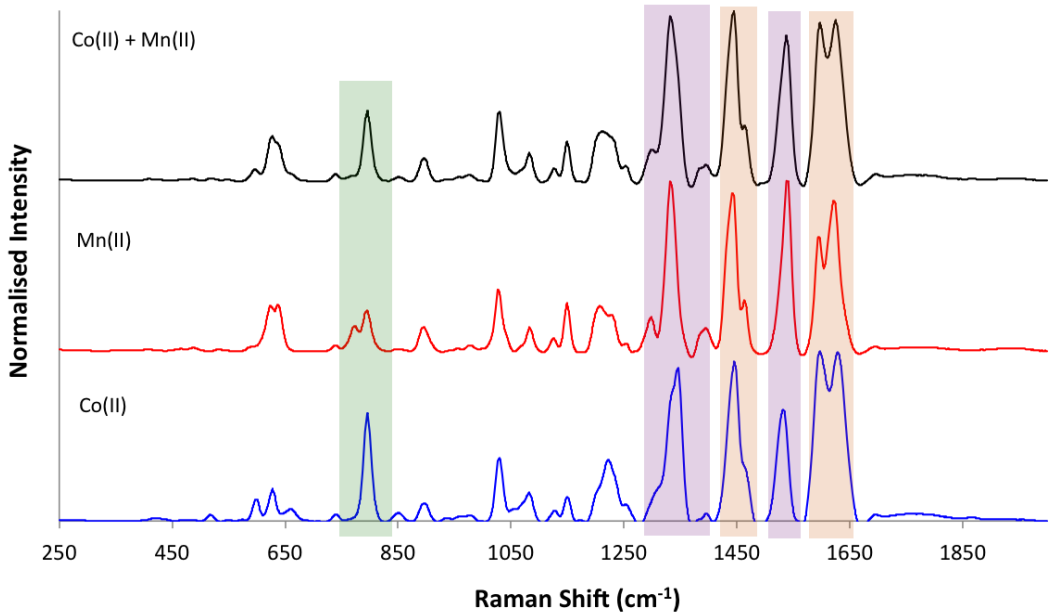

Figure 6.17: Comparison of the SERS spectrum obtained from a mixture of Co(II) and Mn(II) (top, black) to the spectra of the single metal ions, Mn(II) (middle, red) and Cu(II) (bottom, blue) (λ_{ex} = 532 nm, acc. time = 10s)

Table 6.8: The peak frequencies for the mixed metal ion salen complex, compared to the frequencies of the single metal ion salen complexes

	Co(II)	**Mn(II)**	**Co(II) + Mn(II)**
Frequency (cm^{-1})	1628	1621.5	1624.5
	1597	1597	1597
	1531	1538	1538
		1463.5	1463
	1445.5	1441.4	1445.5
	1346.5	1332	1332
		1298	1298.5
	795.5	795.5	795.5
		774.5	

Close examination of this spectrum shows bands that are specific to each metal ion. The green box in Figure 6.17 highlights a band that is an indicator of Co(II), and the purple boxes highlights bands that have frequencies unique to Mn(II). The two other bands in the orange boxes occur at frequencies that are between the characteristic shifts of both

ions, indicating that both Co(II) and Mn(II) are influencing these vibrations. Again, the spectrum from this mixture does not conclusively identify the presence of both metal ions, and the detection of Co(II) could be easily missed.

The SERS spectra of the other metal ion combinations can be found in Appendices XVI – XIX. Again for all mixtures, one metal ion tends to dominate the SERS spectrum however, slight changes relating to the second metal ion can be found upon close inspection. As a result, detection of two metal ions present in a sample is in no way conclusive using this method, however subtle changes can be used to indicate the presence of more than one ion.

6.11 N,N'-bis(salicylaldehyde)–1,2-phenylenediamine (Salophen)

As the sensitivity of the salen system was affected by the more complex matrix of the environmental samples, a new Schiff base was synthesised from the condensation of salicylaldehyde and 1,2-phenylenediamine. This ligand has an extra aromatic ring at the bridge as shown in Figure 6.18. As a result, salophen contains a π-conjugated bridge, unlike salen, and this extra conjugation results in a decreased energy gap between the highest occupied molecular orbital (HOMO) and the lowest occupied molecular orbital (LUMO). Consequently, a red-shifting of the extinction spectrum occurs.[117] The absorption maximum for salophen is therefore closer to the exciting laser wavelength of 532 nm and should therefore result in a stronger SERS enhancement.

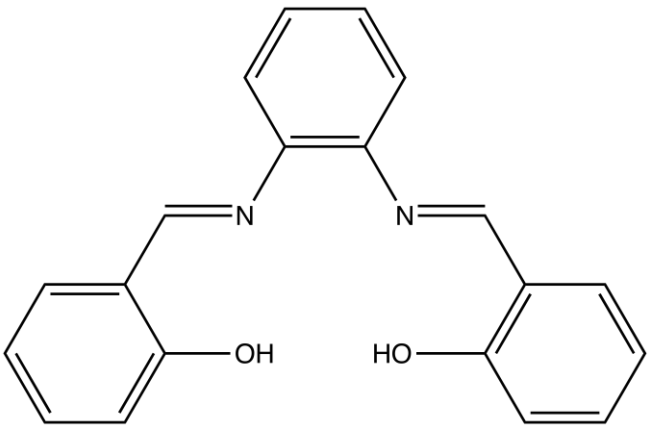

Figure 6.18: Structure of salophen

6.11.1 SERS of Salophen Complexes

Again the SERS spectra of the four different metal-salophen complexes were obtained using the same procedure as for salen. Initially, the same salen concentration of 10 µM was used however, signal saturation occurred using this concentration and as a result, the concentration was decreased to 0.5 µM as this concentration gave a low SERS signal for the free ligand, and an increased response after the addition of the metal ions (see Appendix XXII). The SERS response using 0.5 µM salophen and 0.5 µM of a range of different metal ions is shown in Figure 6.19. The frequencies and assignments for the main bands of interest present in the SERS spectra of the salophen complexes are listed in Table 6.9.

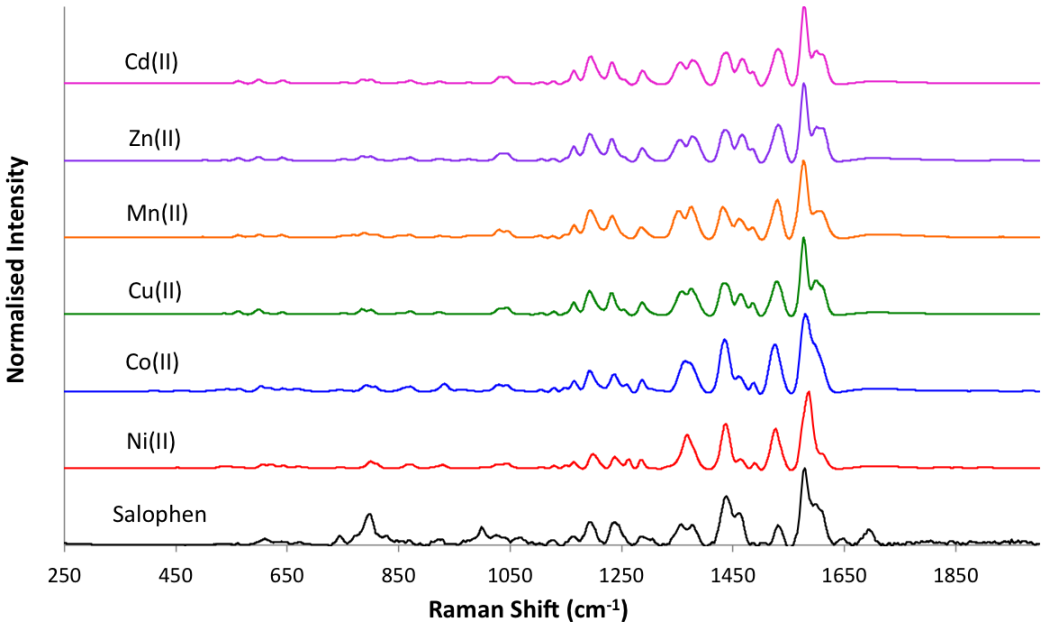

Figure 6.19: Comparison of the SERS spectra of salophen and different metal-salophen complexes. Salophen, black; Ni(II), red; Co(II), blue; Cu(II), green; Mn(II), orange; Zn(II), purple; Cd(II), pink (λ_{ex} = 532 nm, acc. time = 10s)

Table 6.9: Frequencies and assignments of the salophen complexes[118]

	Ni(II)	Co(II)	Other Metal Ions	Tentative Assignment
Frequency (cm^{-1})			1600 (m)	C=N stretch
	1586.5 (vs)	1580 (vs)	1576.5 (vs)	Phenyl, C=C quadrant stretch
	1527 (s)	1524 (s)	1527.5 (s)	Phenyl, semicircular stretch
	1488.5 (w)	1488 (w)	1485 (w)	
	1463 (w)	1459.5 (w)	1463.5 (w)	
	1437.5 (s)	1434.5 (s)	1434.5 (m)	
			1376 (s)	Phenyl, sextant stretch
	1368.5 (m)	1365 (m)	1358 (m)	
	1286.5 (w)	1287 (w)	1287 (w)	Six-membered chelate ring stretch
	1264 (w)	1260 (w)	1253 (m)	
	1237.5 (w)	1237.5 (w)	1233.5 (m)	Phenyl C-N stretch
	1199.5 (w)	1192 (m)	1192 (w)	Phenyl C-O stretch

Again, Ni(II), Cu(II), Co(II) and Mn(II) all produced an increased SERS signal, as too did Cd(II) and Zn(II). However, it can be seen from Figure 6.19 that four of the metal ions – Cu(II), Mn(II), Zn(II) and Cd(II) – produced very similar SERS spectra that could not be easily discriminated. Ni(II) and Co(II) showed slight differences to both the free ligand and other metal-salophen complexes however, they changed the SERS spectrum of salophen in a very similar manner. Nevertheless, Table 6.9 demonstrates that a number of bands for the Ni(II) and Co(II) complexes have slightly different shifts. Firstly, the C=N stretch has a difference in frequency of ~6 cm^{-1} due to the coordination of the different species. This band appears at a lower frequency than for salen as a result of the third

aromatic ring, which results in extra conjugation in the salophen ligand, hence the different frequencies observed in the spectra. It can also be seen that the aromatic stretches also differ by a few wavenumbers. Although the shifts are small, there are a number of bands present in the spectrum that vary upon Ni(II)/Co(II) coordination, and these can therefore be used to support the identification of these species.

6.11.2 PCA

As the differences between the SERS spectra of the salophen-metal complexes were subtle, PCA was applied to the dataset to determine whether the different samples could be separated from each other. The scores plot from this is depicted in Figure 6.20 (the loadings for PC1 and PC2 can be found in Appendices XXIII and XXIV).

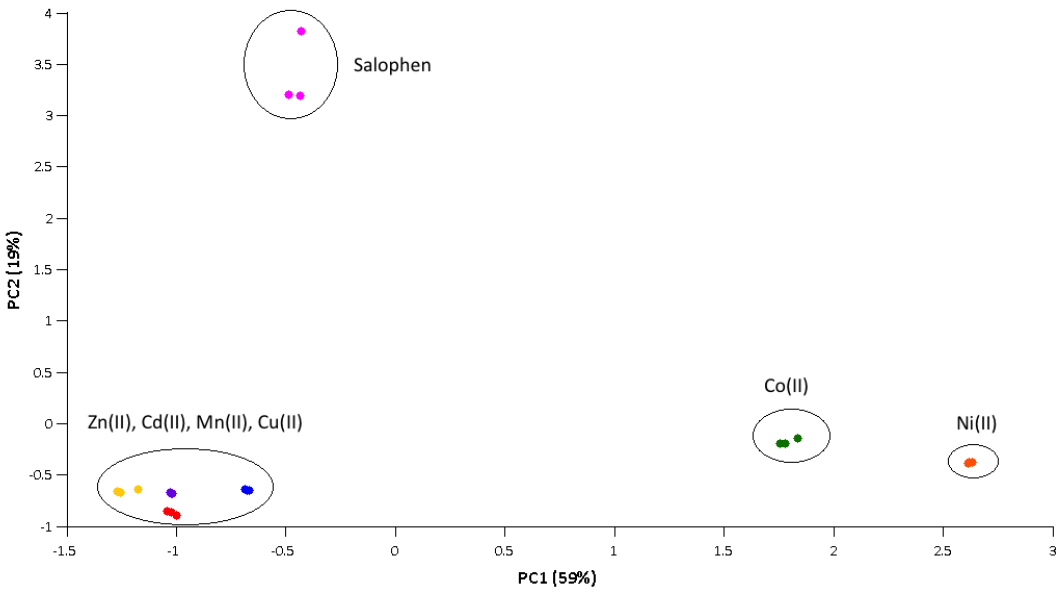

Figure 6.20: PCA scores plot of the different metal-salophen complexes. Salophen ligand, pink; Zn(II), yellow; Cd(II), purple; Mn(II), red; Cu(II), blue; Co(II), green; Ni(II), orange

It can be seen from this scores plot that Zn(II), Cd(II), Mn(II) and Cu(II) all cluster together as expected, confirming that the spectra are identical between each of these metal-salophen complexes. As a result, they cannot be discriminated even using PCA. Co(II) and Ni(II) form groupings separate from the other samples, demonstrating the SERS spectra of these ions are vastly different from all other samples. There is a slight separation of

Co(II) and Ni(II), which is to be expected as these two ions produce frequency shifts in a number of the salophen bands.

From these results, it can be said that only Ni(II) and Co(II) can be confidently identified using salophen. It is hypothesised that the addition of the third aromatic ring at the bridge of salophen results in a loss of flexibility compared to salen and consequently, the metal ions do not alter the SERS spectrum of salophen as profoundly as for salen.

6.11.3 Salophen vs. Salen

It should be noted that although selectivity is lost using salophen as the chelating ligand, the SERS intensity of the metal-salophen complexes are superior to those from the metal-salen complexes. This is to be expected as the absorption maximum is closer to the exciting laser wavelength of 532 nm. This is represented in Figure 6.21, which compares the SERS spectra of Ni(II)-salen and Ni(II)-salophen at a metal ion concentration of 0.5 µM.

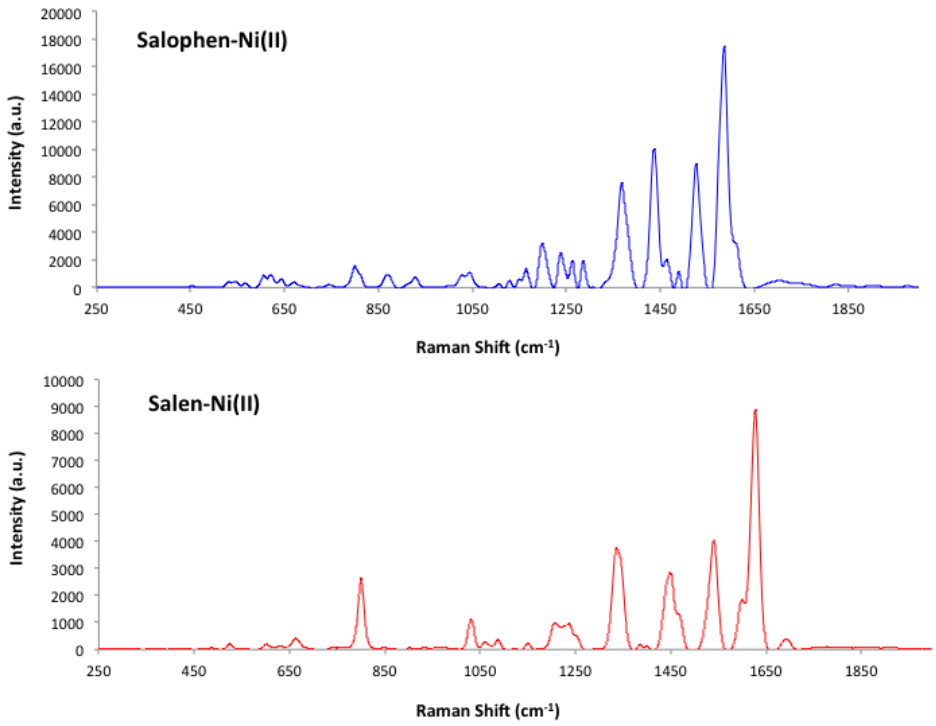

Figure 6.21: Comparison of the SERS response from salen-Ni(II) (bottom, red) and salophen-Ni(II) (top, blue) (λ_{ex} = 532 nm, acc. time = 10s)

It can be seen that the intensity of the Ni(II)-salophen complex is increased by approximately twice as much, demonstrating that salophen does provide a stronger SERS signal due to the addition of the third phenyl ring, as was hypothesised. However, the presence of this aromatic ring results in a loss of selectivity. As salen was shown to discriminate between more metal ions, and Co(II) is not usually deemed hazardous to water samples, work with salophen was discontinued.

6.12 Salicylaldehyde Thiosemicarbazone (SALTSC)

Due to the success of Schiff bases, work continued with this group of molecules. From the results of salen and salophen, it was hypothesised that the vibrational profile of a flexible ligand that contains a chromophore is more likely to be influenced by the coordination of metal ions. Therefore, salicylaldehyde thiosemicarbazide (SALTSC) was investigated next as it is a commercially available thiosemicarbazone that is likely to coordinate to a number of different metal ions.

Thiosemicarbazones are derived from the condensation of aldehydes or ketones with thiosemicarbazide compounds, and therefore can be easily modified by variation of the parent aldehyde/ketone used in the synthesis.[119] These compounds are known to chelate to metal ions, usually as a tridentate O,N,S-donor. As a result, the commercially available salicylaldehyde thiosemicarbazone (SALTSC), shown in Figure 6.22, was investigated as a potential ligand for the SERS detection of metal ions, as the addition of both a hard and soft donor group in one ligand increases the coordination ability towards both hard and soft metal ions.[119]

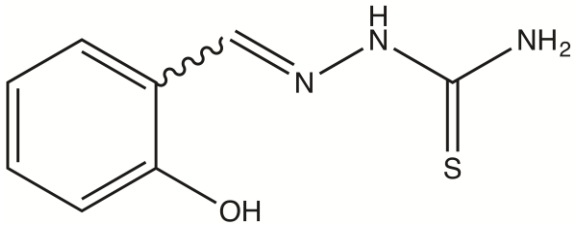

Figure 6.22: Structure of salicylaldehyde thiosemicarbazone (SALTSC)

6.12.1 Concentration Study

In order to get an idea of the concentration of SALTSC required to give monolayer coverage, a brief concentration study was conducted by adding varying concentrations of SALTSC (1 to 10 µM) to both water and a 2.5 µM Ni(II) solution. These were left overnight to allow complete coordination to occur, after which they were added to AgNPs and the SERS spectra collected. The SERS spectra of SALTSC added to water (see Appendix XXV) remained constant from 10 to 5 µM, with slight variation in intensity (1400 to 1800 counts). Below 5 µM, the SERS signal begins to decrease demonstrating that too few SALTSC molecules are present to provide monolayer coverage.

The SERS spectra obtained using d.H_2O were then compared to those obtained by adding Ni(II) to SALTSC, which is shown in Figure 6.23.

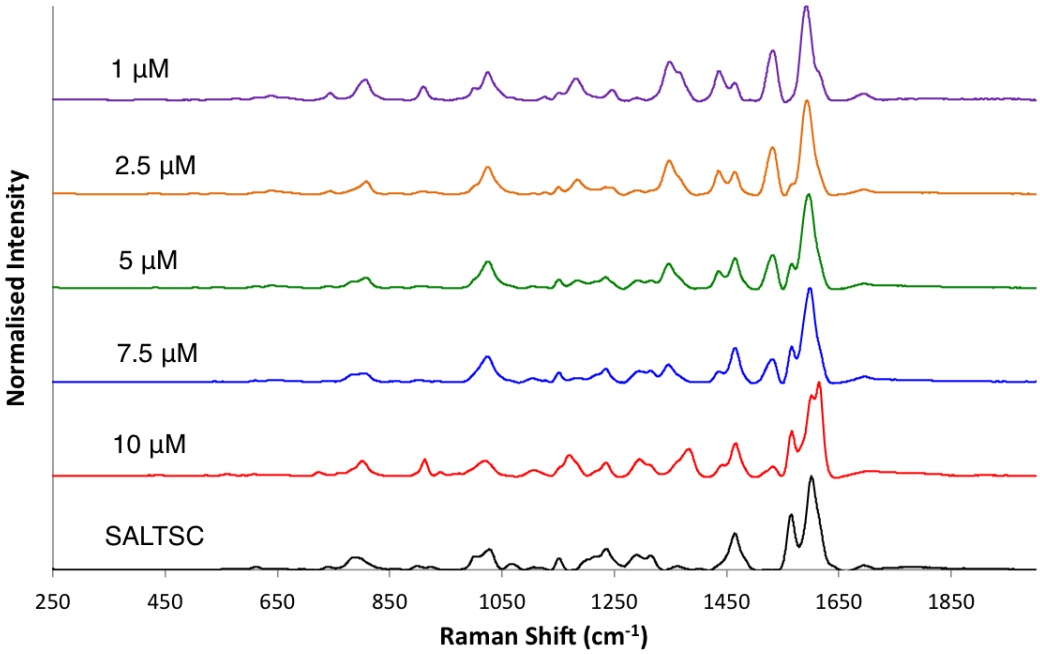

Figure 6.23: Comparison of Ni(II)-SALTSC complexes, with varying concentrations of the ligand. SALTSC-water (50 µM), black; 10 µM SALTSC, red; 7.5 µM SALTSC, blue; 5 µM SALTSC, green; 2.5 µM SALTSC, orange; 1 µM SALTSC, purple (λ_{ex} = 532 nm, acc. time = 10s)

Again, the spectra obtained using higher concentrations of SALTSC had a similar intensity, around 3500 counts which is a slight increase over the SALTSC-water samples. It can be

seen from Figure 6.23 however, that a 10 µM concentration of SALTSC gives a slightly different SERS spectrum as extra bands are observed, likely resulting from above monolayer coverage of the AgNPs. Below 10 µM however, the spectra remain consistent and only at 1 µM SALTSC does the intensity decrease to around 1400 counts, indicating that monolayer coverage is lost at this concentration. As a result, a SALTSC concentration of 5 µM was selected as this appeared to provide the monolayer coverage required for optimal SERS.

6.12.2 SERS of SALTSC-metal complexes

Again, a range of different metal ions were added to a solution of the ligand, which was then left overnight to allow complete coordination. The complex was added to AgNPs and aggregated with salt. Eight metal ions (Ni(II), Cu(II), Co(II), Mn(II), Zn(II), Cd(II), Pb(II), Cr(III)) were tested with this ligand however, only Ni(II), Cu(II) and Co(II) were shown to change the SERS spectrum of the SALTSC ligand. The SERS response from the SALTSC complexes of these metal ions are compared in Figure 6.24, along with the SERS spectrum of the SALTSC ligand. The SERS assignments for SALTSC and its complexes are also listed in Table 6.10. The spectra of the other ions can be found in Appendix XXVI.

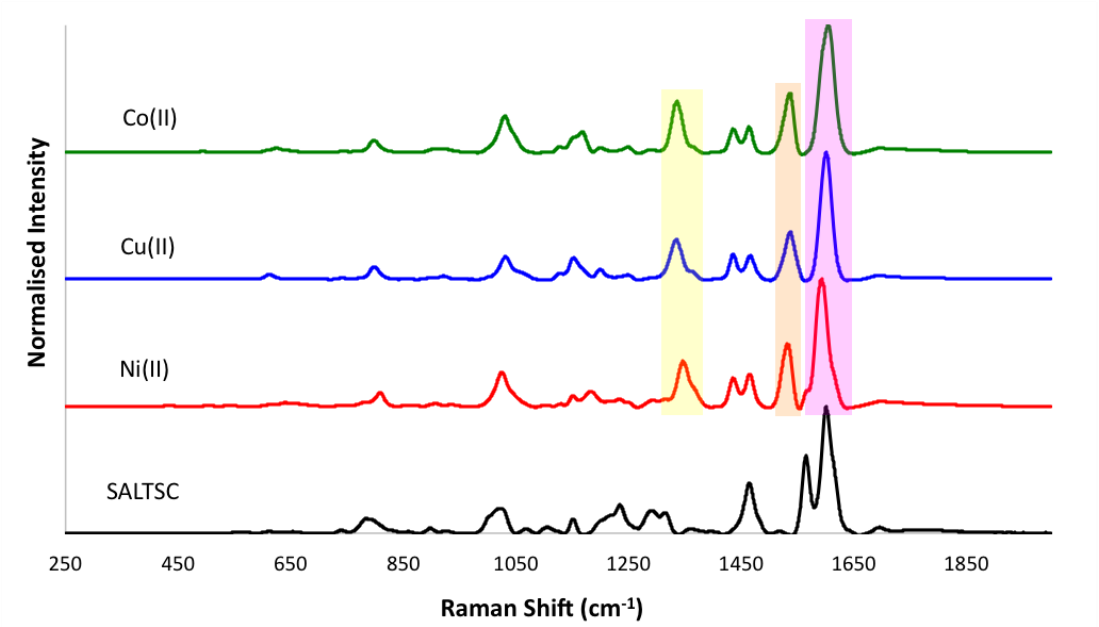

Figure 6.24: SERS spectra of the free SALTSC ligand (black) and the SALTSC complexes of Ni(II) (red), Cu(II) (blue) and Co(II) (green) (λ_{ex} = 532 nm, acc. time = 10s)

Table 6.10: SERS frequencies and assignments of the SALTSC ligand and its Ni(II), Cu(II), Co(II) complexes[120]

	SALTSC	Ni(II)	Cu(II)	Co(II)	Tentative Assignment (cm^{-1})
Frequency (cm^{-1})	1606	1593.5	1600.5	1604	νCN
	1571	1531	1537.5	1537.5	νCC
	1469	1466.5	1466.5	1463.5	
		1434.5	1434.5	1434.5	
	1363.5	1346.5	1335.5	1335.5	βOH, νCC
	1319	1316.5			νCC, νCO
	1296	1294		1290.5	
	1224	1234	1249	1249	νCC, νCN
	1206	1184	1199.5	1199.5	βCCH
	1158	1152.5	1153	1168.5	βCCH
		1126	1126	1126	βCCH, ωHCCC
	1028	1026	1030.5	1030.5	βCCH
	788.5	808.5	799.5	796	ωHCCC

From the comparison of the SERS spectra, it appears as though the spectra from the Ni(II), Cu(II) and Co(II)-SALTSC complexes are very similar. However, inspection of the frequencies show that there are some frequency shifts specific to each metal ion. Firstly, there is a slight shift of 4 cm^{-1} of the C=N stretch for Co(II) and Cu(II) (represented in the pink box in Figure 6.24). This band however has a larger shift for Ni(II), appearing at 1593.5 cm^{-1} and consequently, this can be used as an immediate marker for Ni(II) coordination. Two further bands, highlighted in the yellow and orange boxes, also exhibit a specific shift for Ni(II) coordination. These bands are believed to be due to aromatic stretches, and from Table 6.10, it can be seen that these stretches occur at 1335.5 and 1537.5 cm^{-1} for both Co(II) and Cu(II). However, these bands exhibit relatively large shifts to 1346.5 and 1531 cm^{-1} for Ni(II) and as a result, Ni(II) can be clearly discriminated from

the uncomplexed SALTSC ligand and all other SALTSC-complexes tested. The SERS spectra of the SALTSC complexes of Co(II) and Cu(II) are very similar, however minor differences can be found upon close examination of the SERS spectra. These include the slight frequency shift of the C=N stretch (around 1600 cm^{-1}) and the weak bands in the region of 1150 – 1250 cm^{-1}. These are probably due to a number of vibrational modes, most likely including C-H, C=N and C-C stretches. As these changes are subtle, it would be difficult to confidently distinguish between these two metal ions using this ligand.

6.12.3 PCA

In order to highlight the relationships between the samples, PCA was applied to the dataset. The resulting scores plot is shown in Figure 6.25, and the loadings can be found in Appendices XXVII and XXVIII.

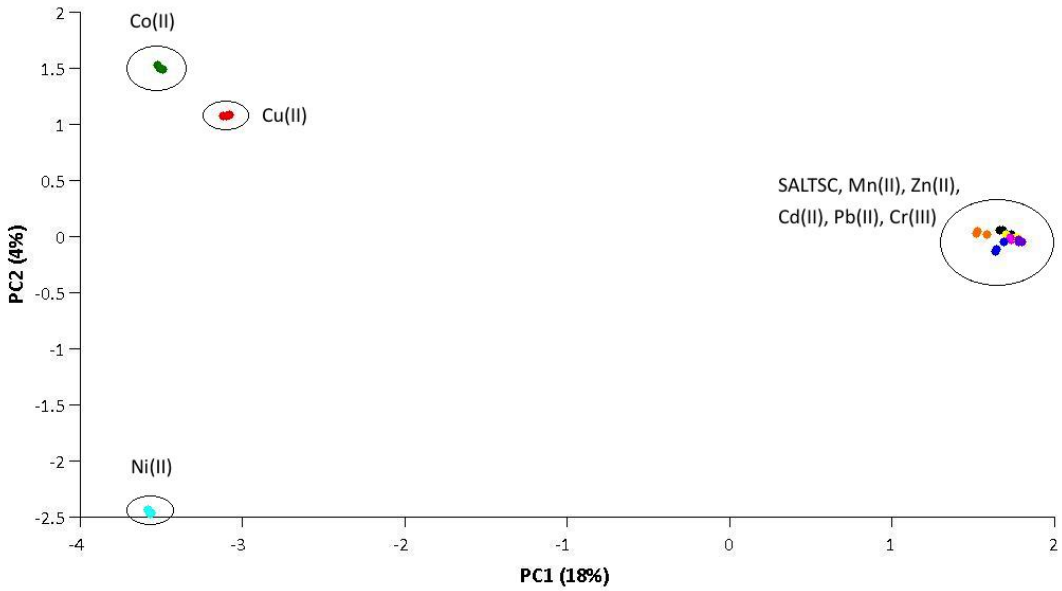

Figure 6.25: PCA scores of SALTSC and its metal complexes. Co(II), green; Cu(II), red; Ni(II), cyan; SALTSC, black; Mn(II), purple; Zn(II), pink; Cd(II), yellow; Pb(II), blue; Cr(III), orange.

The scores plot separates the Ni(II), Cu(II) and Co(II)-SALTSC complexes from all other species, as would be expected. No changes arose from the coordination of Mn(II), Zn(II), Cd(II), Pb(II) or Cr(III) and consequently, they are grouped with the free SALTSC ligand,

indicating that they all have very similar SERS spectra. Unsurprisingly, Ni(II), Cu(II) and Co(II) are well-separated from this grouping as it can be clearly seen that these metal ions significantly alter the SERS spectrum of SALTSC. Ni(II) changes the SERS spectrum of SALTSC most profoundly, as previously discussed, and therefore forms a well-distinct cluster away from all other samples. Co(II) and Cu(II) provide similar SERS spectra however, minor differences result in a slight separation of these two metal ions.

As only one metal ion could be clearly discriminated using this ligand, it was decided to discontinue with SALTSC, as Ni(II) could already be confidently identified using salen, along with three other metal ions. However, this ligand again demonstrates the potential of SERS to be used as an alternative technique for the detection of metal ions.

6.13 Chapter Conclusions

In this chapter, salen was used to coordinate to Ni(II), Cu(II), Co(II) and Mn(II) and these salen complexes were shown to induce unique changes in the SERS spectra that were specific to each metal ion. These changes were clear and discernible enough that no data analysis was necessary in order to distinguish each species however, PCA was applied in order to highlight the reproducibility between various metal ion concentrations. LOD studies were then performed in order to establish the sensitivity of this ligand. For LOD studies conducted using d.H_2O and synthetic f.H_2O, the detection limits for Ni(II), Cu(II) and Mn(II) were all below the recommended WHO limits in drinking water. Co(II) also produced a low LOD however a level is not set by the WHO as ultimately, most Co(II) ends up in soil and sediment. As low detection limits were obtained, investigation of the system using natural environmental samples was conducted. Firstly, f.H_2O was collected from Loch Thom in Greenock and these were spiked with varying concentrations of the metal ions of interest, in order to determine the sensitivity of this system in a real environmental sample. Unfortunately, an interferent was present which impeded the detection of the metal ions at low concentrations. As a result, the detection limits were much higher than those obtained using d.H_2O and were also above the recommended WHO levels. However, the concentrations present in the f.H_2O sample were very low and

did not pose a danger to the environment and consequently, this method was able to show that these species were not present at a harmful level.

Following on from this, a sample of contaminated f.H_2O was obtained from Gourock burn which is known to have leachate issues. This sample was not spiked and analysed as collected. The resulting SERS spectrum was almost identical to that of the salen-Mn(II) complex, apart from a couple of minor differences due to the more complex sample matrix. ICP-MS analysis confirmed that Mn(II) was present at a concentration of 833 ppb, which is above the WHO limit. This system was therefore shown to be capable of detecting this metal ion at a harmful level in a real environmental water sample.

As this method showed potential with f.H_2O, it was decided to examine the SERS response of metal-salen complexes in seawater, which has a much higher salinity. However, the high salt content of seawater resulted in over-aggregation of the AgNPs and consequently, the SERS response was drastically decreased compared to the d.H_2O and f.H_2O, samples. It was concluded therefore that this system would not be appropriate for seawater sampling.

Finally, as environmental waters may contain more than one of the metal ions of interest, mixtures of two metal were analysed. It was discovered that the SERS response resembled one metal ion more than the other, and so identification of both metal ions could easily be missed. Close examination of the spectra indicates the presence of a second metal ion however it was concluded that, although there are hints of a competing ion, the results were not conclusive enough to definitively identify the presence of two metal ions.

Due to the success of salen, further Schiff bases were investigated. Salophen was shown to provide a greater sensitivity however, the drawback of this ligand was the lack of selectivity, as only Ni(II) and Co(II) could be discriminated. SALTSC was also examined and this ligand was found to discriminate Ni(II), Cu(II) and Co(II). Although these ligands did not exceed the potential of salen to detect a number of metal ions, the results supported

the theory that SERS could be used as an alternative technique for the environmental monitoring of metal ions.

7 Conclusions

The aim of this project was to research new responsive nanomaterials that are capable of detecting a range of metal ions for applications in environmental monitoring. The idea behind this is to develop a simple, low-cost alternative to ICP-MS/ICP-AES that can be used for on-site monitoring of metal ions. Therefore, research was focussed on using one ligand to coordinate to metal ions, and using the spectral differences produced by each individual metal ion in order to discriminate between them. As a result, the same sample preparation and ligand is used for the analysis of all metal ions.

Initially, the ability of small Raman reporter molecules to discriminate between metal ions was investigated. The SERS spectra of 4-MBA and 4-MPY did produce subtle frequency shifts of certain bands upon complexation of different metal ions. However, these changes could only be observed at high metal ion concentrations and therefore, these ligands were not deemed suitable for environmental monitoring due to the lack of sensitivity.

Although these ligands were not ideal, they did however demonstrate that the vibrational spectra of certain ligands can change upon metal ion coordination. Therefore, it was hypothesised that chelating ligands would coordinate to the metal ions more strongly, resulting in more profound changes in the SERS spectra of the various complexes.

As bipy can chelate to a number of metal ions and produce a strong SERS signal, this ligand was investigated. It has been shown that six metal ions (Fe(II), Ni(II), Zn(II), Cu(II), Cd(II) and Cr(III)) can be clearly distinguished using a number of different bands in the SERS spectra of bipy, which uniquely changed depending on which species was coordinated. This enabled clear discrimination of the six different metal ions however, the sensitivity desired for environmental sensing was still not achieved, with only Cu(II) and Zn(II) capable of being detected below the recommended WHO limits in drinking water.

As bipy demonstrated that greater frequency shifts and intensity changes are produced with the chelating ligand compared to the small Raman reporter molecules of 4-MBA and 4-MPY, research continued using chelating ligands. Salen was selected next as Schiff bases

are also known to strongly coordinate to metal ions. With salen, a smaller range of metal ions can be detected (only four: Ni(II), Cu(II), Co(II) and Mn(II)), however the changes were much more pronounced and the identity of the metal ion present could be recognised immediately. The sensitivity of this ligand is also improved over bipy, with all metal ions capable of being detected below the recommended WHO limits. Due to this success, real environmental water samples were analysed using this system, where the presence of Mn(II) in a contaminated water sample was achieved.

The bipy and salen ligands can detect a wider range of metal ions compared to similar published work by Tsoutsi *et. al.* and Li *et. al.*, where these authors use terpyridine-modified NPs and L-cysteine functionalsed NPs respectively to discriminate between two metal ions.[69, 71] Our system also has the advantage of using the entire spectral region to discriminate between various metal ions, unlike Kim *et. al.* who use the single CN stretch of cyanide to detect five metal ions, which enables discrimination with greater confidence.[70] Although the detection limits in this work are not as sensitive as those demonstrated in these other publications, the detection limits for salen still fall below those reported by the WHO, and it has also been shown that the salen system can be used in real environmental samples, where high levels of Mn(II) can be successfully detected in contaminated water.

This research has therefore demonstrated the potential of SERS to be a useful tool for the on-site sampling of metal ions. The simple sample preparation used and the clear, characteristic SERS spectra produced by the different metal ions demonstrates its potential as a low-cost alternative to expensive laboratory-based instruments.

8 Future Work

It was clear from Chapter 4 that the small reporter molecules 4-MBA and 4-MPY did not provide the sensitivity required for environmental sensing. Other small Raman molecules, such as mercaptobiphenylcarbonitrile for example, could be investigated as the carbonitrile group should coordinate to a number of metal ions and provide a strong SERS band. However, as chelating ligands provided more sensitive analysis, it is suggested that further research should focus on these ligands.

Coordination of six different metal ions to bipy uniquely altered the bipy spectrum allowing discrimination of Fe(III), Zn(II), Ni(II), Cu(II), Cr(III) and Cd(II). However, this method lacked sensitivity and therefore a pre-concentration step would have to be developed in order to lower the detection limits and make it suitable for the environmental sensing of metal ions. It should also be noted that the concentration of bipy remained constant at 40 µM, even though the concentration of metal ions was lowered. As a result, a huge excess of bipy was present when low metal ion concentrations were added, and could therefore be masking the changes produced from the different metal-bipy complexes. If the concentration of bipy was decreased for the low metal ion concentrations, the characteristic changes may become visible resulting in improved detection limits. This system was also only tested using d.H_2O however, environmental waters are much more complex and may contain analytes that interfere with the detection of the metal ions. Therefore, in order to be used for environmental screening, real water samples, such as fresh, marine and seawater should be investigated in order to determine if this system performs with more realistic samples. As environmental samples are very complex, moving gradually from d.H_2O to tap water or synthetic f.H_2O before moving to real environmental samples would be recommended.

Salen proved to be the most successful ligand at providing a balance between selectivity and sensitivity. However, all research was conducted using water samples and there are other environmental media that can also be adversely affected by heavy metals. It would be interesting therefore to test the SERS sensor with other media such as soil, sediment

or air. Clearly, these samples are much more complex and therefore much greater sample preparation would be necessary.

As salen provided a very promising route to the detection of metal ions using SERS, it is suggested that other Schiff bases should also be investigated. Salophen has been investigated however, only Ni(II) and Co(II) could be discriminated from the other metal ions tested. However, the other four metal ions did show a very different SERS spectrum to the free salophen ligand, with a large increase in SERS response. This ligand could therefore be potentially used to indicate the general presence of metal ions, although only Ni(II) and Co(II) can be selectively detected. It is believed that this system would have a higher sensitivity and therefore provide improved detection limits over salen and the other ligands tested. Clearly, LOD studies would have to be undertaken to confirm this theory. As the extra constraint due to the bridging aromatic ring is thought to be the source of the loss of selectivity, the investigation of other, less rigid Schiff bases could help overcome this problem and there are numerous Schiff bases that can be easily prepared by varying the parent aldehyde/ketone and diamine groups.

Macrocycles and porphyrins are also known to strongly bind to metal ions and could be another class of ligands that could be pursued. However, the constrained system is again likely to impede the SERS detection of metal ions, however these ligands may potentially provide interesting results.

Another group of compounds that could be investigated are spectrophotometric reagents that are used as indicators for metal ions. For example, zincon is used for the determination of zinc and copper, dithizone is used for Cd, Cu, Hg, Zn and Pb, and Eriochrome Black T which is used to estimate Ca(II), Mg(II) and Zn(II) ions. All of these dyes should provide a strong Raman signal and could potentially be used for the SERS detection of various metal ions.

9 References

1. P. B. Tchounwou, C. G. Yedjou, A. K. Patlolla and D. J. Sutton, *EXS*, 2012, **101**, 133-164.
2. S. Eustis and M. A. El-Sayed, *Chemical Society Reviews*, 2006, **35**, 209-217.
3. I. Freestone, N. Meeks, M. Sax and C. Higgitt, *Gold Bulletin*, 2007, **40**, 270-277.
4. M. I. Stockman, *Physics Today*, 2011, **64**, 39-44.
5. M. Faraday, *Philosophical Transactions of the Royal Society of London*, 1857, **147**, 145-181.
6. J. Conde, G. Doria and P. Baptista, *Journal of Drug Delivery*, 2011, **2012**.
7. M.-C. Daniel and D. Astruc, *Chemical reviews*, 2004, **104**, 293-346.
8. P. K. Jain, K. S. Lee, I. H. El-Sayed and M. A. El-Sayed, *The Journal of Physical Chemistry B*, 2006, **110**, 7238-7248.
9. C. J. Murphy, T. K. Sau, A. M. Gole, C. J. Orendorff, J. Gao, L. Gou, S. E. Hunyadi and T. Li, *The Journal of Physical Chemistry B*, 2005, **109**, 13857-13870.
10. L. Guerrini and D. Graham, *Chemical Society Reviews*, 2012, **41**, 7085-7107.
11. V. M. Zamarion, R. A. Timm, K. Araki and H. E. Toma, *Inorganic Chemistry*, 2008, **47**, 2934-2936.
12. A. Smekal, *Naturwissenschaften*, 1923, **11**, 873-875.
13. C. V. Raman and K. S. Krishnan, *Nature*, 1928, **121**, 501-502.
14. E. Smith and G. Dent, *Modern Raman Spectroscopy - A Practical Approach*, John Wiley & Sons, 2005.
15. P. Larkin, *Infrared and Raman Spectroscopy; Principles and Spectral Interpretation*, Elsevier, 2011.
16. M. Fleischmann, P. J. Hendra and A. J. McQuillan, *Chemical Physics Letters*, 1974, **26**, 163-166.
17. D. L. Jeanmaire and R. P. Van Duyne, *Journal of Electroanalytical Chemistry and Interfacial Electrochemistry*, 1977, **84**, 1-20.
18. M. G. Albrecht and J. A. Creighton, *Journal of the American Chemical Society*, 1977, **99**, 5215-5217.
19. K. A. Willets and R. P. Van Duyne, *Annual Review of Physical Chemistry*, 2007, **58**, 267-297.
20. K. Kneipp, H. Kneipp, I. Itzkan, R. R. Dasari and M. S. Feld, *Journal of Physics: Condensed Matter*, 2002, **14**, R597-R624.
21. K. Faulds, A. Hernandez-Santana and W. E. Smith, in *Spectroscopic Properties of Inorganic and Organometallic Compounds: Techniques, Materials and Applications, Volume 41*, The Royal Society of Chemistry, 2010, vol. 41, pp. 1-21.
22. E. V. Efremov, F. Ariese and C. Gooijer, *Analytica Chimica Acta*, 2008, **606**, 119-134.

23. V. N. Pustovit and T. V. Shahbazyan, *The Journal of Chemical Physics*, 2012, **136**, 204701-204706.
24. G. E. Batley, *Integrated Environmental Assessment and Management*, 2012, **8**, 215-215.
25. M. Jaishankar, T. Tseten, N. Anbalagan, B. B. Mathew and K. N. Beeregowda, *Interdisciplinary Toxicology*, 2014, **7**, 60-72.
26. L. Järup, *British Medical Bulletin*, 2003, **68**, 167-182.
27. A. L. Benin, J. D. Sargent, M. Dalton and S. Roda, *Environmental Health Perspectives*, 1999, **107**, 279-284.
28. J. O. Nriagu, *Science of The Total Environment*, 1990, **92**, 13-28.
29. J. G. Farmer, L. J. Eades, M. C. Graham and J. R. Bacon, *Journal of Environmental Monitoring*, 2000, **2**, 49-57.
30. T. E. McKone and J. I. Daniels, *Regulatory Toxicology and Pharmacology*, 1991, **13**, 36-61.
31. M. De Lurdes Dinis and A. Fiúza, in *Environmental Heavy Metal Pollution and Effects on Child Mental Development: Risk Assessment and Prevention Strategies*, eds. I. L. Simeonov, V. M. Kochubovski and G. B. Simeonova, Springer Netherlands, Dordrecht, 2011, pp. 27-50.
32. J. O. Duruibe, M. O. C. Ogwuegbu and J. N. Egwurugwu, *International Journal of Physical Sciences*, 2007, **2**, 112-118.
33. C. J. Smith, S. D. Livingston and D. J. Doolittle, *Food and Chemical Toxicology*, 1997, **35**, 1107-1130.
34. AAS, GFAAS, ICP or ICP-MS? Which technique should I use?, http://www.thermo.com/eThermo/CMA/PDFs/Articles/articlesFile_18407.pdf, 2013).
35. W. E. Federation and A. P. H. Association, *American Public Health Association (APHA): Washington, DC, USA*, 2005.
36. A. M. Mitchell and M. G. Mellon, *Industrial & Engineering Chemistry Analytical Edition*, 1945, **17**, 380-382.
37. A. G. Howard and M. H. Arbab-Zavar, *Analyst*, 1980, **105**, 338-343.
38. H.-H. Wang, Q. Gan, X.-J. Wang, L. Xue, S.-H. Liu and H. Jiang, *Organic Letters*, 2007, **9**, 4995-4998.
39. J. Y. Kwon, Y. J. Jang, Y. J. Lee, K. M. Kim, M. S. Seo, W. Nam and J. Yoon, *Journal of the American Chemical Society*, 2005, **127**, 10107-10111.
40. P. Jiang and Z. Guo, *Coordination Chemistry Reviews*, 2004, **248**, 205-229.
41. C.-C. Huang and H.-T. Chang, *Analytical Chemistry*, 2006, **78**, 8332-8338.
42. R. Metivier, I. Leray and B. Valeur, *Chemical Communications*, 2003, 996-997.
43. E. M. Nolan and S. J. Lippard, *Journal of the American Chemical Society*, 2003, **125**, 14270-14271.
44. F. A. Abebe, C. S. Eribal, G. Ramakrishna and E. Sinn, *Tetrahedron Letters*, 2011, **52**, 5554-5558.
45. K. P. Carter, A. M. Young and A. E. Palmer, *Chemical Reviews*, 2014, **114**, 4564-4601.
46. Y.-X. Yuan, L. Ling, X.-Y. Wang, M. Wang, R.-A. Gu and J.-L. Yao, *Journal of Raman Spectroscopy*, 2007, **38**, 1280-1287.

47. A. Hakonen, P. O. Andersson, M. Stenbæk Schmidt, T. Rindzevicius and M. Käll, *Analytica Chimica Acta*, 2015, **893**, 1-13.
48. C. A. Mirkin, R. L. Letsinger, R. C. Mucic and J. J. Storhoff, *Nature*, 1996, **382**, 607-609.
49. S. S. R. Dasary, A. K. Singh, D. Senapati, H. Yu and P. C. Ray, *Journal of the American Chemical Society*, 2009, **131**, 13806-13812.
50. K. Kneipp, Y. Wang, R. R. Dasari, M. S. Feld, B. D. Gilbert, J. Janni and J. I. Steinfeld, *Spectrochimica Acta Part A: Molecular and Biomolecular Spectroscopy*, 1995, **51**, 2171-2175.
51. K.-C. Ho, P.-J. Tsai, Y.-S. Lin and Y.-C. Chen, *Analytical Chemistry*, 2004, **76**, 7162-7168.
52. H. Gu, K. Xu, C. Xu and B. Xu, *Chemical Communications*, 2006, 941-949.
53. D. S. Grubisha, R. J. Lipert, H.-Y. Park, J. Driskell and M. D. Porter, *Analytical Chemistry*, 2003, **75**, 5936-5943.
54. Y. Xue, H. Zhao, Z. Wu, X. Li, Y. He and Z. Yuan, *Analyst*, 2011, **136**, 3725-3730.
55. J. Liu and Y. Lu, *Journal of the American Chemical Society*, 2003, **125**, 6642-6643.
56. J. S. Lee, M. S. Han and C. A. Mirkin, *Angewandte Chemie*, 2007, **119**, 4171-4174.
57. X. Xue, F. Wang and X. Liu, *Journal of the American Chemical Society*, 2008, **130**, 3244-3245.
58. Y. Kim, R. C. Johnson and J. T. Hupp, *Nano Letters*, 2001, **1**, 165-167.
59. J. R. Kalluri, T. Arbneshi, S. Afrin Khan, A. Neely, P. Candice, B. Varisli, M. Washington, S. McAfee, B. Robinson and S. Banerjee, *Angewandte Chemie*, 2009, **121**, 9848-9851.
60. C.-Y. Lin, C.-J. Yu, Y.-H. Lin and W.-L. Tseng, *Analytical chemistry*, 2010, **82**, 6830-6837.
61. J. Xin, L. Miao, S. Chen and A. Wu, *Analytical Methods*, 2012, **4**, 1259-1264.
62. H. Li, Z. Cui and C. Han, *Sensors and Actuators B: Chemical*, 2009, **143**, 87-92.
63. J. Duan, M. Yang, Y. Lai, J. Yuan and J. Zhan, *Analytica Chimica Acta*, 2012, **723**, 88-93.
64. D. Han, S. Y. Lim, B. J. Kim, L. Piao and T. D. Chung, *Chemical Communications*, 2010, **46**, 5587-5589.
65. M. Mulvihill, A. Tao, K. Benjauthrit, J. Arnold and P. Yang, *Angewandte Chemie*, 2008, **120**, 6556-6560.
66. G. Q. Wang and L. X. Chen, *Chinese Chemical Letters*, 2009, **20**, 1475-1477.
67. J. Yin, T. Wu, J. Song, Q. Zhang, S. Liu, R. Xu and H. Duan, *Chemistry of Materials*, 2011, **23**, 4756-4764.
68. Ž. Krpetić, L. Guerrini, I. A. Larmour, J. Reglinski, K. Faulds and D. Graham, *Small*, 2012, **8**, 707-714.
69. D. Tsoutsi, L. Guerrini, J. M. Hermida-Ramon, V. Giannini, L. M. Liz-Marzan, A. Wei and R. A. Alvarez-Puebla, *Nanoscale*, 2013, **5**, 5841-5846.
70. K. Kim, J. W. Lee and K. S. Shin, *Analyst*, 2013, **138**, 2988-2994.
71. F. Li, J. Wang, Y. Lai, C. Wu, S. Sun, Y. He and H. Ma, *Biosensors and Bioelectronics*, 2013, **39**, 82-87.

72. in *Principles of Surface-Enhanced Raman Spectroscopy*, eds. E. C. L. Ru and P. G. Etchegoin, Elsevier, Amsterdam, 2009, pp. 529-535.
73. P. C. Lee and D. Meisel, *The Journal of Physical Chemistry*, 1982, **86**, 3391-3395.
74. J. Yguerabide and E. E. Yguerabide, *Analytical Biochemistry*, 1998, **262**, 137-156.
75. Y.-Q. Dang, H.-W. Li, B. Wang, L. Li and Y. Wu, *ACS Applied Materials & Interfaces*, 2009, **1**, 1533-1538.
76. S. J. Lee and M. Moskovits, *Nano Letters*, 2010, **11**, 145-150.
77. G. McNay, D. Eustace, W. E. Smith, K. Faulds and D. Graham, *Applied Spectroscopy*, 2011, **65**, 825-837.
78. A. Michota and J. Bukowska, *Journal of Raman Spectroscopy*, 2003, **34**, 21-25.
79. W. Wen-qiang Ma and Yan Fang and Gang-ling Hao and Wei-guo, *Chinese Journal of Chemical Physics*, 2010, **23**, 659.
80. G. Socrates, *Infrared and Raman Characteristic Group Frequencies: Tables and Charts*, Wiley, 2004.
81. F. Bonnier and H. J. Byrne, *Analyst*, 2012, **137**, 322-332.
82. L. Zhang, Y. Bai, Z. Shang, Y. Zhang and Y. Mo, *Journal of Raman Spectroscopy*, 2007, **38**, 1106-1111.
83. J. Hu, B. Zhao, W. Xu, B. Li and Y. Fan, *Spectrochimica Acta Part A: Molecular and Biomolecular Spectroscopy*, 2002, **58**, 2827-2834.
84. R. G. Pearson, *Journal of Chemical Education*, 1968, **45**, 581.
85. F. W. Cagle and G. F. Smith, *Analytical Chemistry*, 1947, **19**, 384-385.
86. G. H. Eom, H. M. Park, M. Y. Hyun, S. P. Jang, C. Kim, J. H. Lee, S. J. Lee, S.-J. Kim and Y. Kim, *Polyhedron*, 2011, **30**, 1555-1564.
87. R. A. Palmer and T. S. Piper, *Inorganic Chemistry*, 1966, **5**, 864-878.
88. W. W. Brandt, F. P. Dwyer and E. D. Gyarfas, *Chemical Reviews*, 1954, **54**, 959-1017.
89. A. G. Brolo, Z. Jiang and D. E. Irish, *Journal of Electroanalytical Chemistry*, 2003, **547**, 163-172.
90. D. P. Butcher, S. P. Boulos, C. J. Murphy, R. C. Ambrosio and A. A. Gewirth, *The Journal of Physical Chemistry C*, 2012, **116**, 5128-5140.
91. M. L. Moss and M. G. Mellon, *Industrial & Engineering Chemistry Analytical Edition*, 1942, **14**, 862-865.
92. WHO, *Iron in Drinking-water*, World Health Organisation, Geneva, 2003.
93. S. Kumar, D. N. Dhar and P. N. Saxena, *Journal of Scientific and Industrial Research*, 2009, **68**, 181-187.
94. A. Prakash and D. Adhikari, *International Journal of Chem Tech Research*, 2011, **3**, 1891-1896.
95. H. Schiff, *Justus Liebigs Annalen der Chemie*, 1864, **131**, 118-119.
96. P. G. Cozzi, *Chemical Society Reviews*, 2004, **33**, 410-421.
97. K. Brodowska and E. Łodyga-Chruścińska, *CHEMIK 2014*, **68**, 129-134.
98. K. C. Gupta and A. K. Sutar, *Coordination Chemistry Reviews*, 2008, **252**, 1420-1450.
99. A. Jarrahpour, D. Khalili, E. De Clercq, C. Salmi and J. M. Brunel, *Molecules*, 2007, **12**, 1720-1730.

100. C. M. da Silva, D. L. da Silva, L. V. Modolo, R. B. Alves, M. A. de Resende, C. V. B. Martins and Â. de Fátima, *Journal of Advanced Research*, 2011, **2**, 1-8.
101. Z. L. You and H. L. Zhu, *Zeitschrift für Anorganische und Allgemeine Chemie*, 2004, **630**, 2754-2760.
102. T. Jeewoth, M. G. Bhowon and H. L. K. Wah, *Transition Metal Chemistry*, 1999, **24**, 445-448.
103. N. Dharmaraj, P. Viswanathamurthi and K. Natarajan, *Transition Metal Chemistry*, 2001, **26**, 105-109.
104. V. K. Gupta, A. K. Singh, M. R. Ganjali, P. Norouzi, F. Faridbod and N. Mergu, *Sensors and Actuators B: Chemical*, 2013, **182**, 642-651.
105. L. Wang, D. Ye and D. Cao, *Spectrochimica Acta Part A: Molecular and Biomolecular Spectroscopy*, 2012, **90**, 40-44.
106. W. H. Hsieh, C.-F. Wan, D.-J. Liao and A.-T. Wu, *Tetrahedron Letters*, 2012, **53**, 5848-5851.
107. L. Wang, W. Qin and W. Liu, *Inorganic Chemistry Communications*, 2010, **13**, 1122-1125.
108. M. Hosseini, Z. Vaezi, M. R. Ganjali, F. Faridbod, S. D. Abkenar, K. Alizadeh and M. Salavati-Niasari, *Spectrochimica Acta Part A: Molecular and Biomolecular Spectroscopy*, 2010, **75**, 978-982.
109. L. Tang, F. Li, M. Liu and R. Nandhakumar, *Spectrochimica Acta Part A: Molecular and Biomolecular Spectroscopy*, 2011, **78**, 1168-1172.
110. Y. W. Choi, G. J. Park, Y. J. Na, H. Y. Jo, S. A. Lee, G. R. You and C. Kim, *Sensors and Actuators B: Chemical*, 2014, **194**, 343-352.
111. *Short-term Methods for Estimating the Chronic Toxicity of Effluents and Receiving Waters to Freshwater Organisms*, 2002.
112. D. H. Busch and J. C. Bailar, *Journal of the American Chemical Society*, 1956, **78**, 1137-1142.
113. K. Nakamoto, P. J. McCarthy and A. E. Martell, *Journal of the American Chemical Society*, 1961, **83**, 1272-1276.
114. J. A. Faniran, K. S. Patel and J. C. Bailar, *Journal of Inorganic and Nuclear Chemistry*, 1974, **36**, 1547-1551.
115. E. M. Nour, A. A. Taha and I. S. Alnaimi, *Inorganica Chimica Acta*, 1988, **141**, 139-144.
116. WHO, *Cobalt and Inorganic Cobalt Compounds*, World Health Organization, Geneva, 2006.
117. J. Cheng, K. Wei, X. Ma, X. Zhou and H. Xiang, *The Journal of Physical Chemistry C*, 2013, **117**, 16552-16563.
118. M. Datta, D. H. Brown and W. E. Smith, *Spectrochimica Acta Part A: Molecular Spectroscopy*, 1983, **39**, 37-41.
119. A. A. Soliman and W. Linert, *Monatshefte für Chemie - Chemical Monthly*, 2007, **138**, 175-189.
120. S. Muthu, E. Elamurugu Porchelvi, M. Karabacak, A. M. Asiri and S. S. Swathi, *Journal of Molecular Structure*, 2015, **1081**, 400-412.

10 Appendices

Appendix I: PC2 loading corresponding to the 4-MBA scores plot

Appendix II: PC3 loading corresponding to the 4-MBA scores plot

Appendix III: Full range SERS spectra of the 4-MPY functionalised AgNPs following addition of different metal ions

Appendix IV: PC2 loading corresponding to the 4-MPY scores plot

Appendix V: PC1 loading corresponding to the solid bipy complexes scores plot

Appendix VI: PC1 loadings corresponding to the bipy-metal complexes scores plot

Appendix VII: PC2 loadings corresponding to the bipy-metal complexes scores plot

Appendix VIII: SERS spectra of metal-salen complexes that did not provide an increased SERS response

Appendix IX: PC1 loadings corresponding to the scores plot of the salen-complexes

Appendix: X: PC2 loadings corresponding to the scores plot of the salen-complexes

Appendix XI: Comparison of the SERS spectra obtained from the metal-salen complexes using synthetic f.H_2O to those obtained using d.H_2O

Appendix XII: Semi-quantitative ICP-MS results of the f.H_2O collected from Loch Thom, Greenock

Appendix XIII: SERS spectra of salen following addition of Fe, Ca, Na and K

Appendix XIV: SERS spectrum obtained from the contaminated f.H_2O collected from Gourock burn

Appendix XV: Ni-salen SERS spectra obtained using $AgNO_3$ to precipitate out chloride from seawater (top) vs. SERS spectrum of Ni-salen in seawater without the addition of $AgNO_3$

Appendix XVI: SERS spectrum obtained after addition of both Ni(II) and Co(II) to salen, compared to the single ion spectra

Appendix XVII: SERS spectrum obtained after addition of both Cu(II) and Co(II) to salen, compared to the single ion spectra

Appendix XVIII: SERS spectrum obtained after addition of both Ni(II) and Cu(II) to salen, compared to the single ion spectra

Appendix XIX: SERS spectrum obtained after addition of both Ni(II) and Mn(II) to salen, compared to the single ion spectra

Appendix XX: ^{1}H NMR spectrum of salophen

Appendix XXI: ^{13}C NMR spectrum of salophen

Appendix XXII: SERS spectrum obtained from the free salophen ligand compared to that obtained from the Ni(II)-salophen complex

Appendix XXIII: PC1 loading corresponding to the scores plot of the salophen-complexes

Appendix XXIV: PC2 loading corresponding to the scores plot of the salophen-complexes

Appendix XXV: SERS spectra of different concentrations of SALTSC with no metal ions coordinated to the ligand

Appendix XXVI: SERS spectra of SALTSC-metal ion complexes that did not alter the spectrum of the ligand

Appendix XXVII: PC1 loading corresponding to the scores plot of the SALTSC-complexes

Appendix XXVII: PC2 loading corresponding to the scores plot of the SALTSC-complexes

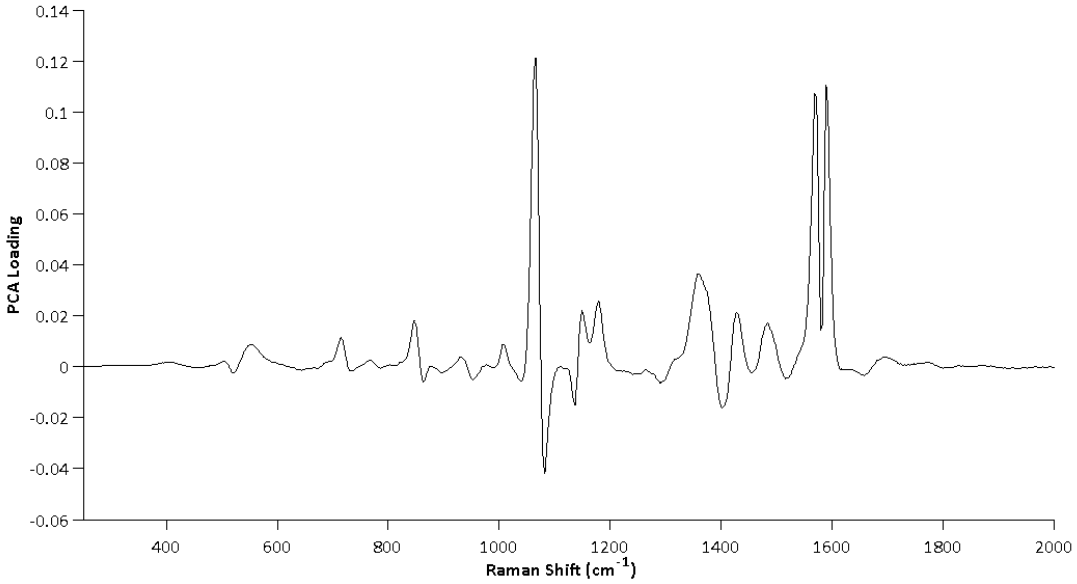

Appendix I: PC2 loading corresponding to the 4-MBA scores plot

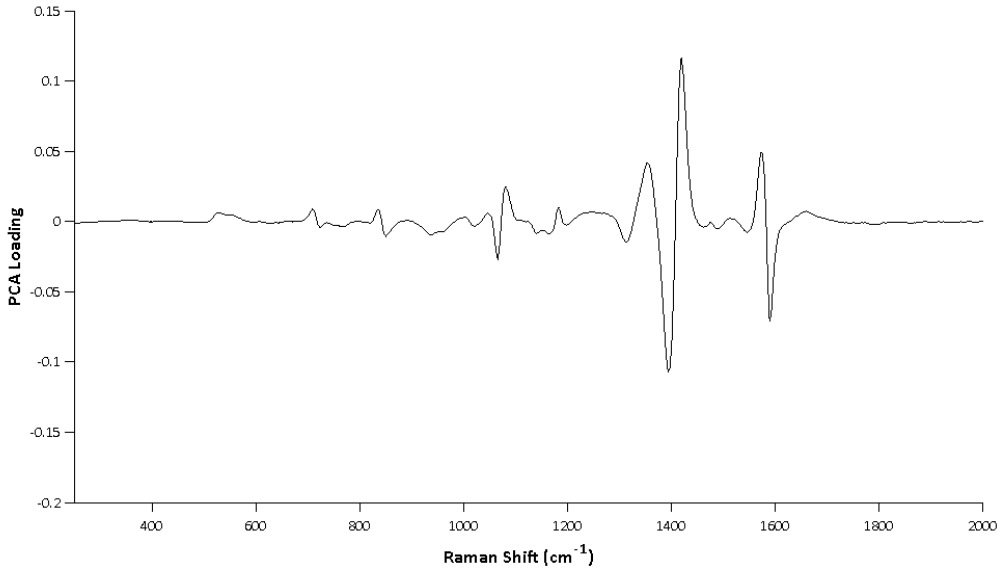

Appendix II: PC3 loading corresponding to the 4-MBA scores plot

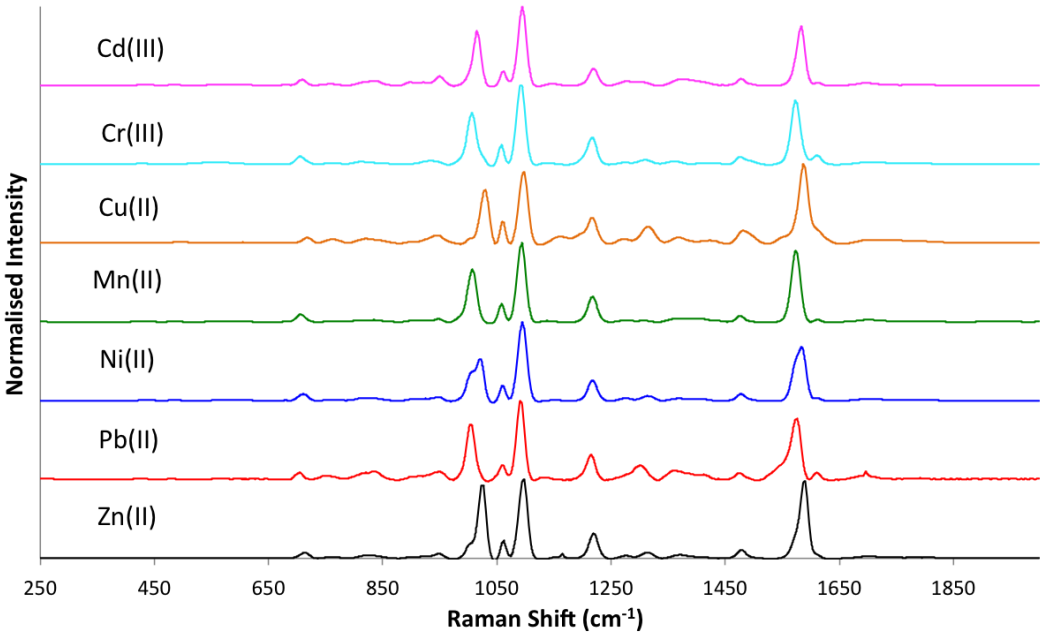

Appendix III: Full range SERS spectra of the 4-MPY functionalised AgNPs following addition of different metal ions (λ_{ex} = 532 nm, acc. time = 10 s)

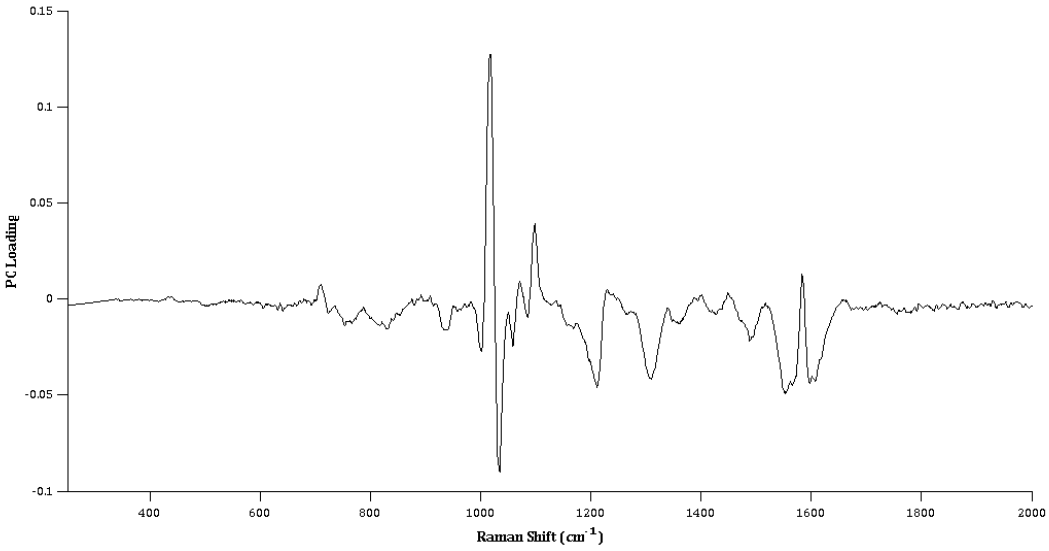

Appendix IV: PC2 loading corresponding to the 4-MPY scores plot

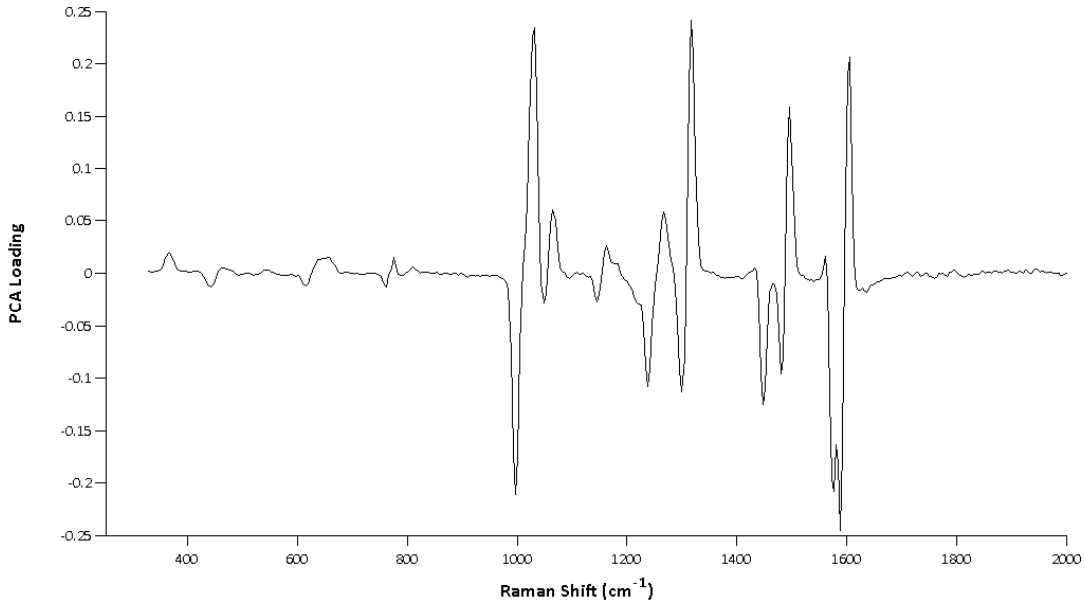

Appendix V: PC1 loading corresponding to the solid bipy complexes scores plot

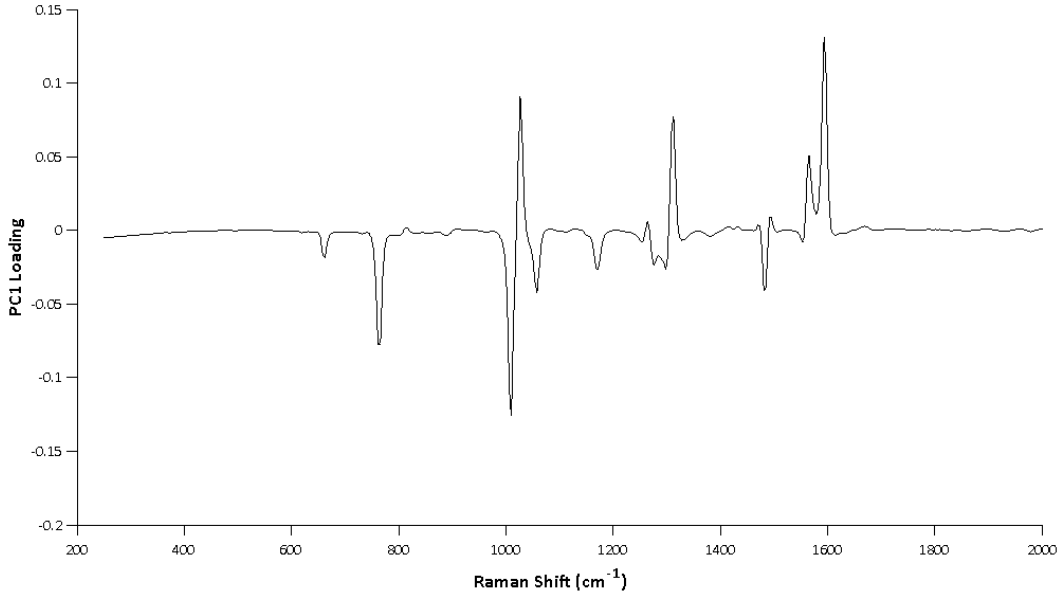

Appendix VI: PC1 loadings corresponding to the bipy-metal complexes scores plot

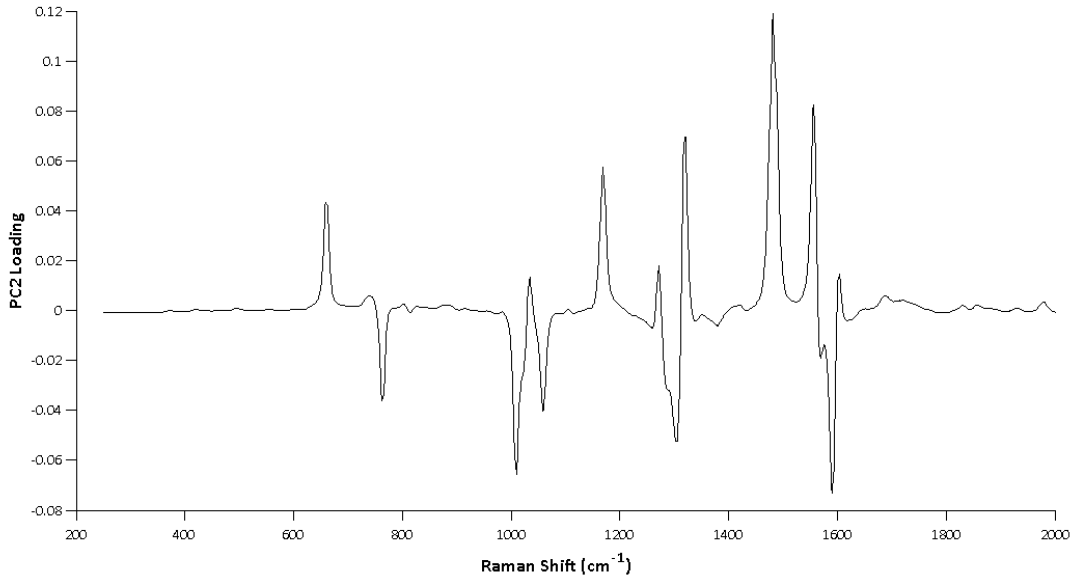

Appendix VII: PC2 loadings corresponding to the bipy-metal complexes scores plot

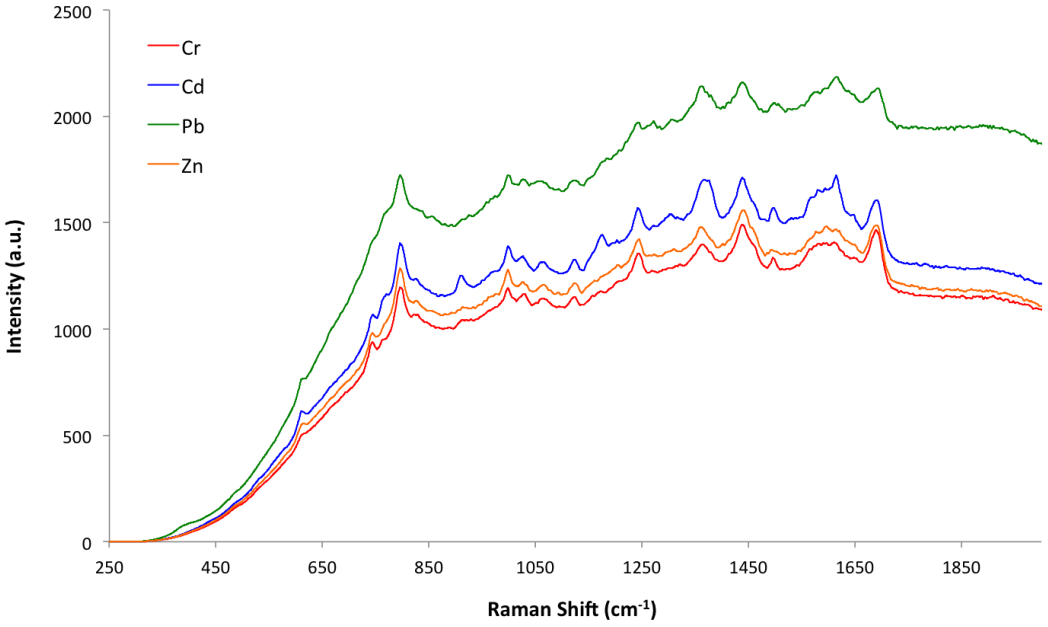

Appendix VIII: SERS spectra of metal-salen complexes that did not provide an increased SERS response (λ_{ex} = 532 nm, acc. time = 10 s)

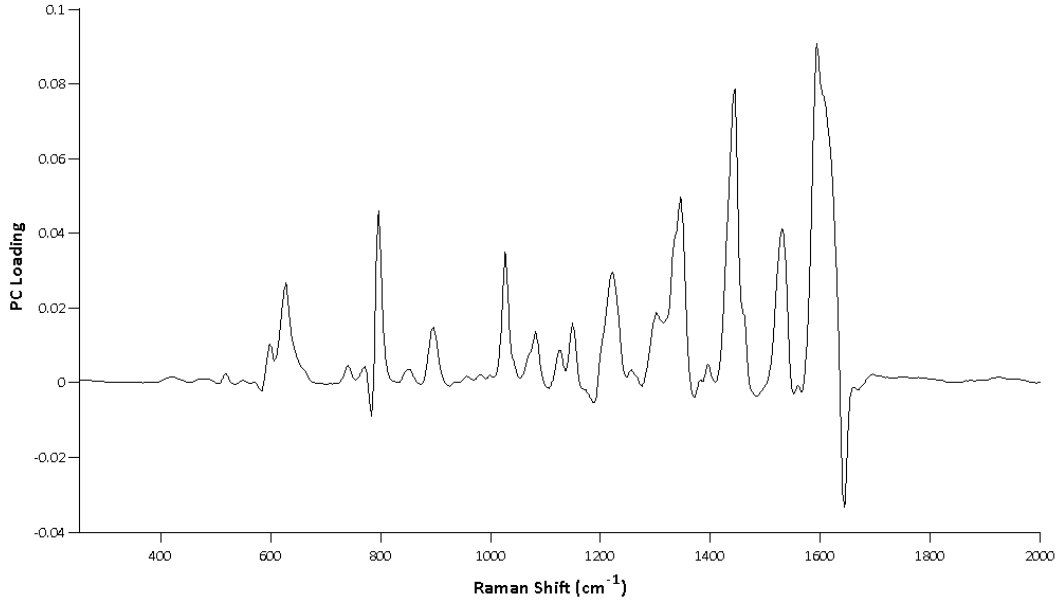

Appendix IX: PC1 loadings corresponding to the scores plot of the salen-complexes

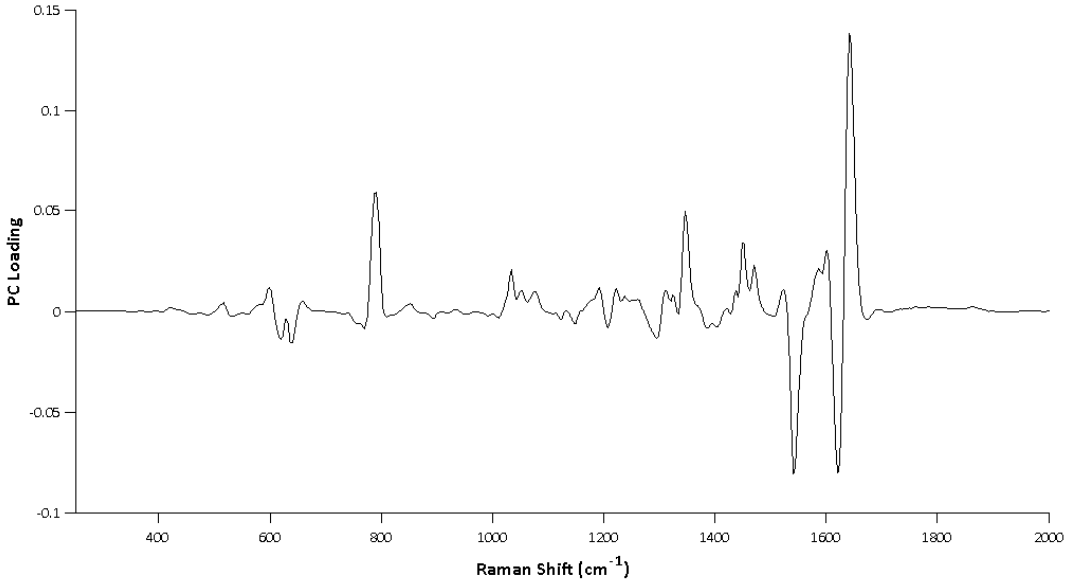

Appendix X: PC2 loadings corresponding to the scores plot of the salen-complexes

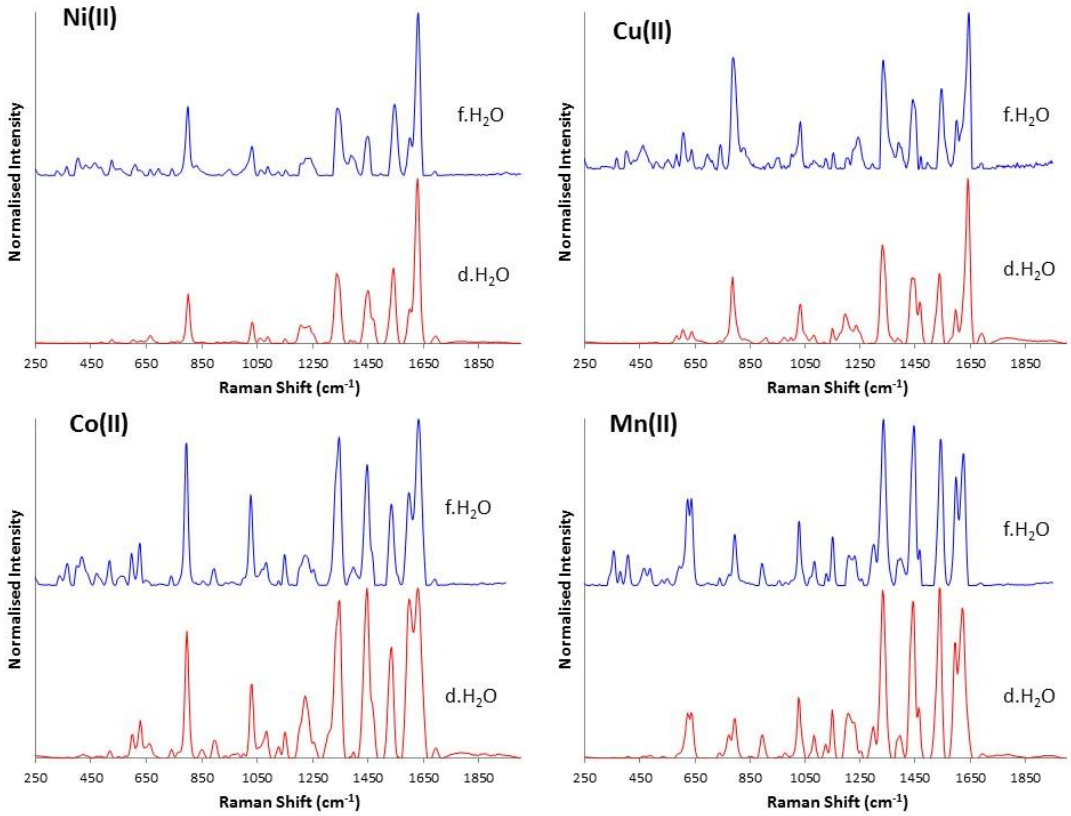

Appendix XI: Comparison of the SERS spectra obtained from the metal-salen complexes using synthetic f.H_2O to those obtained using d.H_2O (λ_{ex} = 532 nm, acc. time = 10 s)

Appendix XII: Semi-quantitative ICP-MS results of the f.H_2O collected from Loch Thom, Greenock

9 Be [1]		11 B [1]		12 C [1]		23 Na [1]		7 Li [1]	
Conc.	SQ Unit	Conc.	SQ Unit	Conc.	SQ Unit	Conc.	SQ Unit	Conc.	SQ Unit
0.00	ng/l	1.56	ug/l	3.45	mg/l	618.95	ug/l	45.44	ng/l
0.98	ng/l	1.66	ug/l	2.57	mg/l	651.00	ug/l	13.89	ng/l
-0.98	ng/l	1.62	ug/l	2.41	mg/l	683.75	ug/l	-4.04	ng/l
24 Mg [1]		27 Al [1]		28 Si [1]		31 P [1]		34 S [1]	
Conc.	SQ Unit	Conc.	SQ Unit	Conc.	SQ Unit	Conc.	SQ Unit	Conc.	SQ Unit
241.03	ug/l	58.77	ug/l	2.12	mg/l	6.07	ug/l	2.98	mg/l
246.21	ug/l	64.38	ug/l	2.22	mg/l	11.99	ug/l	3.38	mg/l
252.83	ug/l	62.38	ug/l	2.23	mg/l	5.97	ug/l	3.61	mg/l
35 Cl [1]		39 K [1]		42 Ca [1]		47 Ti [1]		51 V [1]	
Conc.	SQ Unit	Conc.	SQ Unit	Conc.	SQ Unit	Conc.	SQ Unit	Conc.	SQ Unit
3.11	mg/l	483.29	ug/l	1.12	mg/l	2.19	ug/l	102.71	ng/l
3.22	mg/l	496.77	ug/l	1.18	mg/l	1.68	ug/l	105.50	ng/l
3.43	mg/l	515.82	ug/l	1.22	mg/l	3.53	ug/l	138.59	ng/l
52 Cr [1]		55 Mn [1]		56 Fe [1]		59 Co [1]		60 Ni [1]	
Conc.	SQ Unit	Conc.	SQ Unit	Conc.	SQ Unit	Conc.	SQ Unit	Conc.	SQ Unit

61.74	ng/l	7.11	ug/l	158.19	ug/l	117.58	ng/l	1.04	ug/l
57.09	ng/l	7.26	ug/l	143.08	ug/l	146.21	ng/l	1.13	ug/l
64.30	ng/l	7.62	ug/l	153.41	ug/l	121.93	ng/l	1.03	ug/l
63 Cu [1]		66 Zn [1]		69 Ga [1]		75 As [1]		78 Se [1]	
Conc.	SQ Unit	Conc.	SQ Unit	Conc.	SQ Unit	Conc.	SQ Unit	Conc.	SQ Unit
2.75	ug/l	14.54	ug/l	4.43	ug/l	1.14	ug/l	26.27	ug/l
2.91	ug/l	11.95	ug/l	4.95	ug/l	921.82	ng/l	14.83	ug/l
5.77	ug/l	12.74	ug/l	4.32	ug/l	608.42	ng/l	18.08	ug/l
79 Br [1]		85 Rb [1]		88 Sr [1]		89 Y [1]		90 Zr [1]	
Conc.	SQ Unit	Conc.	SQ Unit	Conc.	SQ Unit	Conc.	SQ Unit	Conc.	SQ Unit
256.67	ug/l	5.32	ug/l	240.94	ug/l	896.42	ng/l	2.12	ug/l
259.59	ug/l	5.82	ug/l	253.28	ug/l	731.94	ng/l	1.22	ug/l
263.56	ug/l	5.86	ug/l	248.09	ug/l	928.40	ng/l	1.74	ug/l
93 Nb [1]		95 Mo [1]		101 Ru [1]		103 Rh [1]		105 Pd [1]	
Conc.	SQ Unit	Conc.	SQ Unit	Conc.	SQ Unit	Conc.	SQ Unit	Conc.	SQ Unit
41.48	ng/l	77.88	ng/l	<9.25814	ng/l	-57.21	ng/l	64.41	ng/l
135.64	ng/l	127.45	ng/l	<9.25814	ng/l	-108.19	ng/l	64.41	ng/l
162.85	ng/l	127.44	ng/l	<9.25814	ng/l	-86.43	ng/l	25.76	ng/l
107 Ag [1]		111 Cd [1]		118 Sn [1]		121 Sb [1]		125 Te [1]	
Conc.	SQ Unit	Conc.	SQ Unit	Conc.	SQ Unit	Conc.	SQ Unit	Conc.	SQ Unit
-10.27	ng/l	<24.58526	ng/l	-444.25	ng/l	381.80	ng/l	<528.00	ng/l
2.28	ng/l	<24.58526	ng/l	-152.88	ng/l	518.84	ng/l	<528.00	ng/l
17.11	ng/l	19.67	ng/l	458.94	ng/l	567.80	ng/l	<528.00	ng/l
127 I [1]		133 Cs [1]		137 Ba [1]		139 La [1]		140 Ce [1]	
Conc.	SQ Unit	Conc.	SQ Unit	Conc.	SQ Unit	Conc.	SQ Unit	Conc.	SQ Unit
36.80	ug/l	71.34	ng/l	180.06	ug/l	1.66	ug/l	2.62	ug/l
39.37	ug/l	117.87	ng/l	179.73	ug/l	1.94	ug/l	2.85	ug/l
40.90	ug/l	229.54	ng/l	185.81	ug/l	1.89	ug/l	2.95	ug/l
141 Pr [1]		146 Nd [1]		147 Sm [1]		153 Eu [1]		157 Gd [1]	
Conc.	SQ Unit	Conc.	SQ Unit	Conc.	SQ Unit	Conc.	SQ Unit	Conc.	SQ Unit
396.75	ng/l	1.14	ug/l	226.61	ng/l	154.28	ng/l	163.48	ng/l
587.36	ng/l	1.37	ug/l	226.62	ng/l	110.64	ng/l	232.49	ng/l
429.49	ng/l	1.17	ug/l	238.87	ng/l	121.55	ng/l	228.87	ng/l
159 Tb [1]		163 Dy [1]		165 Ho [1]		166 Er [1]		169 Tm [1]	
Conc.	SQ Unit	Conc.	SQ Unit	Conc.	SQ Unit	Conc.	SQ Unit	Conc.	SQ Unit
35.42	ng/l	171.62	ng/l	22.88	ng/l	119.93	ng/l	4.48	ng/l
20.76	ng/l	126.04	ng/l	24.65	ng/l	83.58	ng/l	6.47	ng/l
39.70	ng/l	168.95	ng/l	19.36	ng/l	69.04	ng/l	3.98	ng/l
172 Yb [1]		175 Lu [1]		178 Hf [1]		181 Ta [1]		182 W [1]	
Conc.	SQ Unit	Conc.	SQ Unit	Conc.	SQ Unit	Conc.	SQ Unit	Conc.	SQ Unit
24.76	ng/l	12.67	ng/l	76.58	ng/l	2.55	ng/l	63.20	ng/l
54.02	ng/l	18.58	ng/l	54.25	ng/l	1.91	ng/l	-2.34	ng/l
72.03	ng/l	8.44	ng/l	82.97	ng/l	1.91	ng/l	11.70	ng/l
185 Re [1]		189 Os [1]		193 Ir [1]		195 Pt [1]		197 Au [1]	

Conc.	SQ Unit	Conc.	SQ Unit	Conc.	SQ Unit	Conc.	SQ Unit	Conc.	SQ Unit
-20.01	ng/l	<12.16137	ng/l	3.84	ng/l	8.61	ng/l	51.86	ng/l
-16.38	ng/l	<12.16137	ng/l	0.00	ng/l	14.35	ng/l	162.65	ng/l
-25.47	ng/l	<12.16137	ng/l	-4.81	ng/l	17.22	ng/l	320.63	ng/l
202 Hg [1]		205 Tl [1]		208 Pb [1]		232 Th [1]		238 U [1]	
Conc.	SQ Unit	Conc.	SQ Unit	Conc.	SQ Unit	Conc.	SQ Unit	Conc.	SQ Unit
-47.67	ng/l	-185.57	ng/l	681.29	ng/l	-81.69	ng/l	76.17	ng/l
-27.24	ng/l	-212.07	ng/l	628.39	ng/l	29.23	ng/l	73.12	ng/l
-88.53	ng/l	-175.12	ng/l	1.09	ug/l	-46.67	ng/l	53.32	ng/l
45 Sc (ISTD) [1]		72 Ge (ISTD) [1]		115 In (ISTD) [1]		209 Bi (ISTD) [1]			
Conc.	SQ Unit	Conc.	SQ Unit	Conc.	SQ Unit	Conc.	SQ Unit		
N/A	ug/l	N/A	ug/l	N/A	ug/l	N/A	ug/l		
N/A	ug/l	N/A	ug/l	N/A	ug/l	N/A	ug/l		
N/A	ug/l	N/A	ug/l	N/A	ug/l	N/A	ug/l		

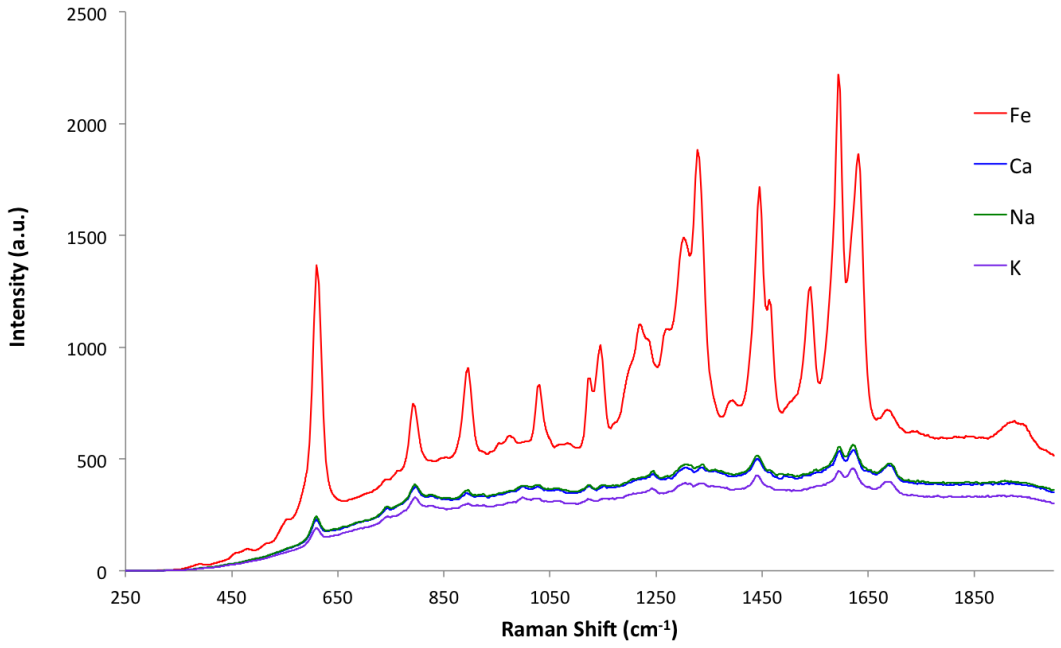

Appendix XIII: SERS spectra of salen following addition of Fe, Ca, Na and K (λ_{ex} = 532 nm, acc. time = 10 s)

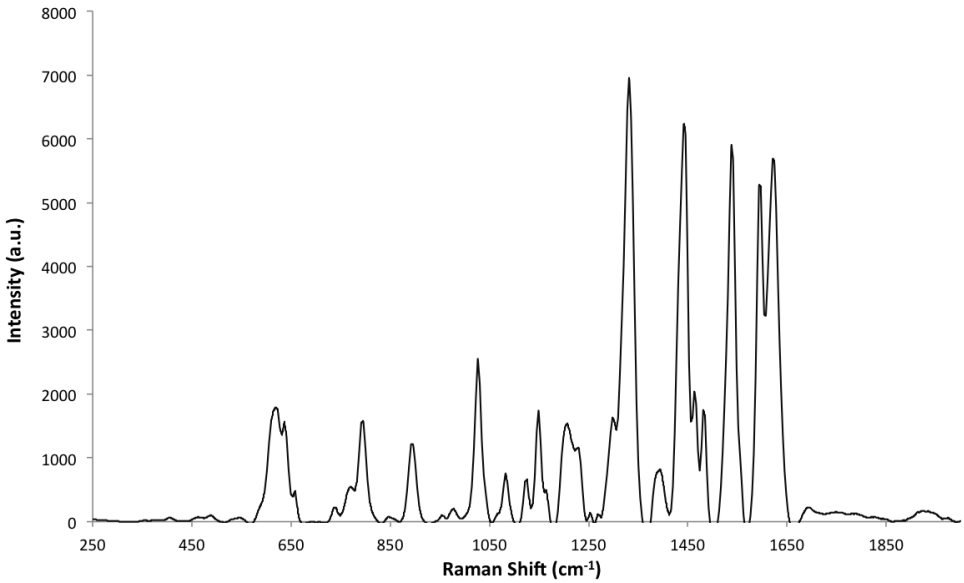

Appendix XIV: SERS spectrum obtained from the contaminated f.H_2O collected from Gourock burn

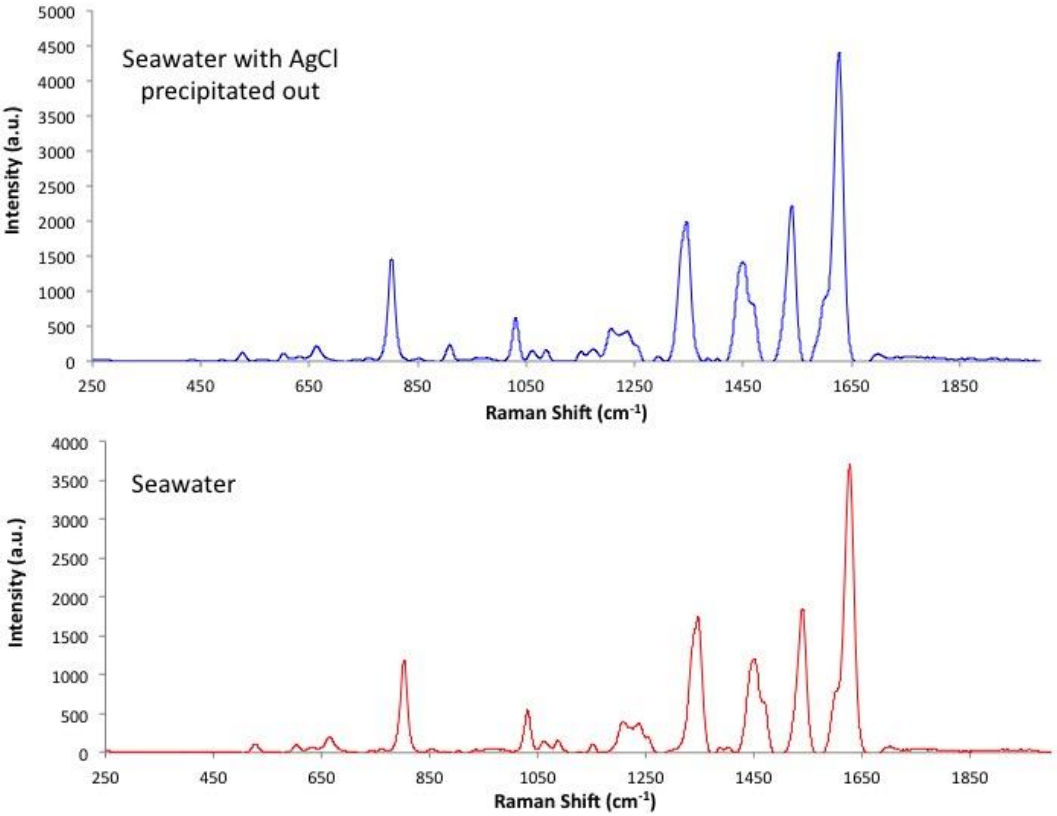

Appendix XV: Ni-salen SERS spectra obtained using $AgNO_3$ to precipitate out chloride from seawater (top) vs. SERS spectrum of Ni-salen in seawater without the addition of $AgNO_3$ (λ_{ex} = 532 nm, acc. time = 10 s)

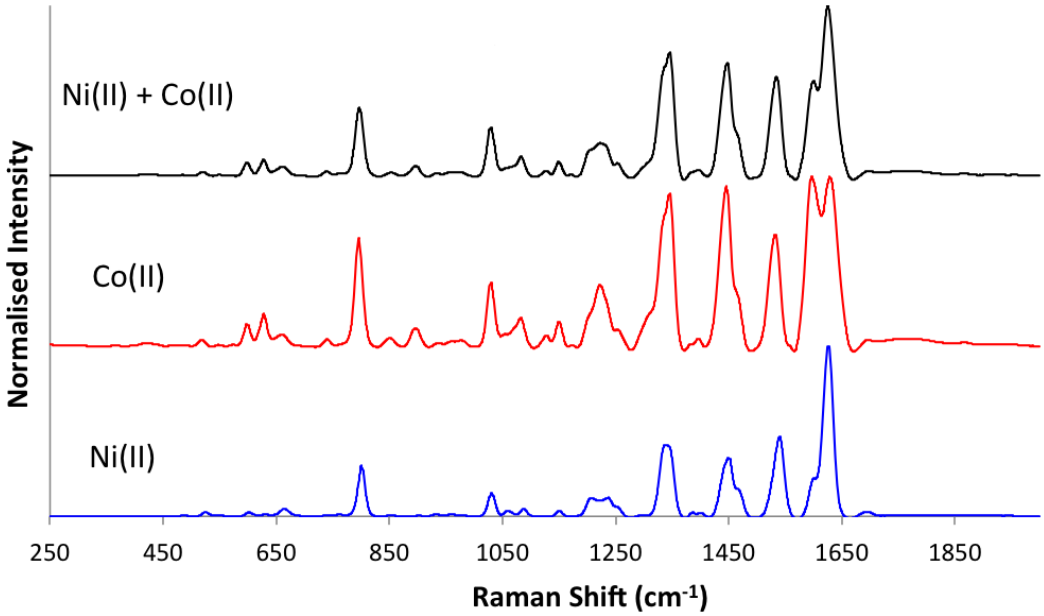

Appendix XVI: SERS spectrum obtained after addition of both Ni(II) and Co(II) to salen, compared to the single ion spectra (λ_{ex} = 532 nm, acc. time = 10 s)

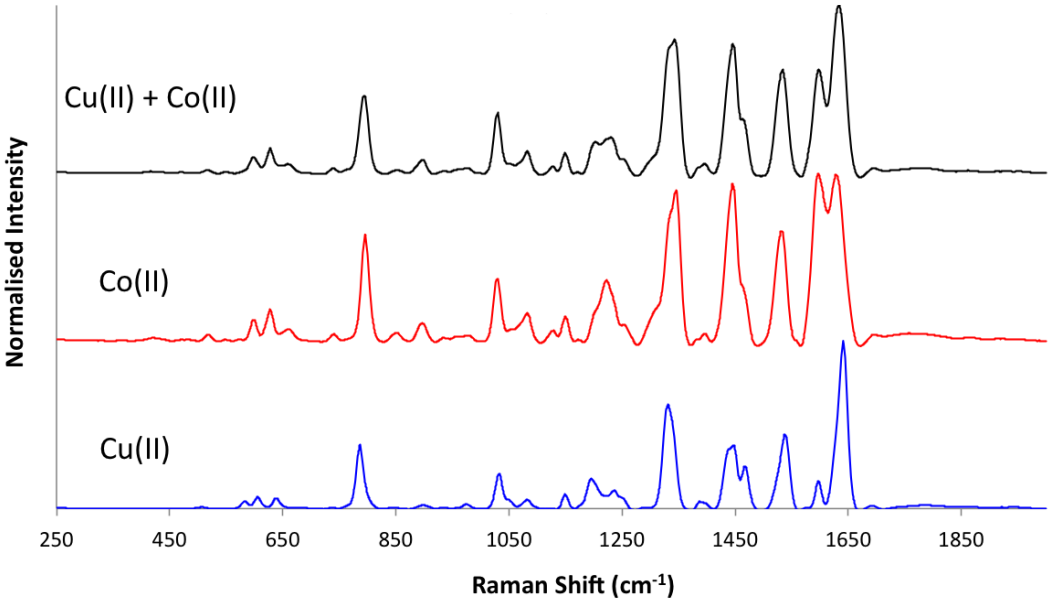

Appendix XVII: SERS spectrum obtained after addition of both Cu(II) and Co(II) to salen, compared to the single ion spectra (λ_{ex} = 532 nm, acc. time = 10 s)

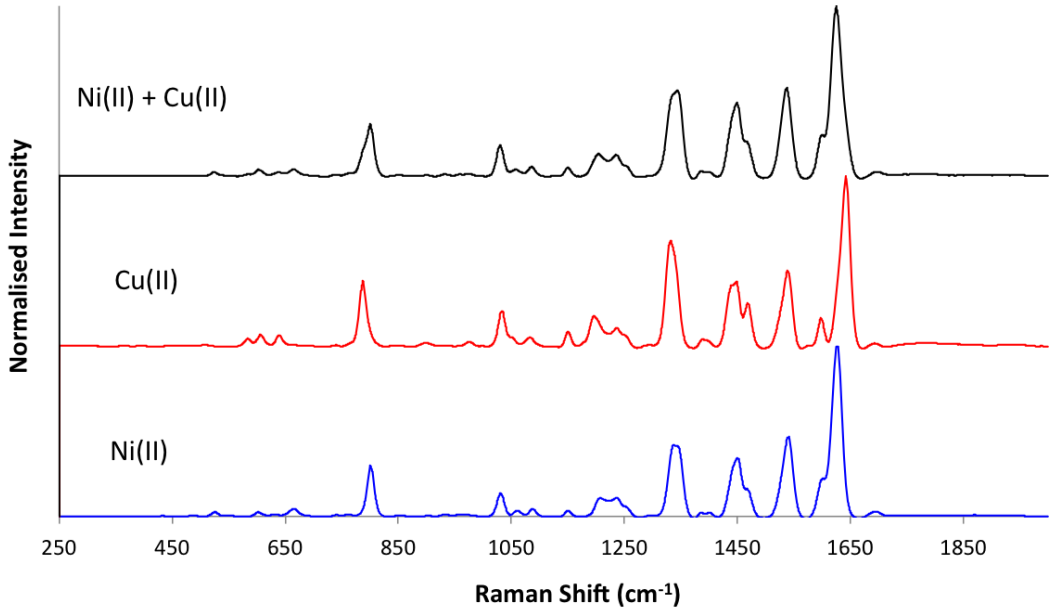

Appendix XVIII: SERS spectrum obtained after addition of both Ni(II) and Cu(II) to salen, compared to the single ion spectra (λ_{ex} = 532 nm, acc. time = 10 s)

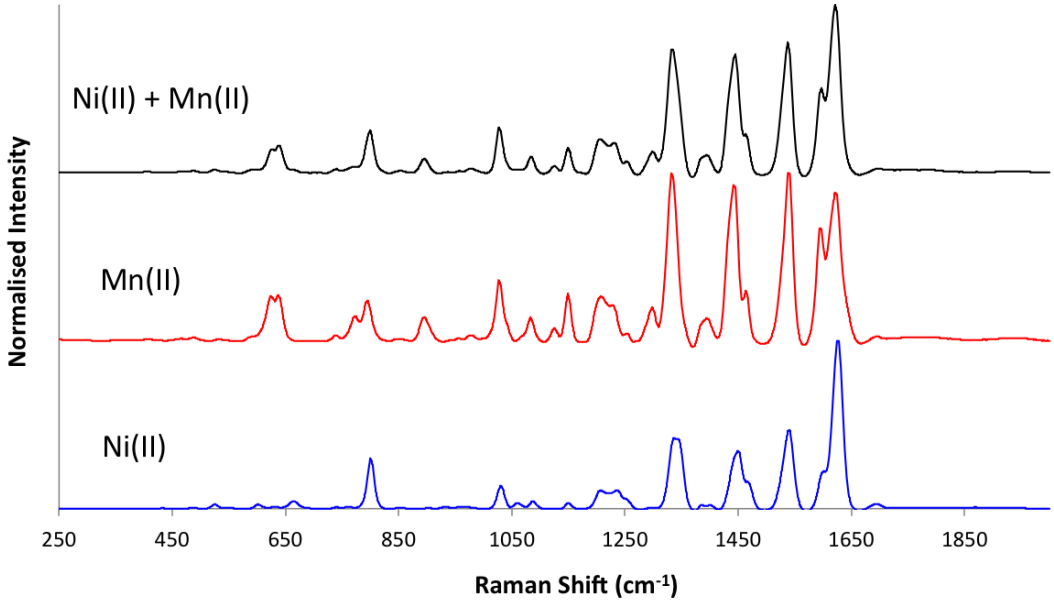

Appendix XIX: SERS spectrum obtained after addition of both Ni(II) and Mn(II) to salen, compared to the single ion spectra (λ_{ex} = 532 nm, acc. time = 10 s)

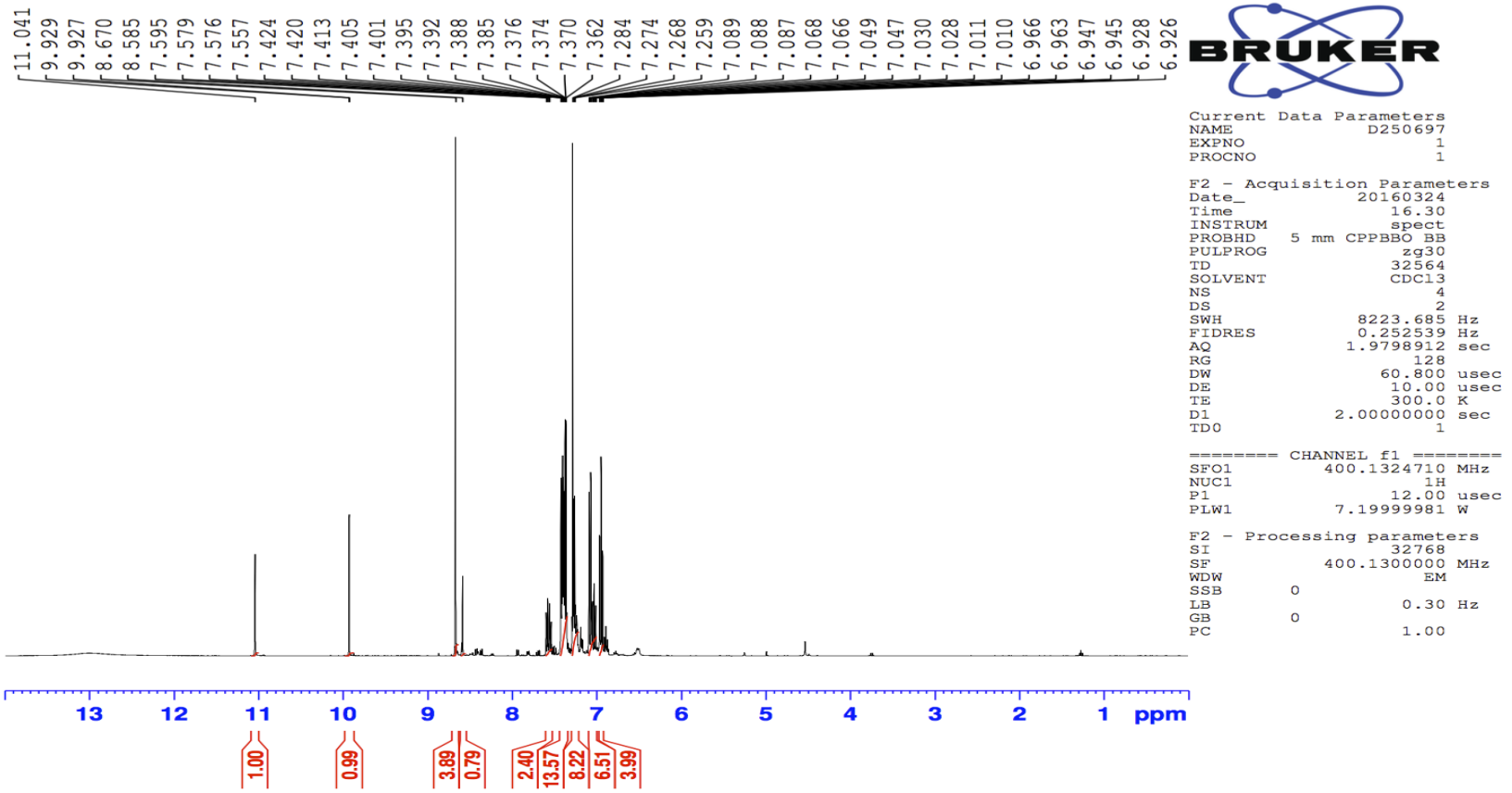

BRUKER

```
Current Data Parameters
NAME                  D250697
EXPNO                       1
PROCNO                      1

F2 - Acquisition Parameters
Date_              20160324
Time                  16.30
INSTRUM               spect
PROBHD    5 mm CPPBBO BB
PULPROG                zg30
TD                    32564
SOLVENT               CDCl3
NS                        4
DS                        2
SWH                8223.685 Hz
FIDRES             0.252539 Hz
AQ                 1.9798912 sec
RG                      128
DW                   60.800 usec
DE                   10.00 usec
TE                   300.0 K
D1                 2.00000000 sec
TD0                       1

======== CHANNEL f1 ========
SFO1            400.1324710 MHz
NUC1                    1H
P1                   12.00 usec
PLW1            7.19999981 W

F2 - Processing parameters
SI                    32768
SF              400.1300000 MHz
WDW                     EM
SSB       0
LB                    0.30 Hz
GB        0
PC                    1.00
```

Appendix XX: ^{1}H NMR spectrum of salophen

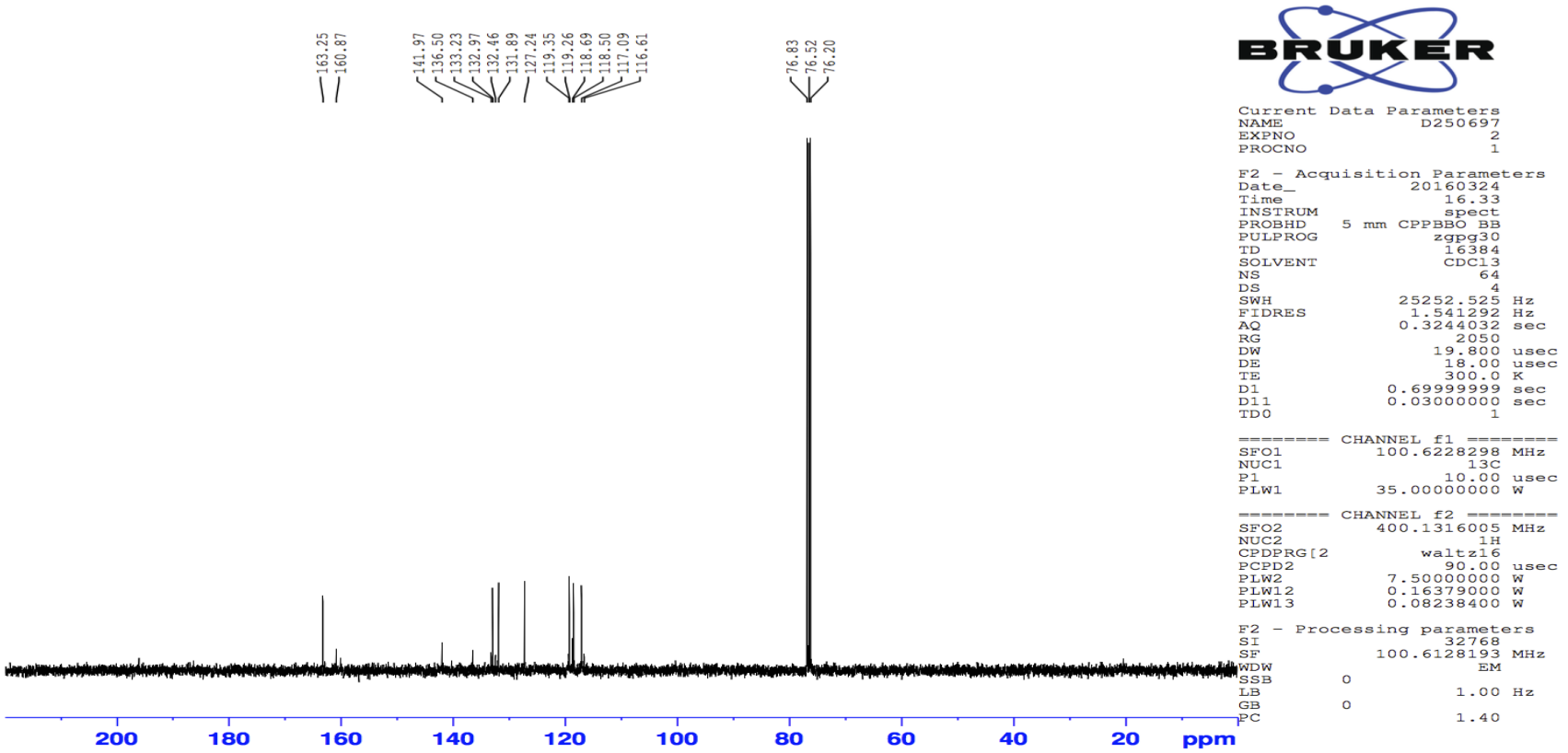

Appendix XXI: ^{13}C NMR spectrum of salophen

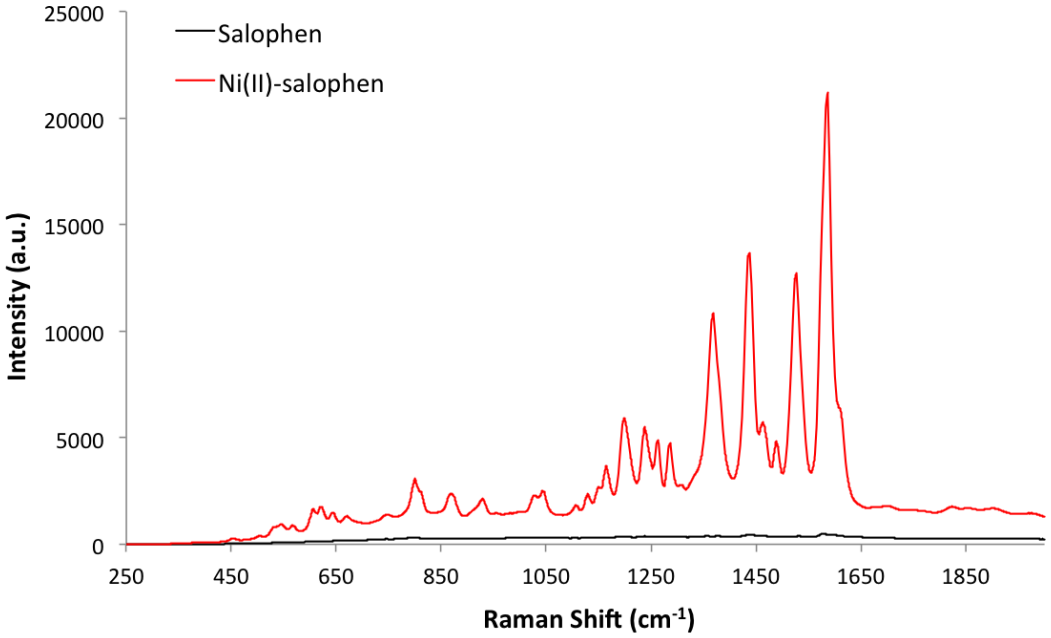

Appendix XXII: SERS spectrum obtained from the free salophen ligand compared to that obtained from the Ni(II)-salophen complex (λ_{ex} = 532 nm, acc. time = 10 s)

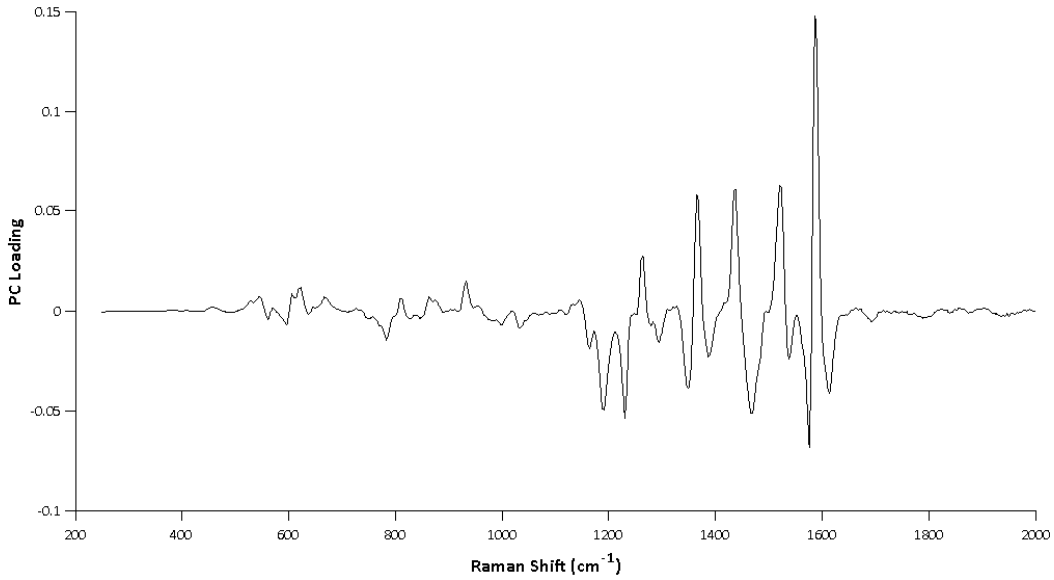

Appendix XXIII: PC1 loading corresponding to the scores plot of the salophen-complexes

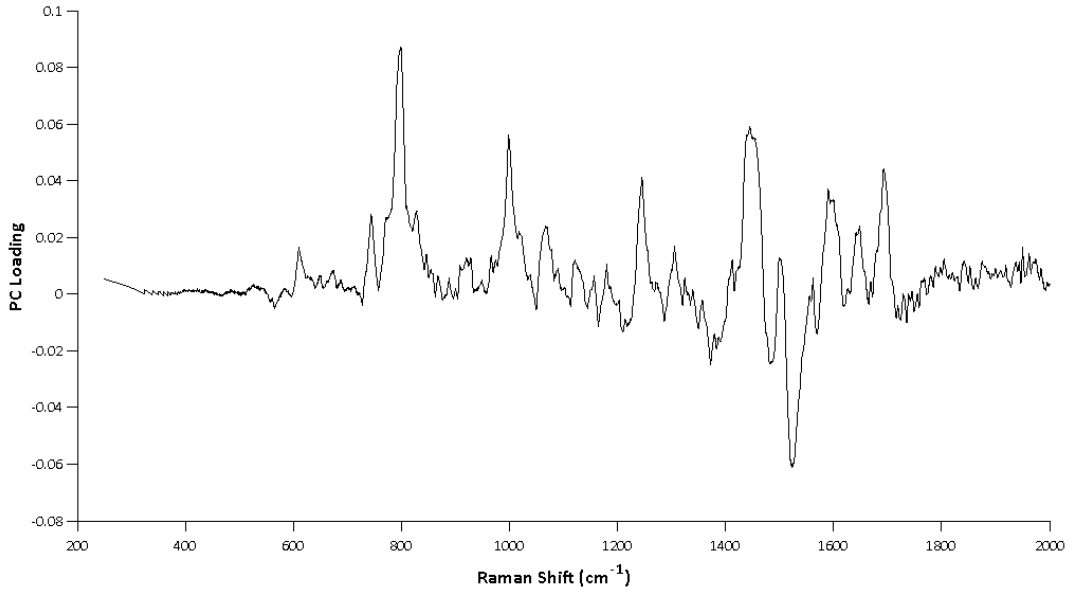

Appendix XXIV: PC2 loading corresponding to the scores plot of the salophen-complexes

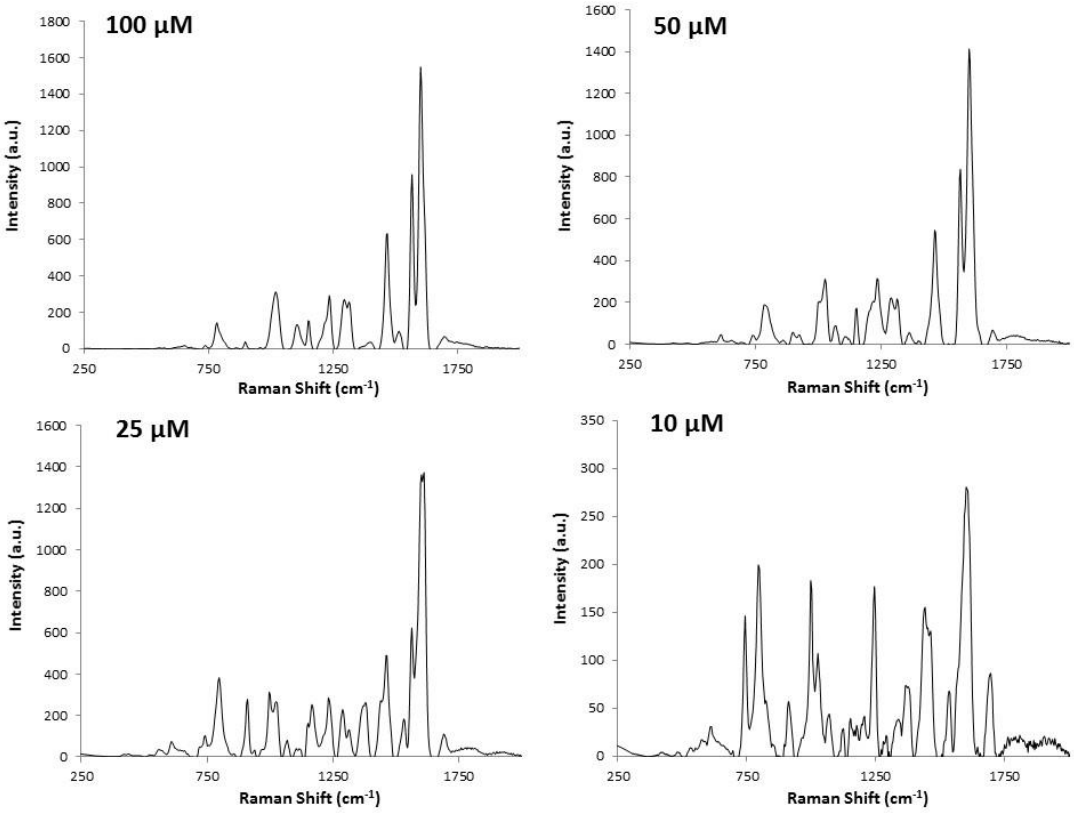

Appendix XXV: SERS spectra of different concentrations of SALTSC with no metal ions coordinated to the ligand (λ_{ex} = 532 nm, acc. time = 10 s)

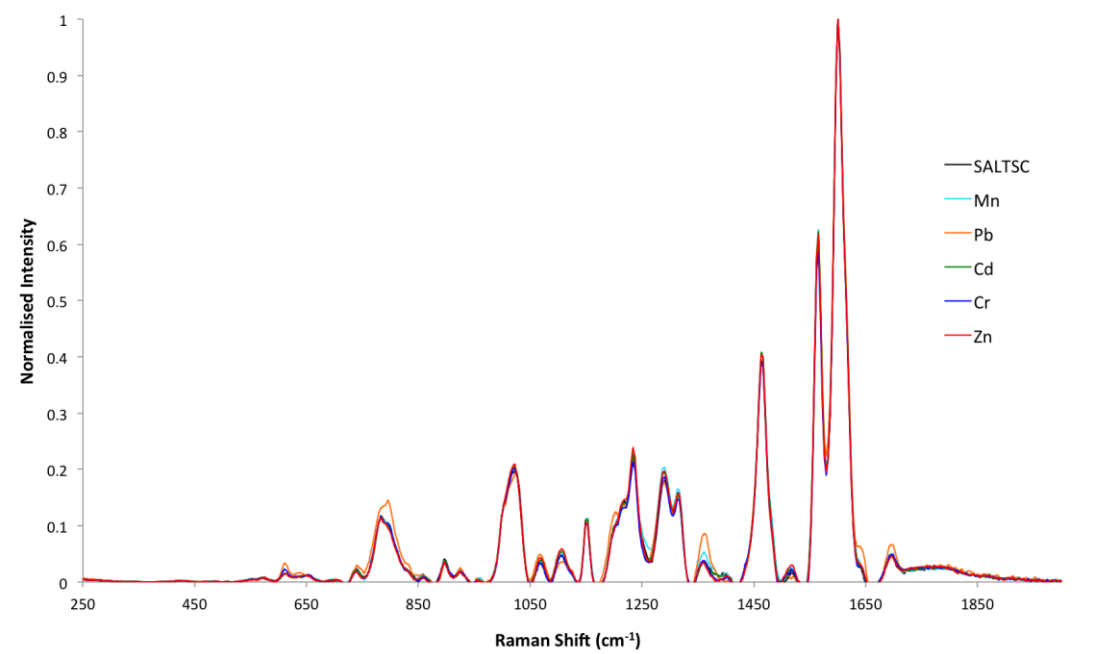

Appendix XXVI: SERS spectra of SALTSC-metal ion complexes that did not alter the spectrum of the ligand (λ_{ex} = 532 nm, acc. time = 10 s)

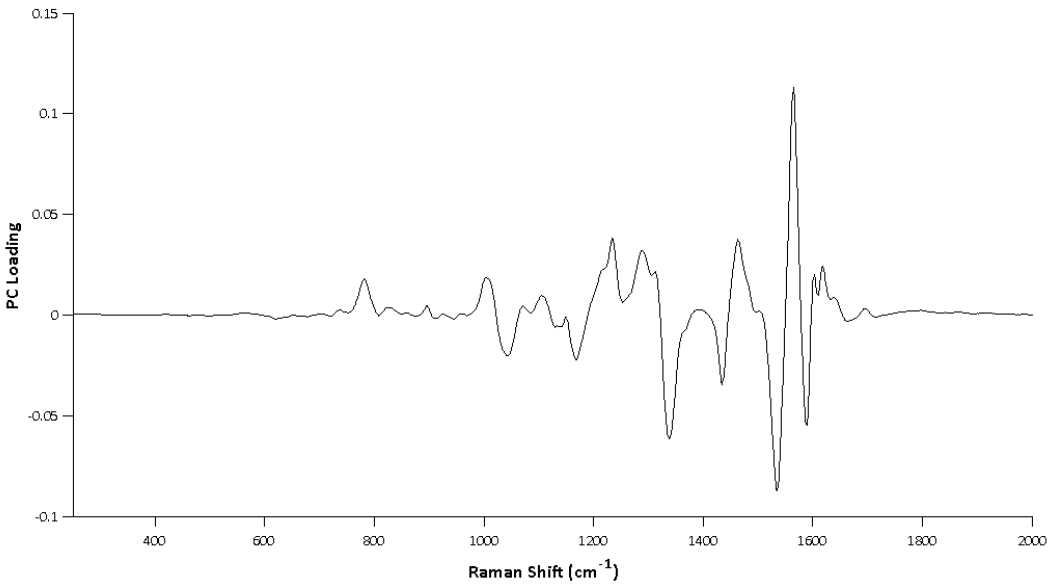

Appendix XXVII: PC1 loading corresponding to the scores plot of the SALTSC-complexes

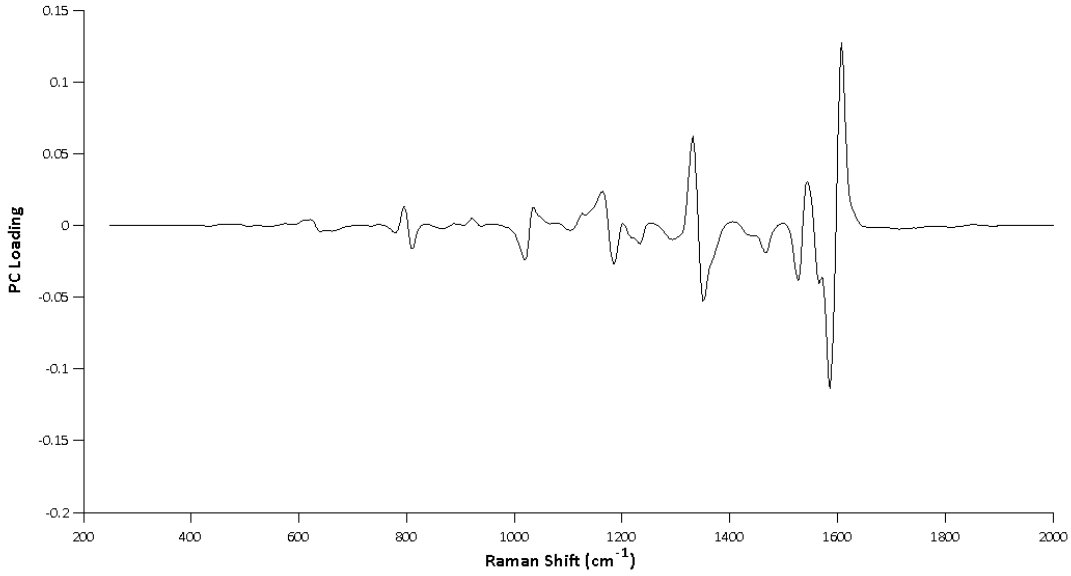

Appendix XXVIII: PC2 loading corresponding to the scores plot of the SALTSC-complexes

Analyst

PAPER

View Article Online
View Journal | View Issue

Cite this: *Analyst*, 2015, **140**, 6538

Determination of metal ion concentrations by SERS using 2,2′-bipyridyl complexes†

Julie Docherty,[a] Samuel Mabbott,[a] W. Ewen Smith,[a] John Reglinski,[b] Karen Faulds,[a] Christine Davidson[b] and Duncan Graham*[a]

Received 27th July 2015,
Accepted 21st August 2015

DOI: 10.1039/c5an01525a

www.rsc.org/analyst

Surface enhanced Raman scattering (SERS) can generate characteristic spectral "fingerprints" from metal complexes, thus providing the potential for the development of methods of analysis for the identification and quantitation of a range of metal ions in solution. The advantages include sensitivity and the use of one ligand for several metals without the need for a specific chromophore. Aqueous solutions of Fe(II), Ni(II), Zn(II), Cu(II), Cr(III) and Cd(II) in the presence of excess 2,2′-bipyridyl (bipy) were analysed using SERS. Specific marker bands enabled the identification of each metal ion and the limit of detection for each metal ion was estimated. Two of the ions, Zn(II) and Cu(II), could be detected below the World Health Organisation's (WHO) recommended limits for drinking water at levels of 0.22 and 0.6 mg L^{-1}, respectively.

Introduction

The identification and detection of metal ions in solution is important in environmental monitoring, industrial process monitoring and biomedical diagnostics.[1] There are several analytical techniques that are available for metal ion determination, such as inductively coupled plasma atomic emission and mass spectrometry (ICP-AES and ICP-MS), atomic absorption spectroscopy (AAS), ultraviolet-visible (UV-Vis) spectroscopy and fluorescence spectroscopy. Of these, ICP-AES and ICP-MS are the most commonly used techniques due to their high sensitivity and throughput capabilities.[2]

UV-Vis and fluorescence spectroscopy are less expensive and more flexible to apply. Using them requires a chromophore to detect metal ion concentrations and relies on detecting the absorption or emission of metal complexes. Among the many examples of the use of absorption spectroscopy are the colourimetric determination of nickel with dimethylglyoxime and arsenic determination using silver diethyldithiocarbamate.[3,4] Fluorescent sensors have also been developed for the detection of many metal ions.[5–11] These sensors are usually designed by linking a receptor molecule, which has a selective affinity for the metal ion of interest, to a fluorophore which exhibits changes in emission on binding to the ion.

Surface enhanced Raman scattering (SERS) can also be used for the detection of metal ions by forming metal complexes. The major advantage of SERS is that it can provide molecularly specific data enabling a range of metals to be identified from the complexes formed with one ligand. There is no need for a chromophore, although one can be present, enabling the use of a much wider range of ligands. As a result, SERS has significant potential to develop methods to unambiguously detect a range of metal ions with the same ligand using the same analytical procedure for each. SERS analysis can also provide lower detection limits than UV-Vis spectroscopy and the sensitivity can be comparable to that of fluorescence spectroscopy.[12] Another benefit of SERS is the wide availability of portable Raman spectrometers, which are becoming better, smaller and cheaper, making it an effective detection technique for the sensing of metal ions in field applications.[13]

SERS sensors using a reporter ligand for the analysis of a single metal ion species have been reported.[14–21] However, the discrimination of different metal ions using SERS has also been published.[22–24] For example, Kim *et al.* have used cyanide for the detection of Cr(III), Fe(III), Fe(II), Ni(II) and Mn(II).[25] The shift in the CN stretch on complexing was monitored using SERS. In the presence of trivalent ions, this band blue-shifted by up to 64 cm^{-1}, whereas for divalent metal ions, it was blue-shifted by 26–35 cm^{-1}. A low detection limit of 1 fM was reported making this method potentially useful for the detection of metal ions in environmental samples. Tsoutsi *et al.* have reported the use of terpyridine for the simultaneous detection of Cu(II) and Co(II) at ultratrace levels.[1] The terpyridine was attached to silver nanoparticles and used as a SERS substrate *via* the dithiocarbamate unit. Complexation with

[a]*Centre for Molecular Nanometrology, WestCHEM, Pure & Applied Chemistry, University of Strathclyde, Technology & Innovation Centre, 99 George Street, Glasgow, G1 1RD, UK. E-mail: duncan.graham@strath.ac.uk*
[b]*WestCHEM, Pure & Applied Chemistry, University of Strathclyde, 295 Cathedral Street, Glasgow, G1 1XL, UK*

†Electronic supplementary information (ESI) available. See DOI: 10.1039/c5an01525a

either Co(II) or Cu(II) produced changes in the vibrational SERS spectra of the terpyridine.

Here we report the use of the chelating ligand 2,2-bipyridyl (bipy) as a reporter as it is known to form complexes with many metals and therefore, one method could be used to detect many different metal ions. The technique is demonstrated using the characteristic spectra produced from Fe(II), Ni(II), Zn(II), Cu(II), Cd(II) and Cr(III) to identify each in solution and obtain detection limits. Bipy forms a red complex with Fe(II) ions which is used as a standard test but for other ions, the complexes formed are either colourless, or are only weakly coloured due to d to d transitions.[26]

Experimental

Chemicals

All reagents were purchased from Sigma-Aldrich and used as received.

Nanoparticle synthesis and characterisation

Silver citrate nanoparticles were prepared using a modified version of the Lee and Meisel method.[27] Briefly, 90 mg of silver nitrate, dissolved in 10 mL water, was added to 500 mL of water and heated to boiling under vigorous stirring. A 1% aqueous solution of sodium citrate was added slowly and the solution boiled for a further 20–30 min before being left to cool to room temperature.

The quality of the colloid was assessed using UV-Vis spectroscopy. Silver colloid made in this way should have a λ_{max} of approximately 400 nm and a full width at half maximum (FWHM) of less than 100 nm in order to be as reasonably close to being monodisperse. The extinction spectrum obtained for the colloid used in this work demonstrated a λ_{max} of 401 nm and a FWHM of approximately 90 nm.

Preparation of samples

Tris(*N*,*N*′-bipyridyl)zinc nitrate, bis(*N*,*N*′-bipyridyl) *O*,*O*′-nitratozinc nitrate and (*N*,*N*′-bipyridyl)zinc bromide were prepared using reported methods.[28]

A stock solution of bipy (5 mM) was prepared by dissolving 78 mg in 100 mL methanol, before dilution with water to reach a concentration of 400 μM. 10 mM stock solutions of the metal nitrate salts were also prepared by dissolving the appropriate amount in water. These were subsequently diluted to give the desired concentrations.

For SERS measurements, 25 μL of each metal ion was added to 25 μL of 400 μM bipy, which was left overnight to allow the complex to form completely. However, leaving the samples for less time also allows discrimination between the metal ions. The bipy–metal complex was then added to 200 μL of Ag citrate colloid before addition of 10 μL of 0.1 M NaCl to induce aggregation. Three replicates of each sample were then analysed using SERS. Metal nitrate salts were used with the exception of Fe(II) where the chloride salt was used instead as no nitrate salt of this metal was commercially available.

Instrumentation

UV-Vis spectra of a 1 in 10 dilution of the colloid in a 1 cm cuvette were collected using a Varian, Cary Win UV 300, dual beam scanning UV-Vis spectrometer (Agilent, Santa Clara, CA) in the wavelength range 200–800 nm.

Raman spectra of the solid bipy complexes were obtained using a WITec Alpha 300 R confocal microscope (WITec, Ulm, Germany) with 532 nm excitation wavelength.

Rapid SERS analysis was conducted using an Avalon Instruments Ltd RamanStation compact benchtop spectrometer (PerkinElmer, Waltham, MA). The system uses a 532 nm diode laser with a laser power of 100 mW. All measurements were carried out using a 10 s exposure time and a resolution of 0.5 cm^{-1} in the range 250–2000 cm^{-1}. The instrument is fitted with a motorised *x*–*y*–*z* sample stage, which accepts 96-well microtitre plates and the instrument's software was used to automatically drive the stage to each well in turn. The instrument was calibrated using an ethanol standard to ensure optimum distance between the sample and the laser aperture.

Results and discussion

Choice of bipy : metal ratio

Bipy can react with a wide range of metal ions to form mono-, bis- or tris-complexes depending on the metal ion and ligand concentration. SERS is sensitive to geometrical changes, consequently this must be taken into account when developing methods for the identification and detection of metal ions. For example, solid Zn(II)–bipy complexes, in each of the mono, bis and tris forms, were synthesised and their Raman spectra obtained (see ESI†). Principal Component Analysis (PCA) was applied to determine if each of the three forms were statistically different from one another, and the scores plot demonstrates that each complex can be successfully separated (Fig. 1). To develop a method to identify and quantify several metal ions, an excess of bipy is maintained ensuring that all complexes are present as the tris form.[29,30]

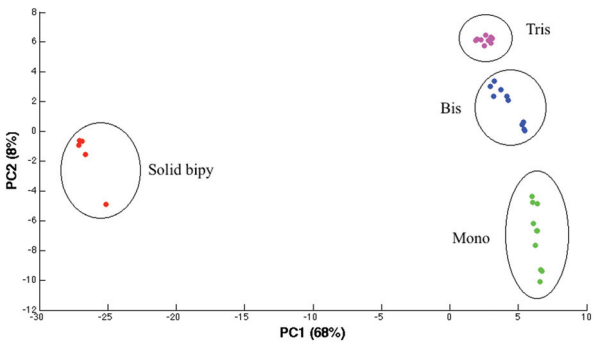

Fig. 1 Scores plot following PCA analysis of the Raman spectra of the solid bipy–Zn(II) complexes in the mono (green), bis (blue) and tris (pink) states. The uncomplexed ligand is also depicted (red) (λ_{ex} = 532 nm, acc. time = 10 s).

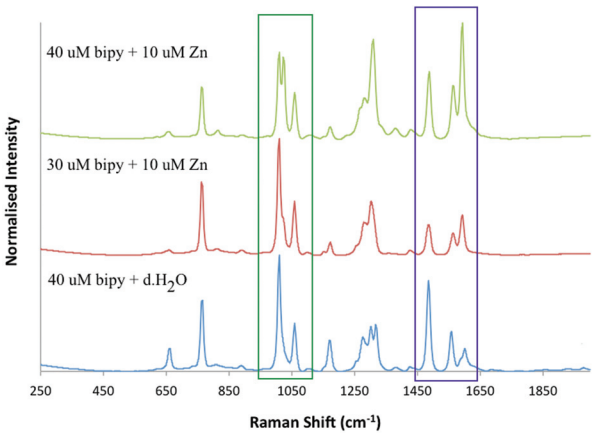

Fig. 2 Comparison of the SERS spectra obtained from 10 μM Zn(II) added to 40 μM (top, green) and 30 μM (middle, red) of bipy. The SERS spectrum of the uncomplexed bipy ligand is also shown (bottom, blue) (λ_{ex} = 532 nm, acc. time = 10 s).

To determine the concentration required to produce the tris complex, SERS was recorded from a series of solutions with equal volumes of between 10 to 100 μM bipy added to a 10 μM Zn(II) solution (see ESI†). The intensity of the aromatic stretches (1400–1600 cm^{-1}) increases with concentration, with the ring breathing mode (1010 cm^{-1}) being the most intense band in the spectrum at low concentrations. Another change is the appearance of a second peak at 1022 cm^{-1} close to the ring breathing mode at higher concentrations. It is thought that the band at 1010 cm^{-1} is due to the adsorption of bipy to the NP surface *via* the nitrogen atoms whereas the second band appearing at 1022 cm^{-1} is due to the Zn(II) complex of bipy. The tris complex forms between 40 μM and 30 μM, above which the spectrum is relatively stable (Fig. 2). A bipy : metal ratio of 4 : 1 was chosen for the method development as this excess forms tris complexes and good discrimination from the uncomplexed ligand.

SERS of 4 : 1 solutions of bipy with Fe(II), Ni(II), Zn(II), Cu(II), Cd(II) and Cr(III) are shown in Fig. 3. Both intensity and frequency changes were observed. The frequencies of the main bands are listed in Table 1 along with their assignments.[31,32]

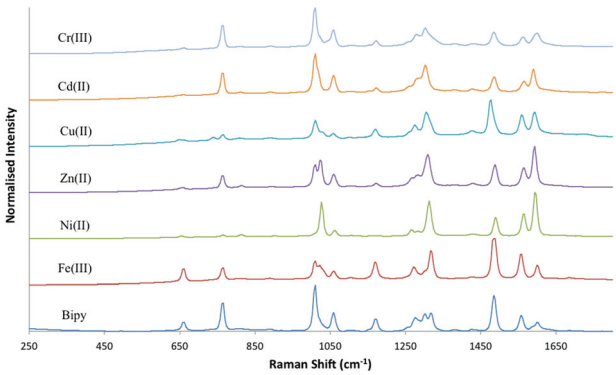

Fig. 3 SERS spectra of bipy complexes using 10 μM of each metal ion. Cr(III), light blue; Cd(II), orange; Cu(II), turquoise; Zn(II), purple; Ni(II), green; Fe(II), red; bipy, dark blue (λ_{ex} = 532 nm, acc. time = 10 s).

First row transition metals: iron to zinc

Fe(II) forms a red coloured complex with bipy, which has an absorption maximum at 522 nm.[26] This maximum occurs close to the exciting wavelength of 532 nm and consequently, molecular resonance will produce greater SERS enhancement for Fe(II) compared to the other metal ions.[33] Therefore, with a concentration of 10 μM Fe(II), signal saturation occurs. As a result, a lower concentration (*i.e.* 1 μM) is displayed in order to compare iron with the other ions. The main difference between Fe(II) and the other ions is the peak ratios of the aromatic stretches. It is evident that the band at 1484 cm^{-1}, attributed to a C=N stretch + C–H in-plane deformation, is the most intense whereas for the other metal ions, it is the bands at around 1010 or 1600 cm^{-1} which are most dominant. The difference in intensities is probably due to molecular resonance. As a result, these bands can be used to discriminate Fe(II) from Ni(II) and Zn(II). Whilst the ratio of the intensities of the Fe(II) aromatic bands are similar to those of the uncomplexed bipy ligand, they are greatly enhanced in the presence of Fe(II) as the stretch at 1484 cm^{-1} becomes the most intense band in the spectrum, compared to the ring breathing mode at 1010 cm^{-1} for uncomplexed bipy. As the metal ions interact *via* the lone pair of electrons on the nitrogens, it is

Table 1 Frequencies of the main bands in the SERS spectra of each metal ion along with their assignments

Wavenumber (cm^{-1})							
Free bipy	Fe(II)	Ni(II)	Zn(II)	Cu(II)	Cd(II)	Cr(III)	Assignment
1010	1010, 1022	1026	1010, 1022	1010 (sh: 1030)	1010	1010	Ring breathing
1275	1279	1267	1268	1275		1279 (sh: 1258)	Ring str. C–C, C–N + C–C inter-ring str. + C–H i.p. def.
1302		1283	1283		1302 (sh: 1280, 1262)	1302	C–C inter-ring str. (*trans*)
1317	1309	1309	1309	1312			C–C inter-ring str. (*cis*)
1485, 1558, 1600	1488, 1562, 1593	1488, 1565, 1594	1488, 1565, 1593	1474, 1559, 1590	1485, 1565, 1590	1484, 1562, 1600	Aromatic stretches

reasonable for the aromatic stretches, which have C=N character, to be affected by the coordination of metal ions. The Fe(II) spectrum also shows unique changes in the inter-ring stretches (~1300 cm^{-1}) that can also be used to help discriminate Fe(II) from the uncomplexed bipy and the other metal ions with greater confidence. Three inter-ring stretches are present in the free ligand spectrum whereas for Fe(II), only two, well-separated bands are observed at 1279 and 1309 cm^{-1}. Finally, a shoulder appears at the ring breathing stretch at 1022 cm^{-1} which assists in differentiating Fe(II)–bipy complexes from the uncomplexed ligand.

Zn(II) and Ni(II) give similar SERS profiles, however there are some differences which discriminate between the two ions. One difference occurs in the ring breathing mode, which is attributed to the physisorption of the nitrogen atoms on the NP surface in the uncomplexed ligand.[31] For Ni(II), this peak occurs at 1026 cm^{-1}, a relatively large blue-shift of 16 cm^{-1} due to the nitrogen atoms coordinating to Ni(II) ions and not physisorbing on the surface of the NP. For Zn(II) however, it is clear that two bands can be observed in the spectrum at 1010 and 1022 cm^{-1}. The difference in the intensity of the band at 1010 cm^{-1} may be due to excess uncomplexed ligand binding to the surface of the NP due to weaker surface attachment of the Zn(II)–bipy complex, whereas the 1022 cm^{-1} stretch is due to the Zn(II)–bipy complex. Nevertheless, this one band can be used to distinguish Zn(II) and Ni(II) from each other, and from the uncomplexed ligand. However, the shape of the bands associated with the inter-ring stretches also differ and therefore, can be used to identify either Ni(II) or Zn(II).

Copper

Copper is subject to the Jahn–Teller effect and forms complexes with distorted geometries. Consequently, the SERS spectrum of the Cu(II)–bipy complex is significantly different from the other first row metals (Fig. 3). The main marker band used for Cu(II) identification is the aromatic stretch at 1474 cm^{-1}. This band occurs between 1484 and 1488 cm^{-1} for all other complexes. The ratio of these aromatic stretches are also characteristic of Cu(II), and the shape of the inter-ring stretches also changes with two stretches observed at 1275 cm^{-1} and 1312 cm^{-1}. Finally, the ring breathing mode slightly differs from that observed in the SERS spectrum of the free ligand as a slight shoulder appears at 1030 cm^{-1}.

Other metals: cadmium and chromium

SERS of cadmium, a main group element, and chromium III, were also obtained (Fig. 3). The inter-ring stretches are the main distinguishing feature for the Cd(II)–bipy complex, with a strong band 1302 cm^{-1} and slight shoulders at 1262 and 1280 cm^{-1}. The aromatic stretches are also a useful indicator for Cd(II) coordination as the ratio of these bands differ from those of the uncomplexed bipy ligand and, although they are in a similar ratio to Ni(II) and Zn(II), their intensities are reduced greatly compared to these ions. The ratio of the aromatic stretches, along with the decreased intensity is a good indication of Cr(III) coordination. The inter-ring stretches

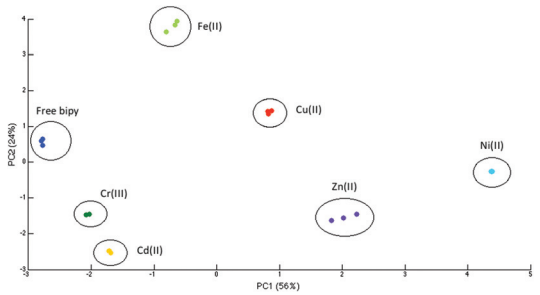

Fig. 4 PCA scores plot of all the metal–bipy complexes studied (3 replicates). Free bipy, dark blue; Fe(II), light green; Cu(II), red; Zn(II), purple; Ni(II), light blue; Cr(III), dark green; Cd(II), yellow.

change with only two bands visible at 1279 cm^{-1} and 1302 cm^{-1}. As a result, Cd(II) and Cr(III) can also be identified by SERS.

Principal component analysis

PCA was a used to extract the data and statistically highlight the differences between the samples, allowing the identification and differentiation of the various complexes. Fig. 4 displays the scores plot for each of the six metal ions, along with uncomplexed bipy. Each sample forms well-separated clusters, demonstrating that each metal–bipy complex has different spectroscopic features, which allow them to be unambiguously identified.

Concentration relationships

The concentration dependence of each complex was determined (Fig. 5) and the detection limits calculated.

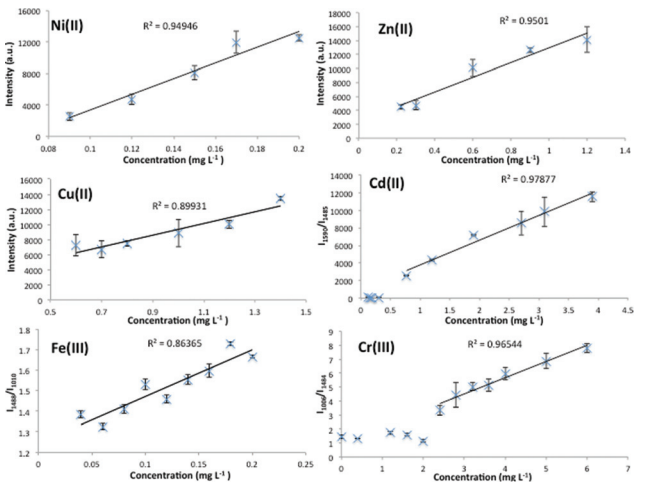

Fig. 5 Concentration relationships for all metal ions. Top left: Ni(II) (I_{1026} *vs.* conc.); top right: Zn(II) (I_{1022} *vs.* conc.); middle left: Cu(II) (I_{1474} *vs.* conc.); middle right: Cd(II) (I_{1590}/I_{1485} *vs.* conc.); bottom left: Fe(II) (I_{1488}/I_{1010} *vs.* conc.); bottom right: Cr(III) (I_{1006}/I_{1484} *vs.* conc.). Error bars represent the standard deviation between the three replicates (λ_{ex} = 532 nm, acc. time = 10 s).

Table 2 Estimated detection limits for all metal ions, compared to the recommended WHO guideline for drinking water

Metal ion	Detection limit (mg L^{-1})	WHO guideline (mg L^{-1})
Cd(II)	0.77 ± 0.07	0.003
Cr(III)	2.4 ± 0.2	0.005
Cu(II)	0.6 ± 0.06	2
Fe(II)	0.02 ± 0.0002	—
Ni(II)	0.087 ± 0.009	0.02
Zn(II)	0.22 ± 0.02	3

The graphs for Ni(II), Zn(II) and Cu(II) were obtained by using a band which was discernible by eye and also specific to each of these ions (1026, 1022 and 1474 cm^{-1}, respectively). The intensities of these bands were plotted against concentration, and the lowest observable detection limit for these species are listed in Table 2, along with the recommended WHO level in drinking water.[34] The uncertainty associated with each metal ion were also calculated by multiplying the % RSD by the LOD. It can be seen from this table that the observable limits for Zn(II) and Cu(II) are below the WHO guideline, suggesting that this system would be capable of detecting hazardous levels of these metal ions in drinking water. However, the limit of Ni(II) would have to be improved in order to detect Ni(II) at the levels necessary, as the level this system can detect is higher than the WHO recommendation.

For Fe(II), Cd(II) and Cr(III), peak ratios were used to determine the observable detection limit as intensity changes were the most unique indicator for the presence of these species. From the graphs, it can be seen that a good linear response is obtained, until a point where the ratios plateau. Again the observable limits are compared to the recommended limits in Table 2. Fe(II) does not have a recommended limit as Fe(II) salts in drinking water are insoluble and therefore precipitate out as insoluble Fe(III) hydroxide.[35] From the comparisons shown in the table, it is evident that the levels for Cd(II) and Cr(III) would also have to be improved to meet WHO limits.

Conclusions

In conclusion, it has been shown that different metal–bipy complexes have unique and characteristic SERS spectra, illustrating the potential of this method for metal ion analysis. Fe (II), Ni(II), Zn(II), Cu(II), Cr(III) and Cd(II) all show specific changes in the SERS spectrum of bipy, enabling the discrimination of these species. PCA was used to group the results according to the variation in their spectra, and each metal ion complex formed distinct clusters proving that they are statistically different from one another. Finally, concentration dependence studies were conducted to determine the sensitivity for each metal ion. A detection limit of 0.22 mg L^{-1} was calculated for Zn(II) and for Cu(II), 0.6 mg L^{-1}, both of which are lower than the recommended limits set out by the WHO. Therefore, this system is sensitive enough for the detection of these ions in environmental water samples, however testing real samples, *e.g.* fresh or marine waters, will have to be completed in order to test the system with more realistic environmental conditions. However, the detection limit for the other species are not sensitive enough to be used directly for environmental monitoring and any method would require a pre-concentration step or further method improvement. Although the detection limits for this system are not as low as for some other reported methods, a wide range of metal ions can be detected using a simple ligand. A number of changes were detected in the spectrum of each complex enabling the discrimination of each complex with greater confidence.

Acknowledgements

This work was supported by the Royal Society of Chemistry's Analytical Chemistry Trust Fund and the Natural Environment Research Council (NERC) [NE/J01771X/1]. DG thanks the Royal Society for support from a Wolfson Research Merit Award. The research data associated with this paper has the following DOI: 10.15129/38671508-b630-4276-820c-2fc6bdbe6fae.

Notes and references

1 D. Tsoutsi, L. Guerrini, J. M. Hermida-Ramon, V. Giannini, L. M. Liz-Marzan, A. Wei and R. A. Alvarez-Puebla, *Nanoscale*, 2013, **5**, 5841–5846.
2 O. T. Butler, W. R. L. Cairns, J. M. Cook and C. M. Davidson, *J. Anal. At. Spectrom.*, 2015, **30**, 21–63.
3 A. M. Mitchell and M. G. Mellon, *Ind. Eng. Chem., Anal. Ed.*, 1945, **17**, 380–382.
4 A. G. Howard and M. H. Arbab-Zavar, *Analyst*, 1980, **105**, 338–343.
5 H.-H. Wang, Q. Gan, X.-J. Wang, L. Xue, S.-H. Liu and H. Jiang, *Org. Lett.*, 2007, **9**, 4995–4998.
6 J. Y. Kwon, Y. J. Jang, Y. J. Lee, K. M. Kim, M. S. Seo, W. Nam and J. Yoon, *J. Am. Chem. Soc.*, 2005, **127**, 10107–10111.
7 P. Jiang and Z. Guo, *Coord. Chem. Rev.*, 2004, **248**, 205–229.
8 C.-C. Huang and H.-T. Chang, *Anal. Chem.*, 2006, **78**, 8332–8338.
9 R. Metivier, I. Leray and B. Valeur, *Chem. Commun.*, 2003, 996–997.
10 E. M. Nolan and S. J. Lippard, *J. Am. Chem. Soc.*, 2003, **125**, 14270–14271.
11 F. A. Abebe, C. S. Eribal, G. Ramakrishna and E. Sinn, *Tetrahedron Lett.*, 2011, **52**, 5554–5558.
12 Y.-X. Yuan, L. Ling, X.-Y. Wang, M. Wang, R.-A. Gu and J.-L. Yao, *J. Raman Spectrosc.*, 2007, **38**, 1280–1287.
13 A. Hakonen, P. O. Andersson, M. Stenbæk Schmidt, T. Rindzevicius and M. Käll, *Anal. Chim. Acta*, 2015, DOI: 10.1016/j.aca.2015.04.010.
14 Ž. Krpetić, L. Guerrini, I. A. Larmour, J. Reglinski, K. Faulds and D. Graham, *Small*, 2012, **8**, 707–714.

15 Y. Xue, H. Zhao, Z. Wu, X. Li, Y. He and Z. Yuan, *Analyst*, 2011, **136**, 3725–3730.
16 J. Li, L. Chen, T. Lou and Y. Wang, *ACS Appl. Mater. Interfaces*, 2011, **3**, 3936–3941.
17 W. Ren, C. Zhu and E. Wang, *Nanoscale*, 2012, **4**, 5902–5909.
18 J. Yin, T. Wu, J. Song, Q. Zhang, S. Liu, R. Xu and H. Duan, *Chem. Mater.*, 2011, **23**, 4756–4764.
19 Y. Wang and J. Irudayaraj, *Chem. Commun.*, 2011, **47**, 4394–4396.
20 M. Mulvihill, A. Tao, K. Benjauthrit, J. Arnold and P. Yang, *Angew. Chem.*, 2008, **120**, 6556–6560.
21 Y. Chen, L. Wu, Y. Chen, N. Bi, X. Zheng, H. Qi, M. Qin, X. Liao, H. Zhang and Y. Tian, *Microchim. Acta*, 2012, **177**, 341–348.
22 L. Guerrini, I. Rodriguez-Loureiro, M. A. Correa-Duarte, Y. H. Lee, X. Y. Ling, F. J. Garcia de Abajo and R. A. Alvarez-Puebla, *Nanoscale*, 2014, **6**, 8368–8375.
23 L. Szabó, K. Herman, N. E. Mircescu, I. S. Tódor, B. L. Simon, R. A. Boitor, N. Leopold and V. Chiş, *J. Mol. Struct.*, 2014, **1073**, 10–17.
24 L. Szabó, K. Herman, N. E. Mircescu, A. Fălămaş, L. F. Leopold, N. Leopold, C. Buzumurgă and V. Chiş, *Spectrochim. Acta, Part A*, 2012, **93**, 266–273.
25 K. Kim, J. W. Lee and K. S. Shin, *Analyst*, 2013, **138**, 2988–2994.
26 M. L. Moss and M. G. Mellon, *Ind. Eng. Chem., Anal. Ed.*, 1942, **14**, 862–865.
27 P. C. Lee and D. Meisel, *J. Phys. Chem.*, 1982, **86**, 3391–3395.
28 G. H. Eom, H. M. Park, M. Y. Hyun, S. P. Jang, C. Kim, J. H. Lee, S. J. Lee, S.-J. Kim and Y. Kim, *Polyhedron*, 2011, **30**, 1555–1564.
29 R. A. Palmer and T. S. Piper, *Inorg. Chem.*, 1966, **5**, 864–878.
30 W. W. Brandt, F. P. Dwyer and E. D. Gyarfas, *Chem. Rev.*, 1954, **54**, 959–1017.
31 D. P. Butcher, S. P. Boulos, C. J. Murphy, R. C. Ambrosio and A. A. Gewirth, *J. Phys. Chem. C*, 2012, **116**, 5128–5140.
32 Z. Luo, B. H. Loo, X. Cao, A. Peng and J. Yao, *J. Phys. Chem. C*, 2011, **116**, 2884–2890.
33 T. J. Dines and R. D. Peacock, *J. Chem. Soc., Faraday Trans. 1*, 1988, **84**, 3445–3457.
34 WHO, *WHO Guidelines for drinking-water quality*, World Health Organization, Geneva, 2011.
35 WHO, *Iron in Drinking-water*, World Health Organisation, Geneva, 2003.

Analyst

PAPER

View Article Online
View Journal | View Issue

Cite this: *Analyst*, 2016, **141**, 5857

Detection of potentially toxic metals by SERS using salen complexes†

Julie Docherty,[a] Samuel Mabbott,[a] Ewen Smith,[a] Karen Faulds,[a] Christine Davidson,[b] John Reglinski[b] and Duncan Graham*[a]

Received 12th July 2016,
Accepted 9th August 2016

DOI: 10.1039/c6an01584k

www.rsc.org/analyst

Surfaced enhanced Raman scattering (SERS) can discriminate between metal complexes due to the characteristic "spectral fingerprints" obtained. As a result, SERS has the potential to develop relatively simple and sensitive methods of detecting and quantifying a range of metal ions in solution. This could be beneficial for the environmental monitoring of potentially toxic metals (PTMs). Here, salen was used as a ligand to form complexes of Ni(II), Cu(II), Mn(II) and Co(II) in solution. The SERS spectra showed characteristic spectral differences specific to each metal complex, thus allowing the identification of each of these metal ions. This method allows a number of metal ions to be detected using the same ligand and an identical preparation procedure. The limit of detection (LOD) was determined for each metal ion, and it was found that Ni(II), Cu(II) and Mn(II) could be detected below the WHO's recommended limits in drinking water at 1, 2 and 2 μg L^{-1}, respectively. Co(II) was found to have an LOD of 20 μg L^{-1}, however no limit has been set for this ion by the WHO as the concentration of Co(II) in drinking water is generally <1–2 μg L^{-1}. A contaminated water sample was also analysed where Mn(II) was detected at a level of 800 μg L^{-1}.

Introduction

Schiff bases were discovered in 1864 by Hugo Schiff and are derived from the condensation between a carbonyl compound and a primary amine.[1] Schiff bases coordinate to a range of metal ions *via* the imine nitrogen and at least one other group, usually linked to the carbonyl compound.[2] They are versatile and are used in a wide variety of applications.[3] For example, aromatic Schiff bases or their metal complexes catalyse a range of reactions and their pharmacological properties have also been widely studied, including their antiviral, antibacterial and antifungal activity.[4–10]

As Schiff bases are good chelating agents, they can also be used detect potentially toxic metals (PTMs). The hazardous and toxic effects that PTMs have on the environment and human health means that monitoring is essential so that the levels present in the environment do not exceed the recommended limits as set out by environmental bodies such as the World Health Organisation (WHO). Methods of PTM quantitation usually use techniques such as ICP-MS/ICP-AES, which are commonly laboratory-based instrumentation and can have high implementation and running costs. As a result, they may not be accessible to all analytical groups, especially those in developing countries and therefore new, simpler, low-cost and potentially portable techniques are required.

Methods using UV-vis spectroscopy and fluorescence to detect metal complexes can potentially overcome these issues. As Schiff bases tend to be coloured, they can undergo a colour change on complexing to metal ions enabling detection of the change by UV-vis spectrometers.[11,12] Schiff base derivatives have also been exploited for the recognition of metal ions using fluorescence detection.[13–15] Recently however, these two techniques have also been combined to provide a single sensor for the detection of multiple metal ions. For example, Tang *et al.* have used a rhodamine B hydrazide methyl-5-formyl-1*H*-pyrrole-2-carboxylate Schiff base that is capable of detecting both Cu(II) and Hg(II) ions, the former colourimetrically and the latter fluorescently.[16] In the presence of Cu(II), the colourless Schiff base changed to pink, accompanied by a new strong absorption band centred at 556 nm. Hg(II) was the only ion amongst 16 tested that showed a fluorescence enhancement. Choi *et al.* have synthesised a Schiff base from 8-hydroxyjulolidine-9-carboxyaldehyde and 1-(3-aminopropyl) imidazole which can colourimetrically detect Fe(II) and Fe(III), while also sensing Zn(II) and Al(III) fluorescently.[17] The Schiff base changed from colourless to orange upon coordination with Fe(II), and to purple with Fe(III). Meanwhile, Zn(II) was the only metal ion (amongst 17 tested) that increased the emission

[a]*Centre for Molecular Nanometrology, WestCHEM, Pure & Applied Chemistry, University of Strathclyde, 99 George St., Glasgow, G1 1RD, UK. E-mail: duncan.graham@strath.ac.uk*
[b]*WestCHEM, Pure & Applied Chemistry, University of Strathclyde, 295 Cathedral Street, Glasgow, G1 1XL, UK*

†Electronic supplementary information (ESI) available. See DOI: 10.1039/c6an01584k

intensity of the Schiff base in a mixture of water and acetonitrile. When the solvent was changed to DMF, Al(III) was the only metal ion to enhance the emission signal. These examples demonstrate the potential of UV-vis and fluorescence to detect metal ions using Schiff bases.

Although colourimetric and fluorometric methods are useful for the determination of metal ions, the drawbacks of these techniques include a lack of selectivity/sensitivity and are liable to interference from other metal ions. However, the main disadvantage is the limited ability to multiplex due to the broad, overlapping signals obtained from these methods. This issue can potentially be overcome by using surface enhanced Raman scattering (SERS) which can give molecularly specific data due to the sharp signals produced. This enables a range of metal ions to be identified *in situ* in solution from complexes formed with a single ligand. In addition, the development of methods using SERS detection which have the potential for environmental monitoring is timely because of the recent development of handheld detectors and the lower costs of some of these units.

This has been demonstrated by Kim *et al.* who have used cyanide for the detection of Cr(III), Fe(III), Fe(II), Ni(II) and Mn(II) in solution.[18] The shift in the CN stretch on complexing was monitored using SERS. In the presence of trivalent ions, this band blue-shifted by up to 64 cm^{-1}, whereas for divalent metal ions, it was blue-shifted by 26–35 cm^{-1}. A low detection limit of 1 fM was reported making this method potentially useful for the detection of metal ions in environmental samples. Tsoutsi *et al.* have reported the use of terpyridine for the simultaneous detection of Cu(II) and Co(II) at ultratrace levels.[19] The terpyridine was attached to silver nanoparticles and used as a SERS substrate *via* the dithiocarbamate unit. Complexation with either Co(II) or Cu(II) produced changes in the vibrational SERS spectra of the terpyridine. We have previously used 2,2′-bipyridyl (bipy) to detect six different metal ions.[20] Each metal ion uniquely alters the SERS spectrum of the bipy ligand upon coordination, and these changes can be used to identify which metal ion is present. It was shown that Zn(II) and Cu(II) could be detected below the WHO's recommended limits of 0.22 and 0.6 mg L^{-1}, respectively.[21]

In this work, a [O,N,N,O] tetradentate bis-Schiff base ligand was synthesised by reacting salicylaldehyde with 1,2-diaminoethane. This ligand (salen) was used to coordinate to Ni(II), Co(II), Cu(II) and Mn(II), and Fig. 1 shows the binding of metal ions to salen. It was found that the SERS spectra of each metal–salen complex was significantly different enabling the unique spectra to be used to identify which metal ion was present. Detection limits were also calculated and to demonstrate the potential utility of the approach, a sample of contaminated water was analysed.

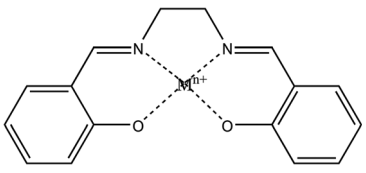

Fig. 1 Diagram representing the coordination of metal ions to salen.

Experimental

Chemicals

All reagents were purchased from Sigma-Aldrich and used as received. Freshwater samples were obtained from Loch Thom, Greenock, UK and contaminated water from Gourock burn, UK.

Nanoparticle synthesis

Silver citrate nanoparticles were prepared by following a modified version of the Lee and Meisel method.[22] Briefly, 90 mg of silver nitrate was added to 500 mL water and heated to boiling under vigorous stirring. A 1% aqueous solution of sodium citrate was added (10 mL) and heating was continued for a further 20 min. The solution was then left to cool to room temperature. In order to assess the quality of the colloid produced, a UV-vis spectrum of the colloid was obtained. Ideally, colloid made in this way should have a λ_{max} of approximately 400 nm and a full width at half maximum (FWHM) of less than 100 nm in order to be as close to monodispersity as possible. The colloid used throughout this work had a λ_{max} of 401 nm and a FWHM of around 90 nm.

Sample preparation

A 5 mM stock solution of salen ($C_{16}H_{16}N_2O_2$) was prepared by dissolving 6.7 mg in 5 mL of acetone, which was subsequently diluted to 100 μM. Metal salt solutions were prepared by dissolving the appropriate amount in distilled water to give the desired concentration.

25 μL of each metal ion solution was added to 25 μL salen (100 μM), which was then left overnight to allow complexation. The complexes can be left for a shorter period of time however, they were left overnight to ensure complete coordination of the metal ions to the ligand. AgNPs (200 μL) were then added to the salen–metal complexes and aggregation was induced by the addition of 10 μL 0.1 M MgBr salt. Three replicates of each standard was prepared and analysed using SERS.

Freshwater obtained from Loch Thom was spiked with varying concentrations of metal ions and analysed using SERS within a couple of days of collection. Environmental samples, such as the freshwater collected for this work, is usually preserved in 2% nitric acid in order to keep the metal ions in solution. However, as this induces aggregation when added to the AgNPs, the samples had to be analysed as soon as possible. An aliquot for ICP-MS analysis was however preserved in nitric acid. Contaminated water from Gourock burn was not spiked and analysed as collected.

Instrumentation

Rapid SERS analysis was conducted using an Avalon Instruments Ltd RamanStation compact benchtop spectro-

meter (PerkinElmer, Waltham, MA). The system uses a 532 nm diode laser with a laser power of 100 mW. All measurements were carried out using a 10 s exposure time and a resolution of 0.5 cm^{-1} in the range 250–2000 cm^{-1}. The instrument is fitted with a motorised *x*–*y*–*z* sample stage which accepts 96-well microtitre plates and the instrument's software was used to automatically drive the stage to each well in turn. The instrument was calibrated using an ethanol standard to ensure optimum distance between the sample and the laser aperture.

When analysing environmental samples, a portable Snowy SnRI instrument was used, which has a 532 nm diode laser with a power of 50 mW (SnRI, Wyoming, USA). All measurements were obtained using a sample volume of 500 μL and a 10 s exposure time.

ICP-MS analysis of the freshwater samples was conducted on an Agilent 7700 instrument (Agilent Technologies, Santa Clara, USA).

Results & discussion

Concentration study

In order to determine a suitable concentration of salen required to give optimal results, a study was conducted by comparing the SERS spectra of different concentrations of salen with no metal ions present, to those obtained when 1 μM Ni(II) was added. The SERS spectra from the uncomplexed salen gives a weak SERS response from the ligand however, upon addition of Ni(II), strong SERS signals are produced. This is shown in the ESI† which compares the SERS response of the free ligand to that of the Ni–salen complex. The results from adding 1 μM Ni(II) to varying concentrations of salen are shown in Fig. 2. It can be seen that the SERS signal increases in intensity as the concentration is increased up to 10 μM salen, at which point the intensity of the signals start to decrease. Above 10 μM, the higher concentrations of salen ligands present at the surface of the nanoparticles can cause over-aggregation of the colloid, or provide multilayer effects which will reduce the effective signal, while below 10 μM, there are too few ligand molecules on the surface which will also reduce the signal. As a result, a concentration of 10 μM salen was used throughout this study as this concentration gave the strongest SERS signals.

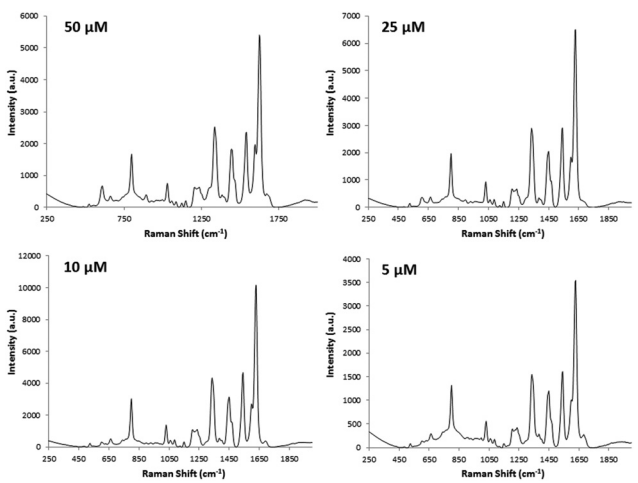

Fig. 2 SERS spectra from different salen concentrations after addition of 1 μM Ni(II). Top left: 50 μM; top right: 25 μM; bottom left: 10 μM; bottom right: 5 μM (λ_{ex} = 532 nm; acc. time = 10 s).

Salen complexes with Ni(II), Co(II), Cu(II) and Mn(II)

To obtain the SERS spectra of the salen complexes, a 2.5 μM solution of each metal salt was added to a solution of salen, followed by addition of AgNPs and aggregation with salt. The spectra acquired are compared in Fig. 3, with the frequencies and assignments of the peaks listed in Table 1.

The spectra of the salen complexes demonstrate that coordination to different metal ions results in clear and distinct changes between each metal complex. Upon coordination to the various metal ions, changes in intensity and frequency of a number of bands can be observed, which are likely to be dependent on the nature of the coordinating metal ion, *e.g.* size, mass, coordination bond strength.[23] One of the main changes between each of the complexes involves the two bands around 1600 cm^{-1}, which are attributed mainly to the C=N stretch of Schiff bases.[23] For Ni(II), a strong band is observed at 1627 cm^{-1}, with a shoulder at 1600 cm^{-1}. However, for Cu(II), this band shifts to 1641 cm^{-1}, with a weak band at 1597 cm^{-1}. For Co(II) and Mn(II), these bands also vary significantly, with two strong bands at 1628 and 1597 cm^{-1} for Co(II), and 1621 and 1597 cm^{-1} for Mn(II). These changes are likely due to the binding of the different metal ions to the nitrogen atoms of the ligand, causing the frequency of these bands to change. The strong differences in these peaks allow them to be used as marker bands for the identification and quantitation of the four metal ions.

Numerous bands can be used to discriminate between the different complexes. For example, the frequencies of other

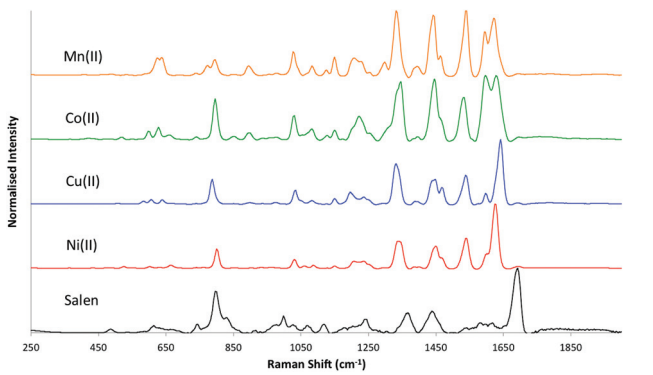

Fig. 3 Comparison of the baseline corrected SERS spectra of the salen complexes studied, using 2.5 μM solutions of each metal ion. Salen, black; Ni(II), red; Cu(II), blue; Co(II), green; Mn(II), orange (λ_{ex} = 532 nm; acc. time = 10 s).

Table 1 Frequencies and tentative assignments of the bands observed in the SERS spectra of the salen complexes[23]

Frequency (cm^{-1})				
Ni(II)	Co(II)	Cu(II)	Mn(II)	Assignment
1627.5 (s)	1628 (s)	1641.5 (s)	1621.5 (s)	C=N/C=C
1600.5 (sh)	1597 (s)	1597 (w)	1597 (s)	
1541 (m)	1531 (m)	1538 (m)	1538 (s)	Aromatic ring stretch
		1467 (m)	1463.5 (m)	
1449 (m)	1445.5 (s)	1448.5 (m)	1441.5 (s)	
		1387.5 (w)	1394.5 (w)	N–CH_2 – symmetric deformation vibration
1335.5 (m)	1346.5 (s)	1331.5 (m)	1332 (s)	CH deformation of alkyl groups
			1298 (w)	
1237.5 (w)	1222.5 (m)	1237.5 (w)	1226.5 (m)	CH_2 wagging vibration
1207.5 (w)		1195.5 (w)	1207 (m)	CH_2 twisting vibration
1149 (w)	1149 (w)	1149 (w)	1149 (m)	C–C stretching
	1129.5 (w)		1125.5 (w)	
1086.5 (w)	1082.5 (w)	1082.5 (w)	1082.5 (w)	C–C stretching
1058.5 (w)				Aromatic C–H in-plane deformation
1030.5 (w)	1030.5 (m)	1034.5 (m)	1026.5 (m)	Ring breathing
			978 (w)	
	896 (w)		896 (w)	
	850.5 (w)			
800 (m)	795.5 (m)	787.5 (m)	795.5 (m)	Aromatic C–H out-of-plane deformation
			774.5 (w)	
	740.5 (w)		740.5 (w)	
663 (w)	662 (w)			
632 (w)	627.5 (w)	640.5 (w)	636.5 (m)	Metal–ligand vibration
601 (w)	597 (w)	605.5 (w)		
		583.5 (w)		

stretches with a significant aromatic contribution also differ, improving the certainty with which the metal ions can be identified. For Ni(II), Cu(II) and Mn(II), an aromatic stretch occurs ~1538 cm^{-1}, however, a relatively large shift of around 7 cm^{-1} occurs for Co(II) and this can be used as a significant marker band for the presence of this metal ion. For the second aromatic stretch, each of the metal ions have a different frequency; 1449, 1467, 1445 and 1463 cm^{-1} for Ni(II), Cu(II), Co(II) and Mn(II), respectively. These changes in the aromatic stretches are likely due to the metal ions binding to the functional groups attached to the ring (the O and N atoms), resulting in changes to the electron density, and hence, polarisability of the ring groups.

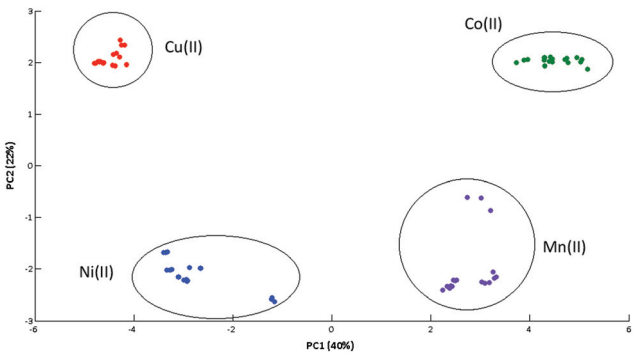

Fig. 4 PCA scores plot of the different salen–metal ion complexes. Ni(II), blue; Cu(II), red; Co(II), green; Mn(II), purple.

Principal component analysis (PCA)

Although the metal ions can be clearly distinguished by examining the SERS spectra, principal component analysis (PCA) was used to extract the data and statistically highlight the differences between the samples. PCA was carried out on 18 samples of each metal ion (three replicates of six different concentrations: 2.5, 2, 1.5, 0.75, 0.5 and 0.25 μM). The scores plot for the four metal ions is shown in Fig. 4.

Each metal ion forms well-separated clusters, emphasising that each complex has different spectroscopic features that allow them to be unambiguously identified. It also shows little variation between the different concentrations of the same metal ion, demonstrating the reproducibility of the spectra from the same complex when the concentration of the metal ion is varied.

Limit of detection (LOD) studies

In order to determine if this method could be used to detect hazardous levels of these metal ions, LODs were calculated from the concentration dependent graphs shown in Fig. 5.

The graphs were constructed by taking the most intense and unique peak for each metal ion and plotting its intensity against concentration. The LODs, calculated by multiplying the standard deviation of the blank sample by 3 and dividing this by the gradient of the line, are listed in Table 2 along with the recommended limits in drinking water as defined by the WHO.[21] From Table 2, it is evident that Ni(II), Cu(II) and Mn(II) can be detected below the WHO's recommended limits at concentrations of 0.001, 0.002 and 0.002 mg L^{-1}, respectively.

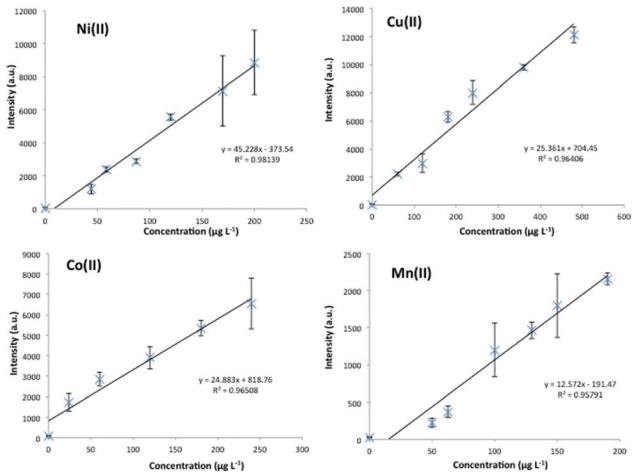

Fig. 5 LOD graphs for each salen–metal complex. Top left: Ni(II) (I_{1627} *vs.* conc.); top right: Cu(II) (I_{1638} *vs.* conc.); bottom left: Co(II) (I_{1597} *vs.* conc.); bottom right: Mn(II) (I_{1332} *vs.* conc.). Error bars represent the standard deviation between the three replicates. (λ_{ex} = 532 nm; acc. time = 10 s).

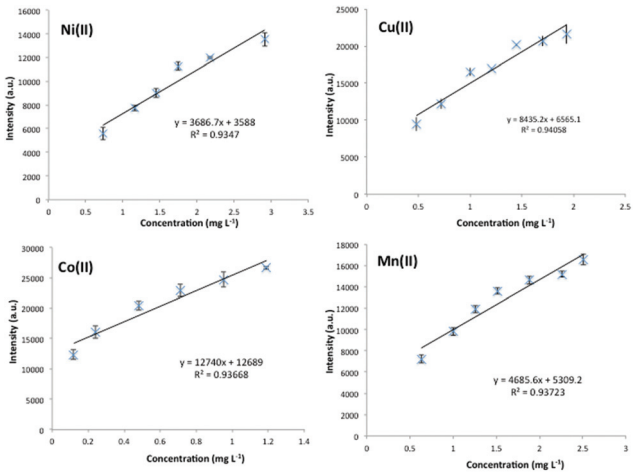

Fig. 6 Concentration dependence of each salen–metal complex in real freshwater. Top left: Ni(II) (I_{1627} *vs.* conc.); top right: Cu(II) (I_{1638} *vs.* conc.); bottom left: Co(II) (I_{1597} *vs.* conc.); bottom right: Mn(II) (I_{1332} *vs.* conc.). Error bars represent the standard deviation between three replicates. (λ_{ex} = 532 nm, acc. time = 10 s).

Table 2 Comparison of the detection limits obtained using distilled water and freshwater. The recommended WHO limits in drinking water are also listed

Metal Ion	Detection limit (d. H_2O) (mg L^{-1})	Lowest observable concentration (real freshwater) (mg L^{-1})	WHO guideline (mg L^{-1})
Co(II)	0.02 ± 0.01	0.12 ± 0.5	—
Cu(II)	0.002 ± 0.02	0.48 ± 1.8	2
Mn(II)	0.002 ± 0.03	0.63 ± 1.8	0.5
Ni(II)	0.001 ± 0.009	0.73 ± 2.7	0.02

Co(II) does not have a recommended limit as it is rarely detected in drinking water, with concentrations usually ranging from 0.1–5 μg L^{-1}, however Co(II) still poses a threat to the environment *via* other media such as soil.[24]

Real freshwater samples

These results demonstrate the ability of this method to detect four metal ions using SERS. However these tests were done using distilled water whereas the composition of environmental samples are more complex, and may contain matrix species that interfere with the detection of the metal ions. Therefore, freshwater was collected from Loch Thom, Greenock in order to test this method with real environmental samples.

Firstly, the composition of the freshwater was obtained using ICP-MS analysis, where the concentration of Ni(II), Cu(II), Co(II) and Mn(II) present was 0.9 ± 0.001, 3.7 ± 1.6, 0.1 ± 0.01 and 17.3 ± 0.08 μg L^{-1}, respectively (n = 3). The freshwater after addition of salen, was then analysed using SERS. However, a large signal was observed which is believed to be from organic material, as the spectrum did not match those from the metal ions of interest, and the concentrations of metal ions in the water sample were not sufficient to cause such a strong signal.

As Ni(II), Cu(II), Co(II) and Mn(II) were not present in the sample at high levels, the freshwater was spiked with varying concentrations of these ions and the SERS spectra acquired. However at lower metal ion concentrations, the SERS spectrum of the interferent dominated, masking features that are specific to each metal ion of interest. The freshwater standard also produced a strong SERS signal and therefore, concentration relationships were plotted as shown in Fig. 6. The lowest observable concentration for each metal ion was subsequently obtained (stated in Table 2) by using the lowest metal ion concentration that clearly produced the characteristic SERS spectrum that is associated with each metal–salen complex. Below this concentration, the SERS spectrum of the interferent dominated and therefore Ni(II), Cu(II), Mn(II) or Co(II) could not be confidently identified. Due to this interferent, the lowest observable concentration for the real freshwater samples were higher than the detection limits of the distilled water, as can be seen in Table 2. Nevertheless, this method was still able to prove that the metal ions were not present in the freshwater at levels likely to have a negative impact on human or environmental health.

Contaminated water

After testing the SERS sensor with natural freshwater, contaminated water was obtained from Gourock burn which is known to have leachate issues due to a nearby landfill site. The SERS spectrum obtained from this water sample was almost identical to that of the Mn(II)–salen complex in distilled water, and these are compared in Fig. 7. The slight differences around 1450 cm^{-1} and 1275 cm^{-1} are attributed to the different sample matrices.

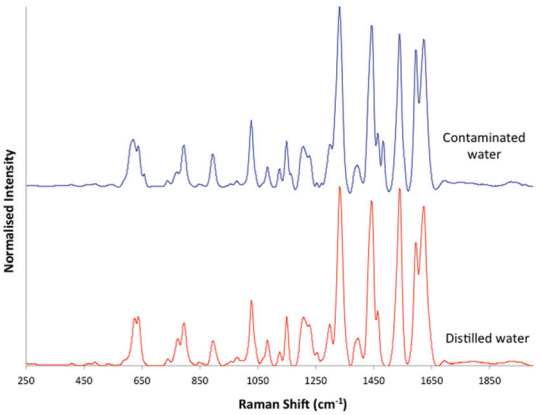

Fig. 7 Comparison of Mn(II)–salen SERS spectrum from contaminated water (top) to the Mn(II)–salen SERS spectrum in distilled water (bottom). (λ_{ex} = 532 nm, acc. time = 10 s).

In order to confirm that Mn(II) was present in the water sample, ICP-MS analysis was conducted and this showed that Mn(II) was indeed present at a concentration of 833 ± 37 μg L^{-1} (n = 3) (the concentrations of Ni(II), Co(II) and Cu(II) were 1.7 ± 0,04, 0.6 ± 0.02 and 1.9 ± 0.07 μg L^{-1}, respectively). The SERS analysis indicated that a Mn(II) concentration of approximately 700 μg L^{-1} was present, as the intensity of the 1332 cm^{-1} stretch (*i.e.* the band used to plot the concentration relationships in Fig. 6) occurred at ~7000 counts, as shown in the ESI† which displays the SERS spectrum obtained from the contaminated freshwater sample. This is reasonably similar to the results of the ICP-MS analysis indicating that this method is capable of detecting high levels of metal ions in contaminated water samples.

Conclusions

It has been demonstrated that a nanoparticle-based sensor has been developed, capable of detecting Ni(II), Cu(II), Co(II) and Mn(II) using SERS. The coordination of each of these metal ions to salen visibly changes the SERS spectrum of this ligand, and the changes produced are specific to each ion. As a result, this allows clear discrimination between each of the analytes. LOD experiments demonstrated that Ni(II), Cu(II) and Mn(II) could be detected below the recommended WHO level in drinking water. However these LODs were obtained using distilled water and therefore, the method was tested using real environmental samples; one freshwater sample with low concentrations of the metal ions of interest, and one contaminated water sample with a high concentration of Mn(II). The uncontaminated water contained an interferent, believed to be organic material, which affected the detection at low concentrations. Nonetheless, it still proved that the metal ions were not present at levels that could be deemed harmful to the environment. The SERS spectrum obtained from the contaminated water showed the presence of Mn(II) and ICP-MS confirmed that this ion was present at a concentration of 833 μg L^{-1}. Therefore, it has been shown that this SERS method for detecting metal ions can be used for the sampling of real environmental samples. ICP-MS is clearly a superior method as it can detect >50 elements at ng L^{-1} levels within a couple of minutes.[25] However, the SERS method described is a much cheaper and simpler alternative that can detect the metal ions of interest at μg L^{-1} levels and using an analysis time of 10 s.

Compared to our previous work using 2,2′-bipyridyl, although a smaller range of metal ions were studied, the sensitivity is improved using salen. The method has also been tested with real environmental water samples and was able to detect the presence of Mn(II) in a contaminated water sample. In regards to similar published work, the detection limits for this research are generally higher, *e.g.* the cyanide system described by Kim *et al.* quote LODs at the fM level while Tsoutsi *et al.* can detect Cu(II) and Co(II) at levels of 6.5 μg L^{-1} and 60 ng L^{-1}, respectively.[18,19] Nevertheless, the detection limits using salen fall below the recommended WHO levels in drinking water and we have also tested our method with natural environmental freshwater in order to ensure that it can be applied to more realistic water samples. Our method also exhibits distinct changes throughout the spectral range which confers greater confidence in the discrimination of the different metal ions. As a result, we have demonstrated the potential of SERS to be used as a low-cost environmental monitoring technique for metal ions.

Acknowledgements

This work was supported by the Royal Society of Chemistry's Analytical Chemistry Trust Fund and the Natural Environment Research Council (NERC) [NE/J01771X/1]. DG thanks the Royal Society for support from a Wolfson Research Merit Award. The research data associated with this paper has the following DOI: 10.15129/38671508-b630-4276-820c-2fc6bdbe6fae. The authors would like to thank Roslyn McIntosh at Inverclyde council for recommending and allowing access to sampling sites.

Notes and references

1 H. Schiff, *Justus Liebigs Ann. Chem.*, 1864, **131**, 118–119.
2 P. G. Cozzi, *Chem. Soc. Rev.*, 2004, **33**, 410–421.
3 A. Prakash and D. Adhikari, *Int. J. ChemTech Res.*, 2011, **3**, 1891–1896.
4 P. G. Cozzi, *Chem. Soc. Rev.*, 2004, **33**, 410–421.
5 K. C. Gupta and A. K. Sutar, *Coord. Chem. Rev.*, 2008, **252**, 1420–1450.
6 A. Jarrahpour, D. Khalili, E. De Clercq, C. Salmi and J. M. Brunel, *Molecules*, 2007, **12**, 1720–1730.
7 C. M. da Silva, D. L. da Silva, L. V. Modolo, R. B. Alves, M. A. de Resende, C. V. B. Martins and Â. de Fátima, *J. Adv. Res.*, 2011, **2**, 1–8.
8 Z. L. You and H. L. Zhu, *Z. Anorg. Allg. Chem*, 2004, **630**, 2754–2760.

9 T. Jeewoth, M. G. Bhowon and H. L. K. Wah, *Transition Met. Chem.*, 1999, **24**, 445–448.
10 N. Dharmaraj, P. Viswanathamurthi and K. Natarajan, *Transition Met. Chem.*, 2001, **26**, 105–109.
11 V. K. Gupta, A. K. Singh, M. R. Ganjali, P. Norouzi, F. Faridbod and N. Mergu, *Sens. Actuators, B*, 2013, **182**, 642–651.
12 L. Wang, D. Ye and D. Cao, *Spectrochim. Acta, Part A*, 2012, **90**, 40–44.
13 W. H. Hsieh, C.-F. Wan, D.-J. Liao and A.-T. Wu, *Tetrahedron Lett.*, 2012, **53**, 5848–5851.
14 L. Wang, W. Qin and W. Liu, *Inorg. Chem. Commun.*, 2010, **13**, 1122–1125.
15 M. Hosseini, Z. Vaezi, M. R. Ganjali, F. Faridbod, S. D. Abkenar, K. Alizadeh and M. Salavati-Niasari, *Spectrochim. Acta, Part A*, 2010, **75**, 978–982.
16 L. Tang, F. Li, M. Liu and R. Nandhakumar, *Spectrochim. Acta, Part A*, 2011, **78**, 1168–1172.
17 Y. W. Choi, G. J. Park, Y. J. Na, H. Y. Jo, S. A. Lee, G. R. You and C. Kim, *Sens. Actuators, B*, 2014, **194**, 343–352.
18 K. Kim, J. W. Lee and K. S. Shin, *Analyst*, 2013, **138**, 2988–2994.
19 D. Tsoutsi, L. Guerrini, J. M. Hermida-Ramon, V. Giannini, L. M. Liz-Marzan, A. Wei and R. A. Alvarez-Puebla, *Nanoscale*, 2013, **5**, 5841–5846.
20 J. Docherty, S. Mabbott, W. E. Smith, J. Reglinski, K. Faulds, C. Davidson and D. Graham, *Analyst*, 2015, **140**, 6538–6543.
21 WHO, *WHO Guidelines for drinking-water quality*, World Health Organization, Geneva, 2011.
22 P. C. Lee and D. Meisel, *J. Phys. Chem.*, 1982, **86**, 3391–3395.
23 G. Socrates, *Infrared and Raman Characteristic Group Frequencies: Tables and Charts*, Wiley, 2004.
24 WHO, *Cobalt and Inorganic Cobalt Compounds*, World Health Organization, Geneva, 2006.
25 H. B. Bradl, *Heavy Metals in the Environment*, Elsevier Academic Press, 2005.